Model Predictive Control
of
Wind Turbines

Martin Klauco

Summary

Wind turbines are the biggest part of the green energy industry. Increasing interest of governments and private companies in this industry calls for continuing innovation in development, construction and operation. Great portion of the operational front lies in designing new and more efficient control strategies.

Control strategy has a significant impact on the wind turbine operation on many levels. First and foremost, it is the electrical power production. Secondly, the cost of power production is directly effected by the controller. On the third count, the lifetime of the turbine and its components is greatly effected by the controller and its performance.

One of control strategies, which can take into account, maximization of power production, minimization of costs and minimization of physical stress is called Model Predictive Control (MPC). In this thesis such control method is explored. Key principles of such control strategy is presented in this research, together with performed simulations. It will be shown, that this method is suitable for wind turbine control, and that it is capable of dealing with all presented issues.

Preface

This thesis was prepared at the department of Informatics and Mathematical Modelling at the Technical University of Denmark in fulfilment of the requirements for acquiring an M.Sc. degree in Electrical Engineering. My supervisors were Niels Kjølstad Poulsen, Mahmood Mirzaei both from IMM DTU and Hans Henrik Niemann from DTU Elektro.

This research deals with controlling and modelling issues of the wind turbines. Main attention was put on design two alternative MPC strategies. These MPC strategies were then compared with baseline PID controller, which is currently running on the actual wind turbines.

Results of this research were presented at GRØN DYST conference held at DTU on June 22, 2012.

Lyngby, July 2012

Martin Klauco

Acknowledgements

I would like to express my deepest gratitude to Niels, for giving me the opportunity to be part of the research at IMM DTU. I would especially like to thank him for his continuous support and guidance. My thanks also goes to Mahmood, with whom I spent countless hours consulting technical stuff and implementation. Furthermore I would like to thank Henrik for his insight and ideas during project development.

Nomenclature

Acronyms

MPC	Model Predictive Control
FMPC	Frequency Weighted Model Predictive Control
RHC	Receding Horizon Control
HAWT	Horizontal Axis Wind Turbine
WT0	Model of the Wind Turbine, considering only rotor speed as a state
WT1	Model of the Wind Turbine, considering also tower for-aft movement

Physical Quantities

R	m	rotor disc radius
ρ	$kg.m^{-3}$	specific weight of the air (density)
ω_r	$rad.s^{-1}$	angular velocity of the rotor
J	$kg.m^2$	moment of inertia
P	W	power
$\dot{m}$	$kg.s^{-1}$	mass flow of the air moving against rotor disc
F_t	N	thrust force affecting the tower
x_t	m	tower displacement
M_t	kg	total mas of the HAWT
D_t	$N.m^{-1}.s^{-1}$	tower dampening constant
K_t	$N.m^{-1}$	tower spring constant

Notation related to Modelling and Control

x	state vector
y	output vector
y_m	output measurements vector
u	control input vector
d	state disturbance vector
A	state space system matrix
B	state space control matrix
C	state space output matrix
D	state space direct matrix
E_x	state space state disturbance matrix
E_y	state space output disturbance matrix
L	Estimator gain (Kalman filter gain)
$G_{u,x}$	Transfer function from input u to state x (or output y)
$R_{c,d}$	covariance matrix in continuous (discrete) time
H	curvature matrix (quadratic programming)
g	first order coefficient vector (quadratic programming)
$n_{u,x,y}$	number of inputs, states and outputs

$"\,\hat{}\,"$	denotes estimation of given variable
$"\,s\,"$	denotes steady state values of given variable
$"\,_0\,"$	denotes linearization point
$"\,*\,"$	denotes coordinates of maximum of the c_p curve

Sets

$\mathbb{R}^n$	Vector of real numbers
$\mathbb{R}^{n \times m}$	Matrix of real numbers
$\mathbb{S}_+$	Symmetric positive definite matrix
$\mathbb{I}^{n \times m}$	Identity matrix
$diag(x_{1,..,n})$	diagonal matrix with diagonal entries $x_1, ..., x_n$
$diag(M_1, ..., M_n)$	block diagonal matrix with diagonal blocks $M_1, ..., M_n$

Contents

Introduction

Every control strategy implemented on processes has two main objectives. Ensure maximum yield, and minimize the cost. Since this project deals with wind turbine control, the objective is to maximize the power output, and minimize the costs of achieving previously mentioned objective. In this case, we not only want to minimize the cost of control activity, but also minimize physical stress of the device itself, thus prolonging the life of the turbine.

One of the control method, which can fulfil those objective is called Model Predictive Control (MPC).

1.1 Horizontal Axis Wind Turbine Overview

The most common type of wind turbines we usually deal with is the horizontal axis wind turbine. The rotor disc, consisting of three blades (fig. 1.1) is responsible for capture of the wind energy. The hub together with blades is constructed in such way, that the angle of the blades against wind direction can be changed. This angle is also called the pitch angle, denoted as β and it is one of the control inputs to the system.

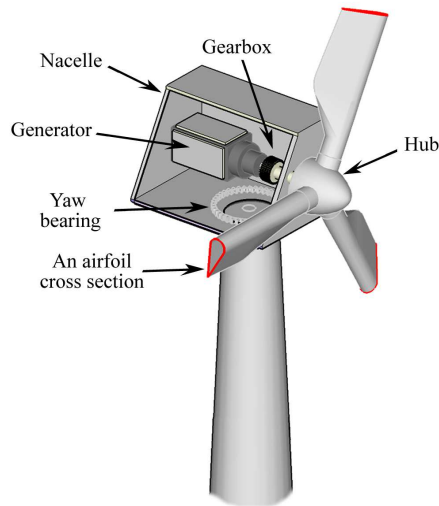The conversion mechanism from wind power to electrical power is shown in

Figure 1.1: Horizontal Axis Wind Turbine (HAWT)

picture 1.2. The second control input to the system is the speed of the generator, or the generator torque - T_g. With these two control action, rotational speed of the rotor ω_r and generated electrical power P_e can be controlled. We have to mention, that in case of HAWT, nacelle yaw angle is controlled as well, but it is assumed that direction of wind speed does not change, so it is committed from control design in this project.
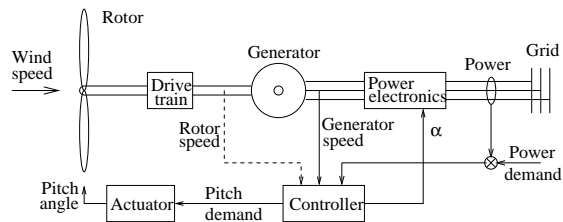

Figure 1.2: Generator with controller (Xin, 1994)

1.2 Survey of Wind Turbine Control

Standard and most common approach, that has been used on controlling the wind turbines all over the world are single-input-single-output (SISO) loops

(Jonkman et al., 2009). So far this control approach has proven to have satis-factory performance. This control strategy si more than suitable to handle the primary control objective, specifically produce maximum power (Laks et al., 2009).

However, when the wind turbine industry is on the rise more advanced control strategies are needed. The main control objective remain the power production, but secondary tasks arise, e.g. decreasing structural fatigue, thus prolonging the lifetime of the turbine and its components. In order to fulfil these objectives, multiple-input-multiple-output (MIMO) methods must be used. For such pur-pose robust model predictive control has been proposed (Mirzaei et al., 2012b). Another approach presented by (Østergaard et al., 2008) propose linear param-eter varying control strategy, as an advanced gain scheduling method in order to control wind turbine in entire considered wind speed interval. These meth-ods are based on linear models. It will be shown, that system dynamics change with increasing wind speed. This means, that estimation or measurement of the wind speed is required, based on which LTI models. Also MPC control or LQ control are based on state feedback, so state estimator is required when using such controllers.

Above presented methods consider collective blade pitch control action. Since the wind speed is not constant throughout the rotor disc, individual blade pitch control has been proposed (Bossanyi, 2003). In paper presented by (Mirzaei et al., 2012a) is proposed individual blade pitch robust model predictive con-troller together with wind speed measurements over the prediction horizon. This proves to have significant advantages when harsh wind speed conditions occurs i.e. wind shears.

1.3   Model Predictive Control Overview

Model predictive control (MPC) is an advanced MIMO optimal control strat-egy. The basic principle of MPC lies in predicting the future states of the plants, then formulating an cost function which reflects control objective and imposing additional constraints on inputs, states or outputs. MPC problem is often for-mulated as a quadratic programming problem (Boyd and Vandenberghe, 2009; Nocedal and Wright, 1999), which is solved at each sampling instance to obtain optimal control inputs.

MPC has become one the most used process control tools mainly in chemical industry like distillation columns (Ahmad and Wahib, 2007), but also oil re-fineries and such (Nikolaou, 2001). Main advantage of it in such applications

is the way of handling huge time delays. Advantages of MPC are also used in electrical power industry (Larsson, 2004), smart grids optimization and design (Bendtsen et al., 2010) etc. Theory behind Model Predictive Control is further discussed in chapter 4.

1.4   Project overview

Every process control design must begin with deriving mathematical model of the process. In our case it is the Wind-Turbine. Once the mathematical model is formulated, MPC design is explained. In this project we will focus on two approaches of controlling the HAWT.

In the controller design we will focus on the MPC design. Two approaches of MPC control will be explained. First, the most common one, where the tuning parameters of the controller are weighting matrices (Camacho and Bordons, 2007). In second part of MPC design we will focus on frequency weighted MPC control design. Advantages and disadvantages of MPC strategies will be explained. Furthermore Kalman filtering for state and disturbance estimation is going to be discussed (Kalman, 1960; Pannocchia and Rawlings, 2003).

In order to demonstrate the performance of the model predictive control strategy, detailed deterministic simulations are shown along with long time stochastic simulations. Performance of standard MPC is then compared with the frequency weighted MPC design. The effects of the frequency weights (filters) are going to be explained as well. Furthermore these two MPC strategies will be compared with currently implemented PID controllers (Jonkman et al., 2009; J. Jonkman and Bir, 2007); it will be shown, that MPC design has stabilized the power output of the HAWT, and that it minimizes the physical stress to the turbine.

Model of Wind Turbine

2.1 Model of the HAWT

Kinetic energy of the wind is the driving force of the power generation in wind-turbine. The following formula shows hot to calculate kinetic energy of an object

$$E = \frac{1}{2}mv^2 \tag{2.1}$$

where m is mass and v is speed of object and E is the kinetic energy. The mechanical power is defined as a first derivative of energy with respect to time:

$$P = \frac{\mathrm{d}E}{\mathrm{d}t} \tag{2.2}$$

Since the speed is considered constant, we can combine equations 2.1 and 2.2 together

$$P = \frac{1}{2}\frac{\mathrm{d}m}{\mathrm{d}t}v^2 = \frac{1}{2}\dot{m}v^2 \tag{2.3}$$

where $\dot{m}$ is considered as mass flow. In case of HAWT, the mass flow is the air moving against rotor disc, therefore we can write:

$$\dot{m} = \pi R^2 \rho v \tag{2.4}$$

where ρ is the density of the air, R is the length of the blades and v is the speed of the wind. The equation 2.5 shows how to calculate the power stored in the wind, which is moving against the wind turbine (Xin et al., 1997; Burton et al., 2001).

$$P_w = \frac{1}{2}\dot{m}v^2 = \frac{1}{2}\rho\pi R^2 v^3 \tag{2.5}$$

It is only natural, that the wind turbine cannot extract 100% of the power stored in the wind. The coefficient, which determines how much power is actually converted into electrical energy is called *power extraction coefficient* or C_P value. This value is function of pitch angle and tip speed ratio. The maximum mechanical power, available in the wind speed is expressed in equation 2.6.

$$P_r = \frac{1}{2}\rho\pi R^2 v^3 C_p(\lambda, \beta) \tag{2.6}$$

Power coefficient $C_P(\lambda, \beta)$ is a function of tip speed ratio (TSR) λ, (eq. 2.7) and pitch β. The c_p curve is displayed on the figure 2.1.

$$\lambda = \frac{R\omega_r}{v} \tag{2.7}$$

The rotation movement of the rotor is given by formula 2.8:

$$J\frac{d\omega_r}{dt} = Q_r - N_g T_g \tag{2.8}$$

Where J is the inertia of the system, Q_r is aerodynamic torque, N_g is gear ratio and T_g is the generator torque. Aero dynamic torque is given as ratio between mechanical power, and rotational speed ω_r (eq. 2.9).

$$Q_r = \frac{P_r}{\omega_r} \tag{2.9}$$

In similar fashion like $C_p(\lambda, \beta)$ curve, is defined $C_t(\lambda, \beta)$ curve (fig. 2.2). Based on c_t coefficient we can calculate the thrust force F_t imposed by the wind on the tower (eq. 2.10).

Thrust force:

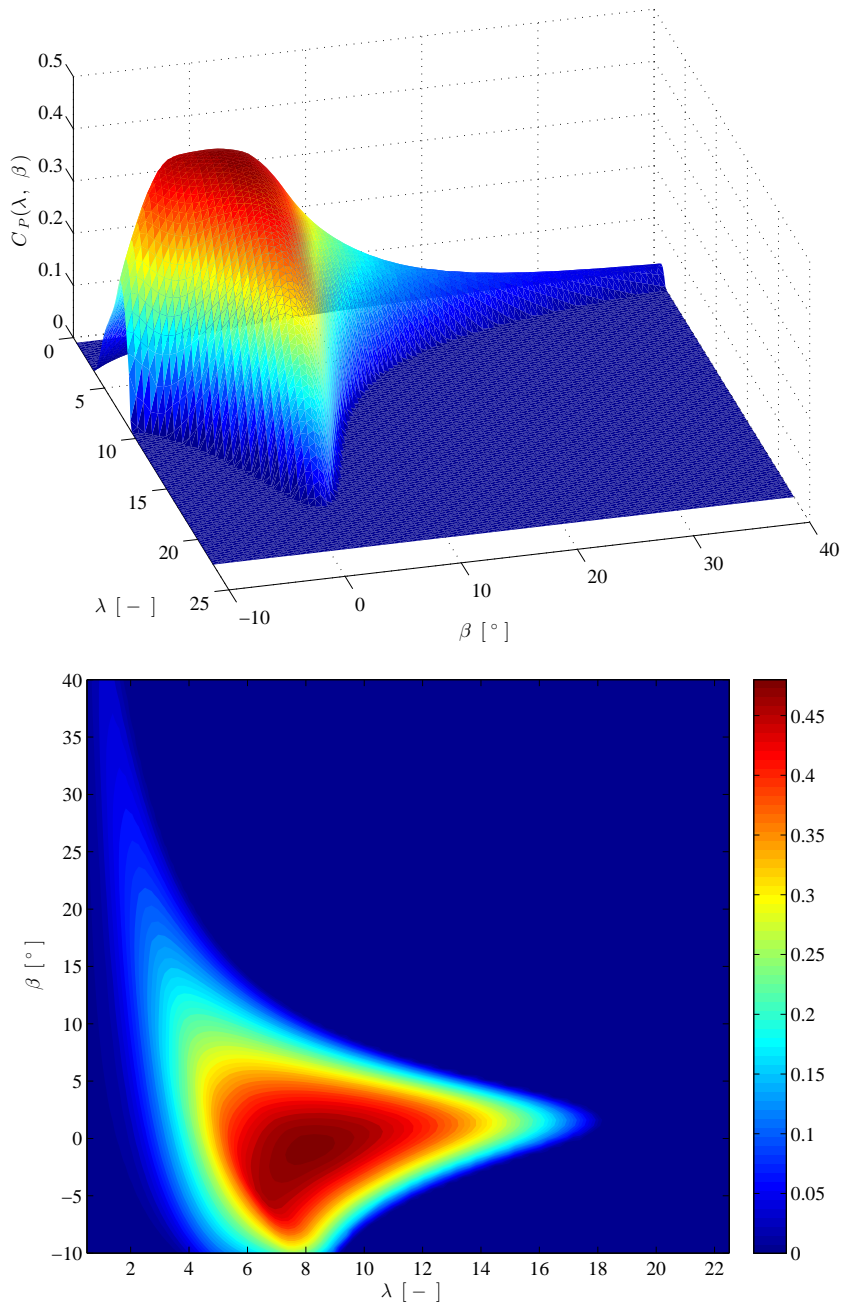$$F_t = \frac{1}{2}\pi\rho R^2 v^2 c_t(\lambda, \beta) \tag{2.10}$$

Figure 2.1: C_P curve used in calculation throughout this project. Maximum of this curve is equal to 0.4861
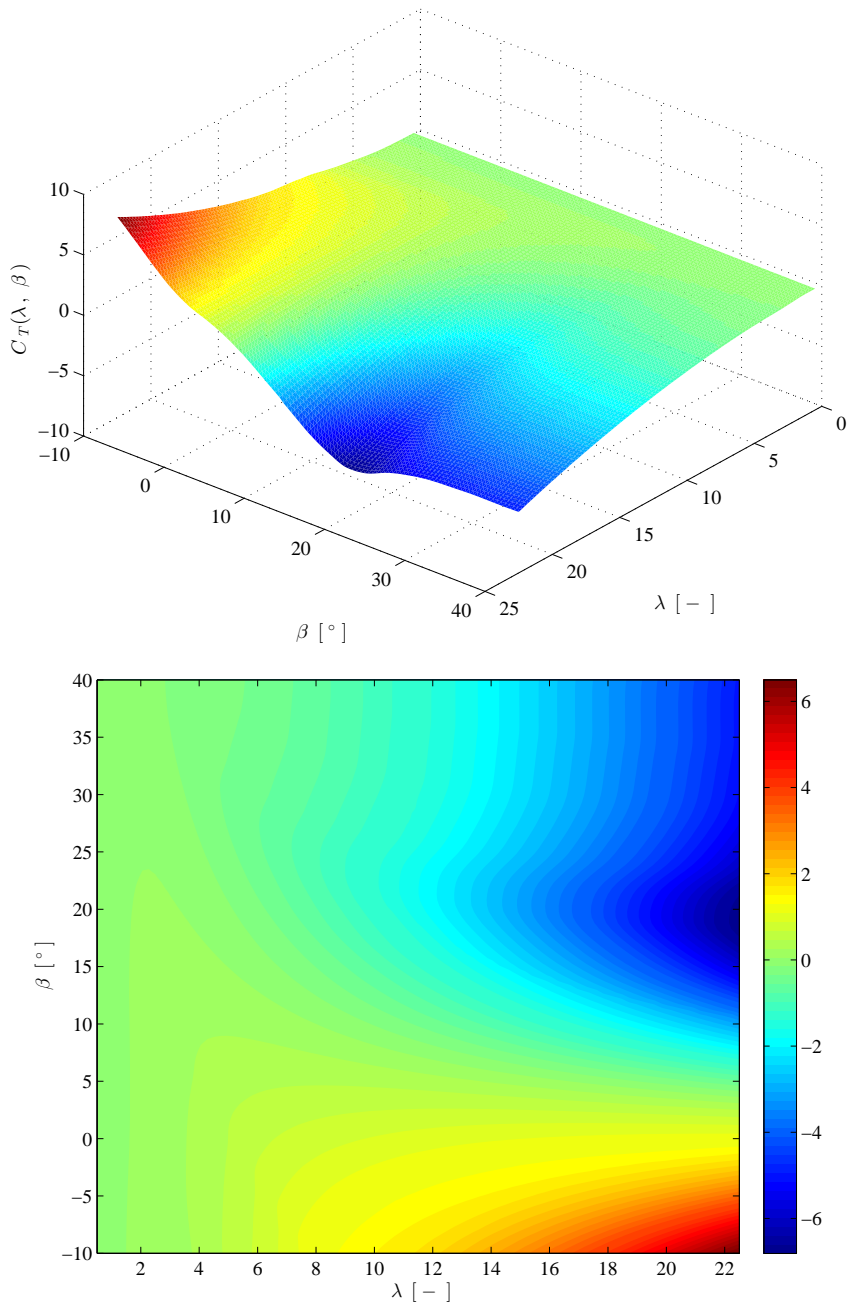
Figure 2.2: Thrust coefficient

Tower for-aft movement can be represented by second order system (Hansen, 2008). Equation 2.11 shows the relation between thrust force, tower speed of displacement $\dot{x}_t$ and tower displacement x_t. Mass constant M_t, structural damping factor D_t and spring constant K_t can be found in (Henriksen, 2007).

$$F_t = M_t\ddot{x}_t + D_t\dot{x}_t + K_tx_t \tag{2.11}$$

Stationary value of tower displacement is calculated:

$$x_{t,0} = \frac{F_t}{K_t} \tag{2.12}$$

2.2 Wind speed model

Effective wind speed is approximated by second order transfer function 2.13. Where parameters k, p_1, p_2 are functions of mean wind speed (Xin et al., 1997; Henriksen, 2007). Values for these parameters can be found in figure 2.3.

$$v_t = \frac{k}{(p_1s + 1)(p_2s + 1)}e_t; \quad e_t \in N_{iid}(0,1) \tag{2.13}$$

A substitution 2.14 has been introduced in order to obtain continuous state space model of the wind speed, this mode is expressed in 2.15.

$$\begin{array}{ccc} x_1 & = & v \\ x_2 & = & \dot{v} \end{array} \tag{2.14}$$

$$\begin{bmatrix} \dot{x}_1 \\ \dot{x}_2 \end{bmatrix} = \begin{bmatrix} 0 & 1 \\ a_1 & a_2 \end{bmatrix} \begin{bmatrix} x_1 \\ x_2 \end{bmatrix} + \begin{bmatrix} 0 \\ b_1 \end{bmatrix} e_t \tag{2.15}$$

yielding:

$$\dot{x} = A_cx + B_ce_t \tag{2.16}$$

As far, as we are only interested in wind speed itself, not wind acceleration, output C matrix for this state space model will be:

$$C = [1 \ 0] \tag{2.17}$$

(a) Gain

(b) Noise Variance
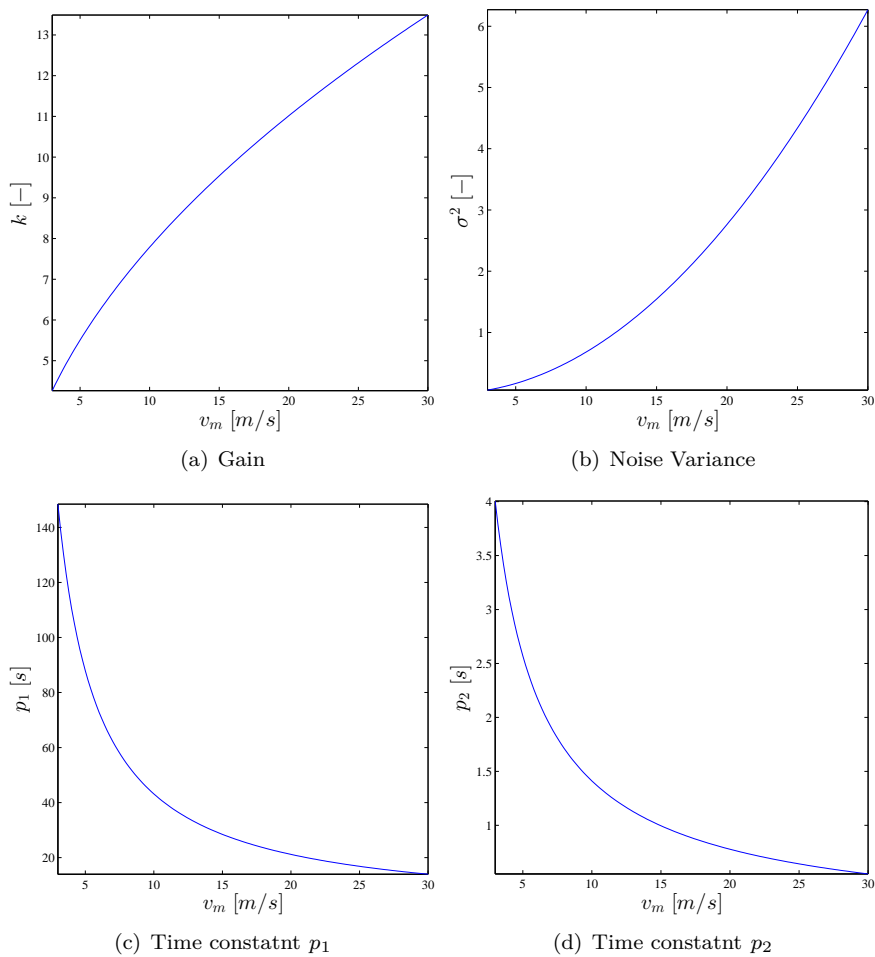
(c) Time constatnt p_1

(d) Time constatnt p_2

Figure 2.3: Wind speed model parameters for transfer function defined in equation 2.13

Coefficients in A_c matrix can be simply calculated from transfer function presented earlier (eq. 2.13).

$$a_1 = -\frac{1}{p_1 p_2} \qquad a_2 = -\frac{p_1 + p_2}{p_1 p_2} \qquad b_1 = \frac{k}{p_1 p_2} \qquad (2.18)$$

Covariance matrix in continuous time for wind speed model is given in equation 2.19, where the intensity I is equal to 1.

$$R_c = BIB^T \qquad (2.19)$$

In order to better understand how the variance of the wind speed changes with increasing mean wind speed, stationary distribution of the output of the state space model is calculated. Using Lyapunov equation in continuous time (eq. 2.20) we calculate the stationary distribution of the states X. The variance of the wind speed can be then calculated using formula 2.21. Result is shown in figure 2.3(b).

$$0 = A_c X + X A_c^T + R_c \qquad (2.20)$$

$$\sigma^2 = CXC^T \qquad (2.21)$$

Since discrete time simulations has been performed, continuous model must be discretized. The target discrete time state space model is shown in 2.22. In which x is the state vector. The variable v_k is the discrete time value of the effective wind speed and v_m is the mean wind speed.

$$x_{k+1} = A_d x_k + R_d e_k \qquad (2.22a)$$
$$v_k = C x_k + v_m \qquad (2.22b)$$

In our case covariance matrix R_c must be also discretized. For calculation we used procedure thoroughly described in (Brown and Hwang, 1997; Åström, 1970). For an illustration this procedure will be shortly explained. First matrix F is constructed (eq. 2.23), then matrix G is calculated using formula 2.24. Note, that when using MATLAB for this calculation, matrix exponential `expm` must be used. In order to obtain the discrete time covariance matrix and discrete time system matrix, matrix G is split into sub-matrices like suggested in 2.24
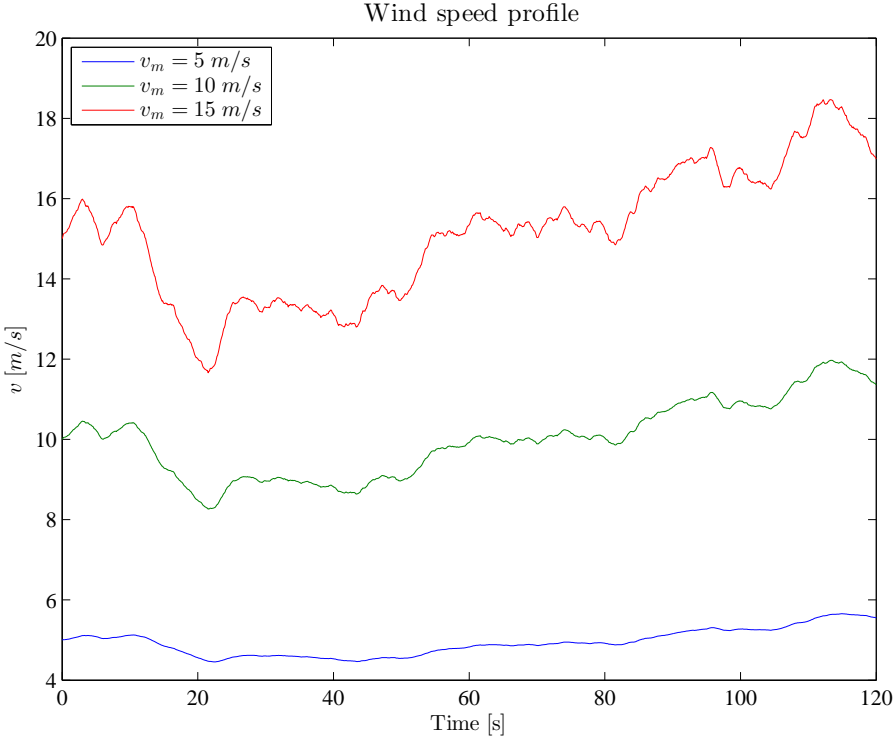
Figure 2.4: Generated wind profile for different mean wind speeds

and 2.25. Equation 2.26 shows the covariance matrix in discrete time. Sampling time τ_s was set to 0.1 s. This sampling time was also used on discretization of state space models.

$$F = \begin{bmatrix} -A & R_c \\ 0 & A^T \end{bmatrix} \tag{2.23}$$

$$G = e^{F\tau_s} = \begin{bmatrix} M_{11} & M_{12} \\ 0 & M_{22} \end{bmatrix} \tag{2.24}$$

$$\begin{aligned} M_{12} &= A_d^{-1} R_d \\ M_{22} &= A_d^T \end{aligned} \tag{2.25}$$

$$R_d = M_{22}^T M_{12} \tag{2.26}$$

Using the discrete time state space model, we can generate the wind speed profile for discrete time simulations. On figure 2.4 are shown profiles for different mean wind speeds. In order to demonstrate the difference in the variance, same set of random numbers were used.

More data about wind turbines standards and wind speed definitions can be found in (IEC-CDV, 2004).

2.3 Operational and Stationary Analysis

Horizontal Axis Wind Turbine operates in 4 operational modes. These operational region are defined by rotational speed ω_r, generated power P_e and by wind speed v. Values of rotational speed can be found on figure 2.5. Figure 2.6 shows the stationary value for power output.

Region 1 (R-I) - Low Region: Angular velocity of the rotor is kept at its minimum value, $\omega_{r,1} = 6.9 \ rpm$. In this region, power is maximized. In order to do that pitch values are found for given TSR, so the value of c_p is maximum possible. The wind speed interval for this region is $v \ \in \ < 3, \ 5.6 > \ m/s$.

Region 2 (R-II) - Mid Region: In this region the maximum of the $c_p(\lambda, \ \beta)$ curve is reached. Velocity of the rotor rise linearly with the wind speed (eq. 2.27). Power is again maximized in this region. Pitch values and TSR values are kept constant. $\lambda^\star$ and $\beta^\star$ denotes the coordinates of the maximum of the c_p curve. The wind speed interval for this region is $v \ \in \ < 5.6, \ 10 > \ m/s$

$$\omega_{r,2} = \frac{\lambda^\star R}{v} \qquad (2.27)$$

Region 3 (R-III) - High Region: Rotor speed is kept at its nominal value $\omega_{r,3} = 12.1 \ [rpm]$. Also in this region power is maximized. The pitch values are found, so the values of power coefficient c_p is maximum possible, given λ. The wind speed interval for this region is $v \ \in \ < 10, \ 11.2 >$

Region 4 (R-IV) - Top Region: Both power output and angular velocity is kept at their respective nominal values. c_p values are calculated from formula 2.28. The wind speed interval for this region is $v \ \in \ < 11.2, \ 25 > \ m/s$

$$c_p(\lambda, \ \beta) = \frac{2P_{nom}}{\rho \pi R^2 v^3} \qquad (2.28)$$

Definition of the operational modes of the HAWT is resulting in stationary values of individual quantities linked to HAWT, like c_p values (fig. 2.7). Following by figures which display stationary values of pitch β and TSR λ with respect to wind speed (figures 2.8 and 2.9).
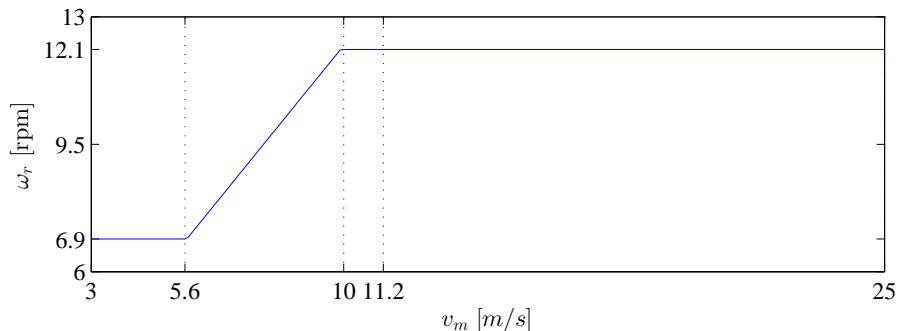

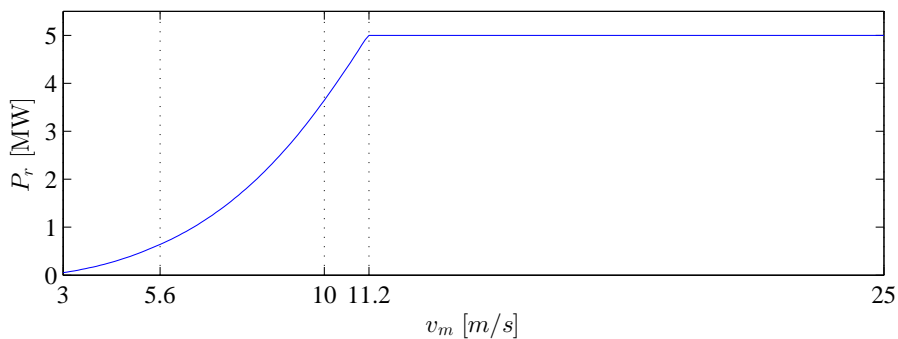**Figure 2.5:** Steady state values of angular velocity of the rotor (ω_r)

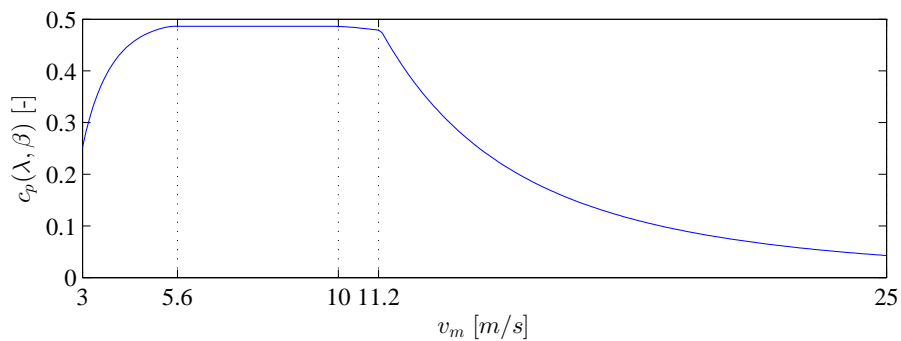**Figure 2.6:** Mechanical power (P_r) generated by the rotor

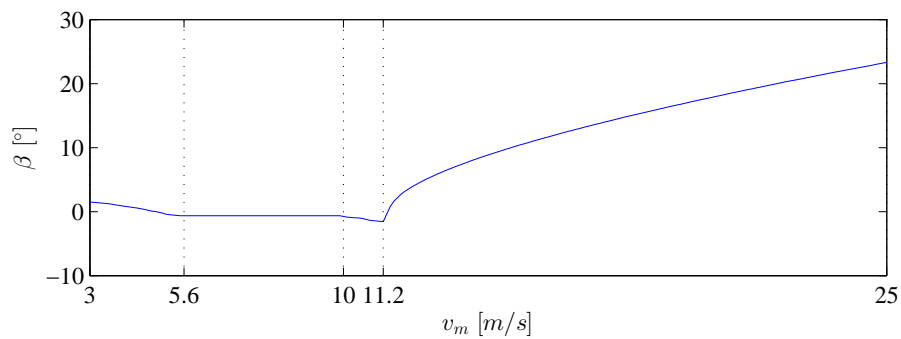**Figure 2.7:** Steady state values of power extraction coefficient (c_p)

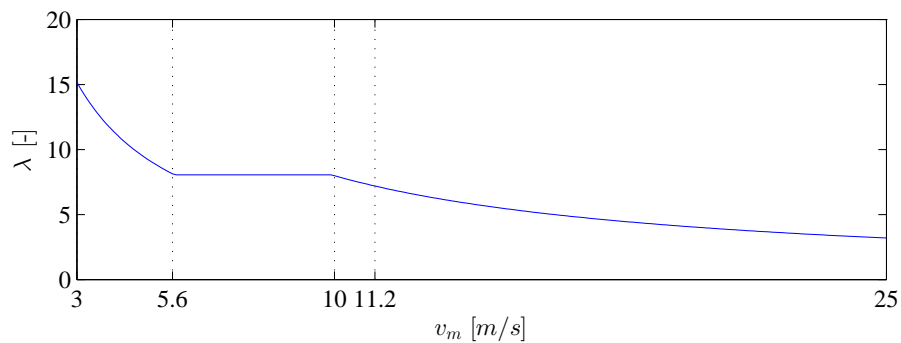**Figure 2.8:** Steady state values of pitch (β)

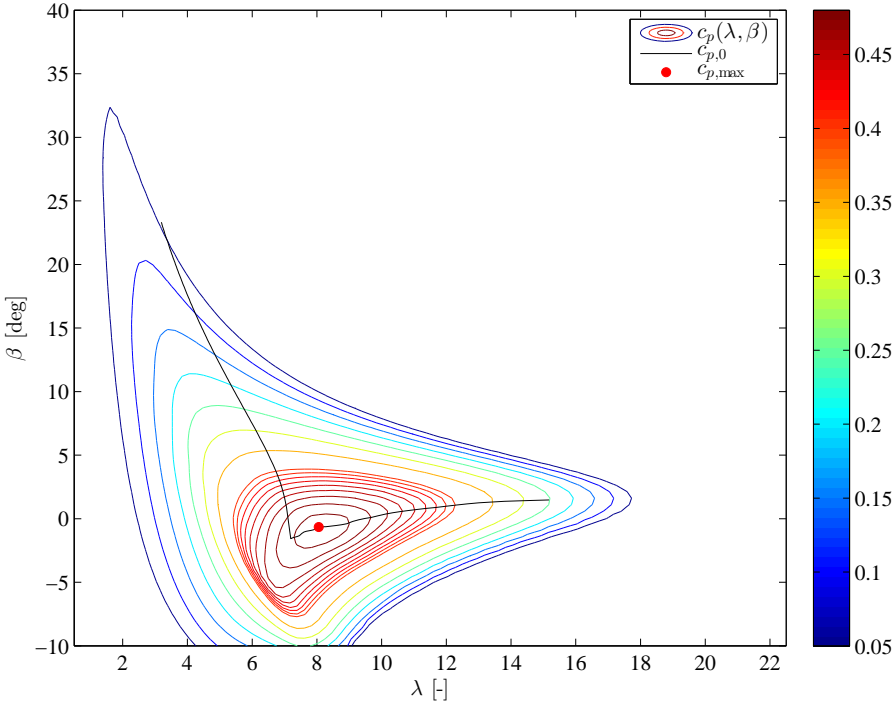**Figure 2.9:** Steady state values of TSR (λ)

Figure 2.10: Contour plot of $c_p(\lambda, \beta)$ curve

Figure 2.10 shows contour plot of the C_p curve, with the stationary values of the TSR, and pitch. Stationary values of $c_p(\lambda, beta)$ are denoted as c_p^0. This figure is crucial for understating the definitions of operational modes. In low wind speeds, TSR is high, and pitch values are found so in order to get maximum c_p value (first three regions). In second region, the pitch is kept constant, the maximum of the c_p. However in the top region, when the objective is to control the power, the pitch is calculated so generated power is equal to nominal power.

Once we calculated these basic quantities, which describes behaviour of the rotor angular velocity at every wind speed, we can calculate values of c_t curve (fig. 2.11), and thrust force F_t (fig. 2.12) as a function of wind speed. Stationary value of tower displacement x_t as a function of wind speed is shown on figure 2.13.
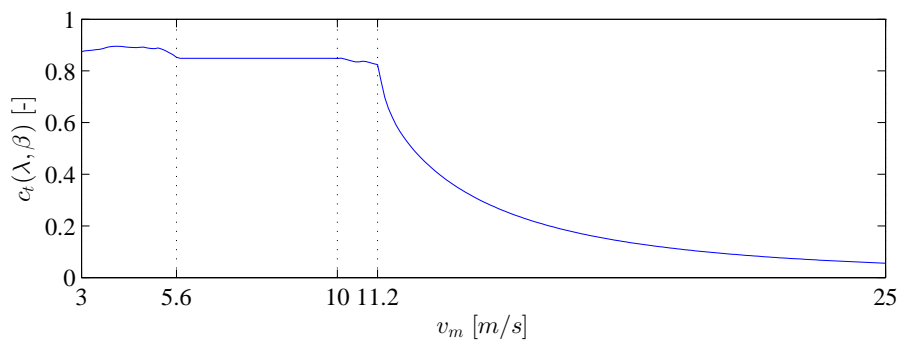
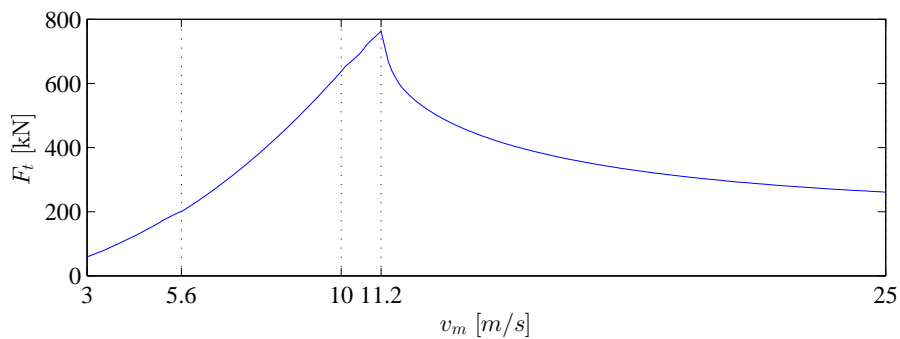**Figure 2.11:** Steady state values of thrust force coefficient (c_t)

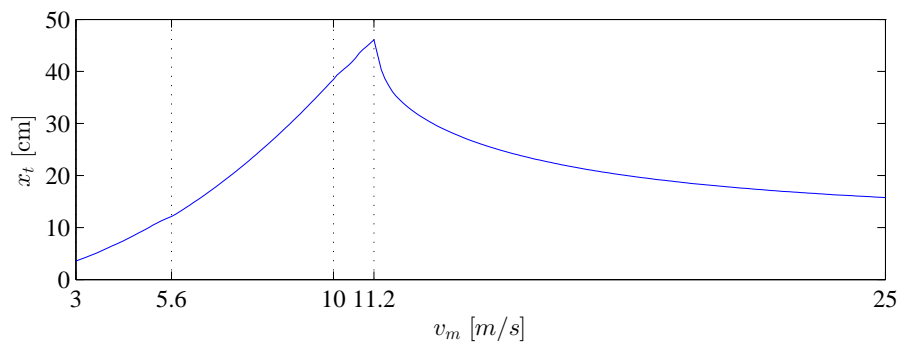**Figure 2.12:** Thrust force (F_t) affecting the rotor

Figure 2.13: Tower displacement ($x_{t,0}$) in steady state

2.4 Linearization

In order to design linear model, on which is based the MPC controller, proper derivatives of physical quantities must be found. Model considered in this project is a third order system (eq. 2.29) with two control inputs (2.30). Wind speed is considered as a disturbance.

$$x = \begin{bmatrix} \omega_r \\ x_t \\ \dot{x}_t \end{bmatrix} \qquad (2.29)$$

$$u = \begin{bmatrix} \beta \\ T_g \end{bmatrix} \qquad (2.30)$$

Differential equations that describes the system behaviour are:

$$J\dot{\omega}_r = Q_r - N_g T_g \qquad (2.31a)$$
$$F_t = M_t \ddot{x}_t + D_t \dot{x}_t + K_t x_t \qquad (2.31b)$$

Once the tower for-aft movement is considered as a part of the model (Hansen, 2008), then we also have to consider relative wind speed v_r (eq. 2.32). It is obvious, that if the steady state point is reached, relative wind speed is equal to actual wind speed. The relative wind speed will be the operating point on which is based the linearization of the states related to the tower movement.

$$v_r = v - \dot{x}_t \qquad (2.32a)$$
$$v = v_r + \dot{x}_t \qquad (2.32b)$$

Linearization of non-linear system presented in equation 2.31 takes place using very well-known first order Taylor series expansion. Partial derivatives respective functions in eq. 2.31 given all states, control and disturbance variables must be found.

First we will introduce derivatives of the aerodynamic torque with respect to considered variables.

$$\left. \frac{\partial Q_r}{\partial \omega_r} \right|_{\omega_{r0}} = \frac{1}{\omega_{r0}} \left. \frac{\partial P_r}{\partial \omega_r} \right|_{\omega_{r0}} - \frac{P_{r0}}{\omega_{r0}^2} \qquad (2.33)$$

$$\left.\frac{\partial Q_r}{\partial \beta}\right|_{\beta_0} = \frac{1}{\omega_{r0}} \left.\frac{\partial P_r}{\partial \beta}\right|_{\beta_0} \tag{2.34}$$

$$\left.\frac{\partial Q_r}{\partial \beta}\right|_{v_0} = \frac{1}{\omega_{r0}} \left.\frac{\partial P_r}{\partial v}\right|_{v_0} \tag{2.35}$$

Then we further continue with the respective derivatives of the mechanical power P_r.

$$\left.\frac{\partial P_r}{\partial \omega_r}\right|_{\omega_{r0}} = \frac{1}{2}\rho \pi R^2 v^3 \left.\frac{\partial c_p(\lambda, \beta)}{\partial \lambda}\right|_{\lambda_0} \cdot \left.\frac{\partial \lambda}{\partial \omega_r}\right|_{\omega_{r0}} \tag{2.36}$$

$$\left.\frac{\partial P_r}{\partial \beta}\right|_{\beta_0} = \frac{1}{2}\rho \pi R^2 v^3 \left.\frac{\partial c_p(\lambda, \beta)}{\partial \beta}\right|_{\beta_0} \tag{2.37}$$

$$\left.\frac{\partial P_r}{\partial v}\right|_{v_0} = \frac{1}{2}\rho \pi R^2 \left(3v_0^2 c_p(\lambda_0, \beta_0) + v^3 \left.\frac{\partial c_p(\lambda, \beta)}{\partial \lambda}\right|_{\lambda_0} \cdot \left.\frac{\partial \lambda}{\partial v}\right|_{v_0} \right) \tag{2.38}$$

Since the $\dot{x}_t$ is considered as a state variable, derivatives of Q_r and F_t with respect to $\dot{x}_t$ must be calculated as well. Understanding the relation presented in equation 2.32, following expression can be written:

$$\left.\frac{\partial P_r}{\partial \dot{x}_{t,0}}\right|_{\dot{x}_{t,0}} = \left.\frac{\partial P_r}{\partial v}\right|_{v_0} \tag{2.39}$$

Respective partial derivatives of TSR:

$$\frac{\partial \lambda}{\partial \omega_r} = \frac{R}{v} \tag{2.40}$$

$$\frac{\partial \lambda}{\partial v} = -\frac{R\omega_r}{v^2} \tag{2.41}$$

Derivatives of C_P with respect to λ and β (eq: 2.42) must be found numerically using various interpolation methods. Values of these derivatives as a function of wind speed can be seen on figures 2.14 and 2.15.
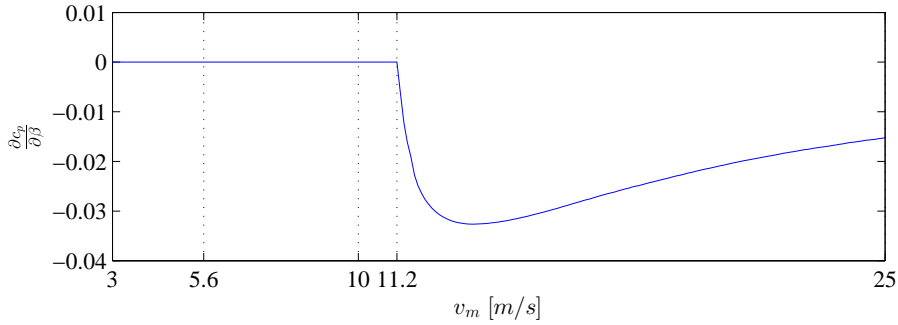
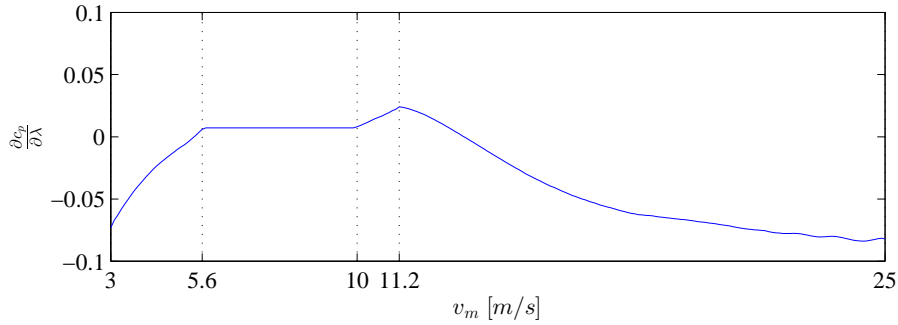**Figure 2.14:** Values of partial derivative of C_p with respect to β

Figure 2.15: Values of partial derivative of C_p with respect to λ

$$\left. \frac{\partial c_p(\lambda, \beta)}{\partial \beta} \right|_{\beta_0} \tag{2.42a}$$

$$\left. \frac{\partial c_p(\lambda, \beta)}{\partial \lambda} \right|_{\lambda_0} \tag{2.42b}$$

Model of the tower for-aft movement was made linear, so we can easily write state space representation (eq. 2.43) of that differential equation (eq. 2.31b).

$$\begin{bmatrix} \dot{x}_t \\ \ddot{x}_t \end{bmatrix} = \begin{bmatrix} 0 & 1 \\ -\frac{K_t}{M_t} & -\frac{D_t}{M_t} \end{bmatrix} \begin{bmatrix} x_t \\ \dot{x}_t \end{bmatrix} + \begin{bmatrix} 0 \\ \frac{1}{M_t} \end{bmatrix} F_t \tag{2.43}$$
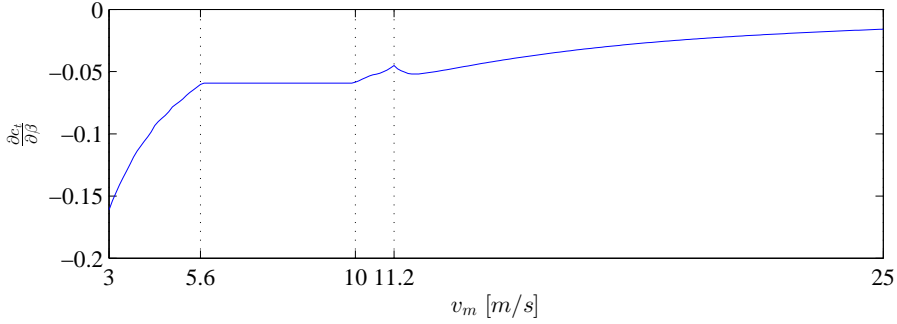
Figure 2.16: Values of partial derivative of C_t with respect to β

Next partial derivatives of thrust force F_t are expressed:

$$\frac{\partial F_t}{\partial \omega_r}\bigg|_{\omega_{r,0}} = \frac{1}{2}\pi\rho R^2 v^2 \left.\frac{\partial c_t(\lambda,\beta)}{\partial \lambda_0}\right|_{\lambda_0} \left.\frac{\partial \lambda}{\partial \omega_r}\right|_{\omega_{r,0}} \qquad (2.44)$$

$$\frac{\partial F_t}{\partial \beta}\bigg|_{\beta_0} = \frac{1}{2}\pi\rho R^2 v^2 \left.\frac{\partial c_t(\lambda,\beta)}{\partial \beta_0}\right|_{\beta_0} \qquad (2.45)$$

$$\frac{\partial F_t}{\partial v}\bigg|_{v_0} = \frac{1}{2}\pi\rho R^2 \left(2v c_t^0(\lambda,\beta) + v^2 \left.\frac{\partial c_t(\lambda,\beta)}{\partial \lambda_0}\right|_{\lambda_0} \left.\frac{\partial \lambda}{\partial v}\right|_{v_0}\right) \qquad (2.46)$$

$$\frac{\partial F_t}{\partial \dot{x}_t}\bigg|_{\dot{x}_{t,0}} = \frac{\partial F_t}{\partial v}\bigg|_{v_0} \qquad (2.47)$$

Similarly derivatives of C_t curve with respect to λ and β (eq: 2.48) must be found numerically using some interpolation methods. Figures 2.16 and 2.17 shows values of these derivatives as a function of wind speed.

$$\left.\frac{\partial c_t(\lambda,\beta)}{\partial \beta}\right|_{\beta_0} \qquad (2.48a)$$

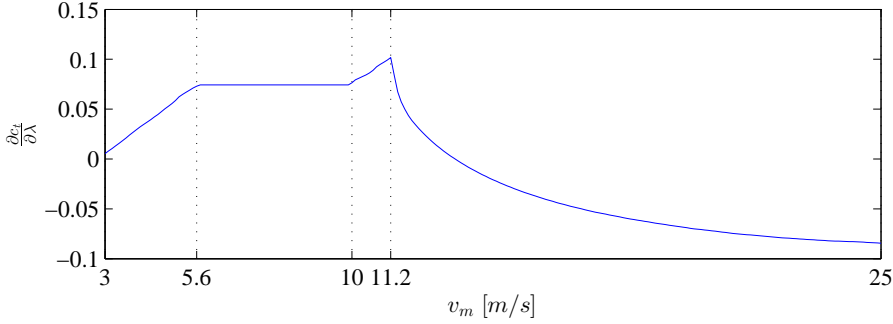$$\left.\frac{\partial c_t(\lambda,\beta)}{\partial \lambda}\right|_{\lambda_0} \qquad (2.48b)$$

Figure 2.17: Values of partial derivative of C_t with respect to λ

Once all partial derivatives are introduced, we can construct the state space representation 2.49 of the third order non-linear model presented in eq. 2.31.

$$
\begin{bmatrix} \dot{\omega}_r \\ \dot{x}_t \\ \ddot{x}_t \end{bmatrix} = \begin{bmatrix} \frac{1}{J} \left. \frac{\partial Q_r}{\partial \omega_r} \right|_{\omega_{r0}} & 0 & -\frac{1}{J} \left. \frac{\partial Q_r}{\partial \dot{x}_t} \right|_{\dot{x}_{t,0}} \\ 0 & 0 & 1 \\ \frac{1}{M_t} \left. \frac{\partial F_r}{\partial \omega_r} \right|_{\omega_{r0}} & \frac{K_t}{M_t} & -\frac{D_t}{M_t} - \frac{1}{M_t} \left. \frac{\partial F_t}{\partial \dot{x}_t} \right|_{\dot{x}_{t,0}} \end{bmatrix} \begin{bmatrix} \omega_r \\ x_t \\ \dot{x}_t \end{bmatrix} +
$$
$$
+ \begin{bmatrix} \frac{1}{J} \left. \frac{\partial Q_r}{\partial \beta} \right|_{\beta_0} & -\frac{N}{J} \\ 0 & 0 \\ \frac{1}{M_t} \left. \frac{\partial F_t}{\partial \beta} \right|_{\beta_0} & 0 \end{bmatrix} \begin{bmatrix} \beta \\ T_g \end{bmatrix} + \begin{bmatrix} \frac{1}{J} \left. \frac{\partial Q_r}{\partial v_r} \right|_{v_0} \\ 0 \\ \frac{1}{M_t} \left. \frac{\partial F_t}{\partial v_r} \right|_{v_0} \end{bmatrix} v_t \tag{2.49}
$$

Proper state space description can be written after deviation variables are introduced 2.50. Resulting state space model is formulated in 2.51

$$
x = \begin{bmatrix} \omega_r - \omega_{r,0} \\ x_t - x_{t,0} \\ \dot{x}_t - 0 \end{bmatrix} \qquad u = \begin{bmatrix} \beta - \beta_0 \\ T_g - T_{g,0} \end{bmatrix} \qquad v = \begin{bmatrix} v_t - v_m \end{bmatrix} \tag{2.50}
$$

$$
\dot{x} = Ax + Bu + B_v v \tag{2.51}
$$

Throughout simulations these measurements have been considered:

$$
y = \begin{bmatrix} P_e \\ \omega_r \\ \ddot{x}_t \end{bmatrix} \tag{2.52}
$$

The generated electrical power is calculated by expression in eq. 2.53. In this model we are neglecting the generator efficiency.

$$P_e = N_g T_g \omega_r \qquad (2.53)$$

The output matrix equation can be expressed as follows.

$$
\begin{bmatrix} P_e \\ \omega_r \\ \ddot{x}_t \end{bmatrix} =
\begin{bmatrix}
N_g T_{g,0} & 0 & 0 \\
1 & 0 & 0 \\
\frac{1}{M_t} \frac{\partial F_r}{\partial \omega_r}\Big|_{\omega_{r0}} & \frac{K_t}{M_t} & -\frac{D_t}{M_t} - \frac{1}{M_t} \frac{\partial F_t}{\partial v_r}\Big|_{v0}
\end{bmatrix}
\begin{bmatrix} \omega_r \\ x_t \\ \dot{x}_t \end{bmatrix} +
$$
$$
+ \begin{bmatrix} 0 & N_g \omega_{r,0} \\ 0 & 0 \\ 0 & 0 \end{bmatrix}
\begin{bmatrix} \beta \\ T_g \end{bmatrix} +
\begin{bmatrix} 0 \\ 0 \\ \frac{1}{M_t} \frac{\partial F_t}{\partial v_r}\Big|_{v0} \end{bmatrix} v
\qquad (2.54)
$$

Knowing the relation between tower for-aft acceleration and speed to be:

$$\dot{x}_t = \int \ddot{x}_t dt \qquad \ddot{x}_t(0) = 0 \qquad (2.55)$$

Based on equation 2.55 output part of the state space model can be simplified and rewritten into representation in 2.56, yielding 2.57. This simplification will prove to be useful in order to mitigate some tuning issues of the Kalman filter. However, if we are working with more advanced simulation software and only access to tower for-aft acceleration measurement is accessible, this approach still can be used. The only difference would be that we need to introduce an integrator before this signal is used in estimator.

$$
\begin{bmatrix} P_e \\ \omega_r \\ \dot{x}_t \end{bmatrix} =
\begin{bmatrix} N_g T_{g,0} & 0 & 0 \\ 1 & 0 & 0 \\ 0 & 0 & 1 \end{bmatrix}
\begin{bmatrix} \omega_r \\ x_t \\ \dot{x}_t \end{bmatrix} +
\begin{bmatrix} 0 & N_g \omega_{r,0} \\ 0 & 0 \\ 0 & 0 \end{bmatrix}
\begin{bmatrix} \beta \\ T_g \end{bmatrix} +
\begin{bmatrix} 0 \\ 0 \\ 0 \end{bmatrix} v +
\begin{bmatrix} P_{e,0} \\ \omega_{r,0} \\ 0 \end{bmatrix} \quad (2.56)
$$

$$y = Cx + Du + y_0 \qquad (2.57)$$

Once the state space model is introduced, stability analysis can be done. Table 2.1 shows eigenvalues of system matrix at certain wind speed. Eigenvalues in

C-Time and D-Time are presented. Sampling frequency has been chosen as $f_s = 10\ Hz$. Table shows eigenvalue for rotational speed state denoted as λ_{ω_r}, and eigenvalues for tower for-aft movement states denoted as λ_t.

Notice decreasing values of λ_{ω_r} with increasing wind speed (in both C-Time and D-Time). The eigenvalues related to tower movement are rising up to the 11 m/s, and then decreasing (C-Time). This is consistent with calculation of thrust force F_t, which is increasing up tp the critical wind speed (11.2 m/s) and then decreasing (fig. 2.12).

Table 2.1: Eigenvalues

wind speed	C-Time		D-Time	
	λ_{ω_r}	λ_t	λ_{ω_r}	λ_t
3	-0.0179	$-0.0683 \pm 1.9772i$	0.9982	$0.9738 \pm 0.1951i$
5	-0.0269	$-0.0789 \pm 1.9776i$	0.9973	$0.9728 \pm 0.1949i$
7	-0.0349	$-0.0922 \pm 1.9784i$	0.9965	$0.9715 \pm 0.1947i$
9	-0.0463	$-0.1118 \pm 1.9788i$	0.9954	$0.9696 \pm 0.1944i$
11	-0.0574	$-0.1156 \pm 1.9823i$	0.9943	$0.9691 \pm 0.1947i$
13	-0.0795	$-0.1122 \pm 1.9750i$	0.9921	$0.9696 \pm 0.1940i$
15	-0.1368	$-0.1109 \pm 1.9713i$	0.9864	$0.9698 \pm 0.1937i$
17	-0.2039	$-0.1098 \pm 1.9676i$	0.9798	$0.9700 \pm 0.1934i$
19	-0.2639	$-0.1087 \pm 1.9642i$	0.9740	$0.9702 \pm 0.1930i$
21	-0.3325	$-0.1076 \pm 1.9605i$	0.9673	$0.9703 \pm 0.1927i$
23	-0.4102	$-0.1056 \pm 1.9570i$	0.9598	$0.9706 \pm 0.1924i$
25	-0.4806	$-0.1032 \pm 1.9540i$	0.9531	$0.9709 \pm 0.1922i$

2.5   Step Responses

Evaluating step responses are vital in order to understand system behaviour. In control of wind turbine, two control inputs are considered pitch angle (β), generator torque (T_g) and wind speed (v), which is considered as disturbance. Step changes are made in all these inputs. Two sets of responses are considered. One in partial load, when the linearization point is set to 7 m/s, and in full load with linearization point 15 m/s. Throughout this project, pitch is considered as control input number 1 (u_1), and generator torque as input number 2 (u_2).

2.5.1   Partial Load Case

Figure 2.18 shows the step change profile applied to the system in partial load. Notice that, LTI model is not tracking the non-linear in case of rotational speed and power output (fig. 2.19(a)). This is caused by the fact, that the partial derivative of c_p with respect to pitch is zero in partial load (fig. 2.14). Notice, that this problem is not encountered in case tower for-aft movement (fig. 2.19(b)).

Based on this reason, that we cannot control rotational speed with pitch action, β is not considered as control input in partial, which leaves us only with generator torque as a control action in partial load (further explanation will be given in chapter 5).
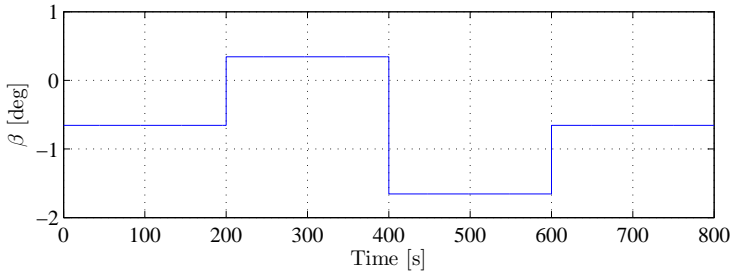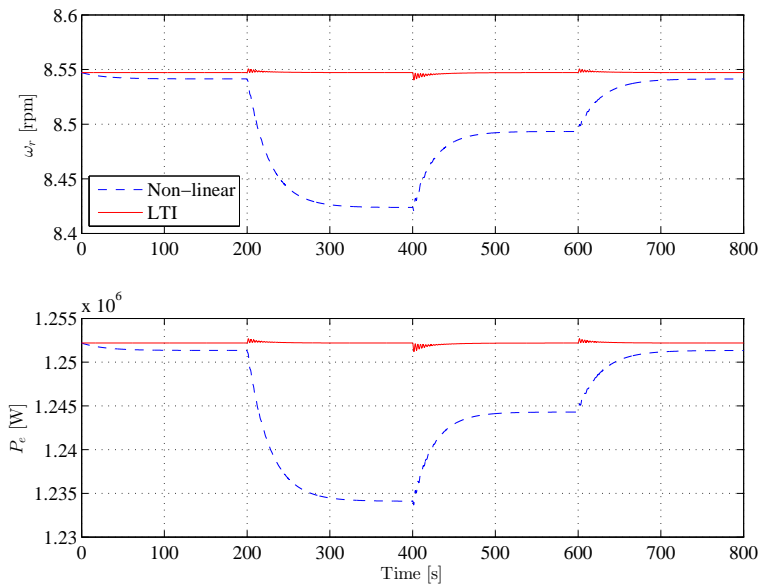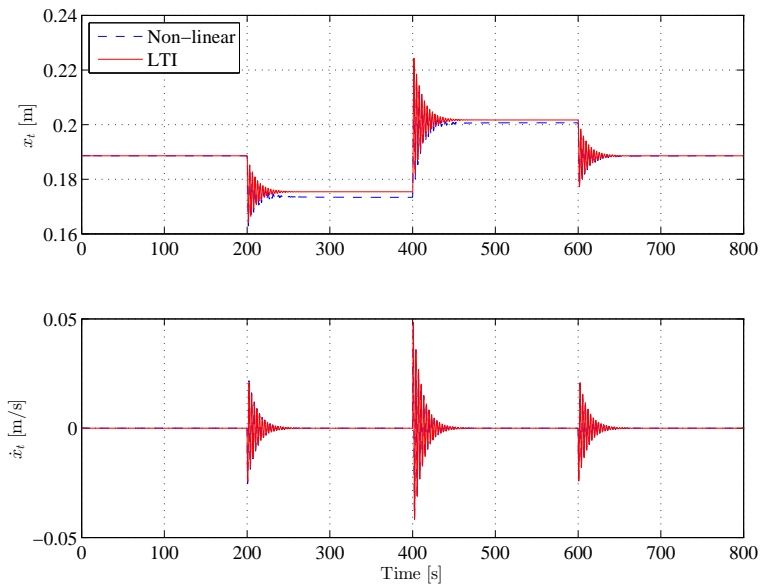

Figure 2.18: Step changes in pitch control action

(a) Measurements - P_e and ω_r

(b) Tower displacement x_t and speed of displacement $\dot{x}_t$

Figure 2.19: Response to change in pitch (β) control input (fig. 2.18)

When made step changes in generator torque input (2.20) or wind speed(2.21), LTI model and non-linear track themselves within acceptable margin. Notice the effect of the generator torque effect on electrical power (fig. 2.22(a)). This is caused by non-zero D matrix in the state space model. Since there is no direct relation between tower for-aft movement, changes in the tower displacement and speed of the tower displacement are very small (fig. 2.22(b)).
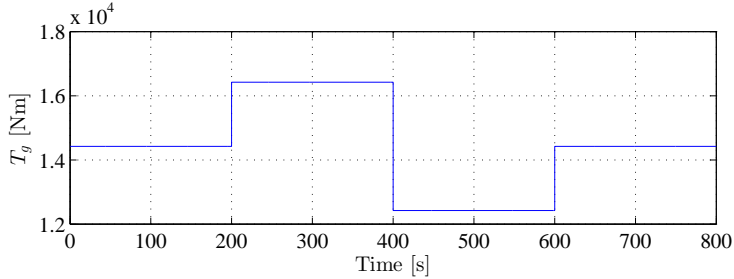
Figure 2.20: Step changes in generator torque control action
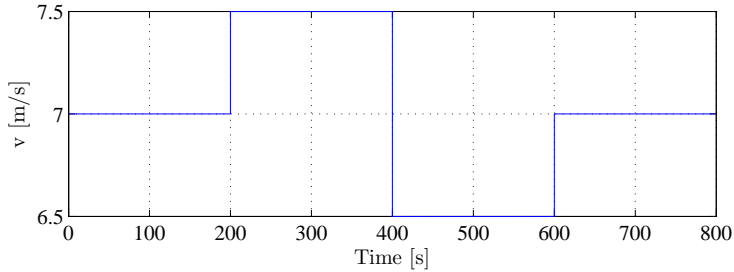
Figure 2.21: Step changes in wind speed

Response to step changes in the wind speed is shown in figure 2.23. Notice slow response of the rotational speed to the step in wind speed. Same response can be seen without any other influences on generated power, it will result only in different scale (fig. 2.23(a)). Differences between non-linear model and linear model are slightly increased, in tower for-aft movement, when harsh step change is made in wind speed at time $t = 200\ s$ (fig. 2.23(b)).
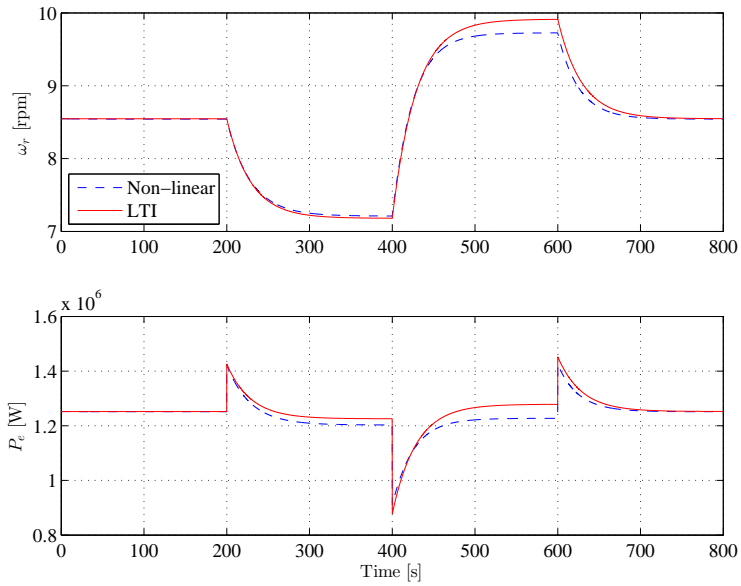
(a) Measurements - P_e and ω_r
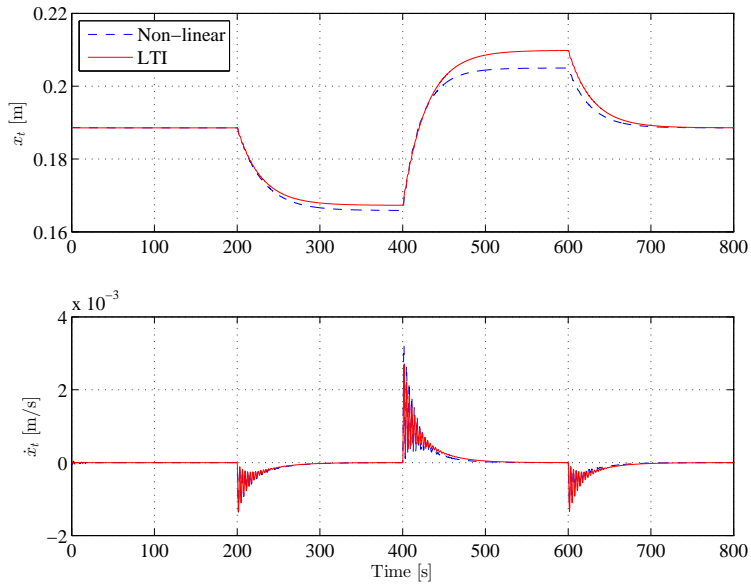
(b) Tower displacement x_t and speed of displacement $\dot{x}_t$

Figure 2.22: Response to step changes in generator torque input (fig. 2.20)

(a) Measurements - P_e and ω_r

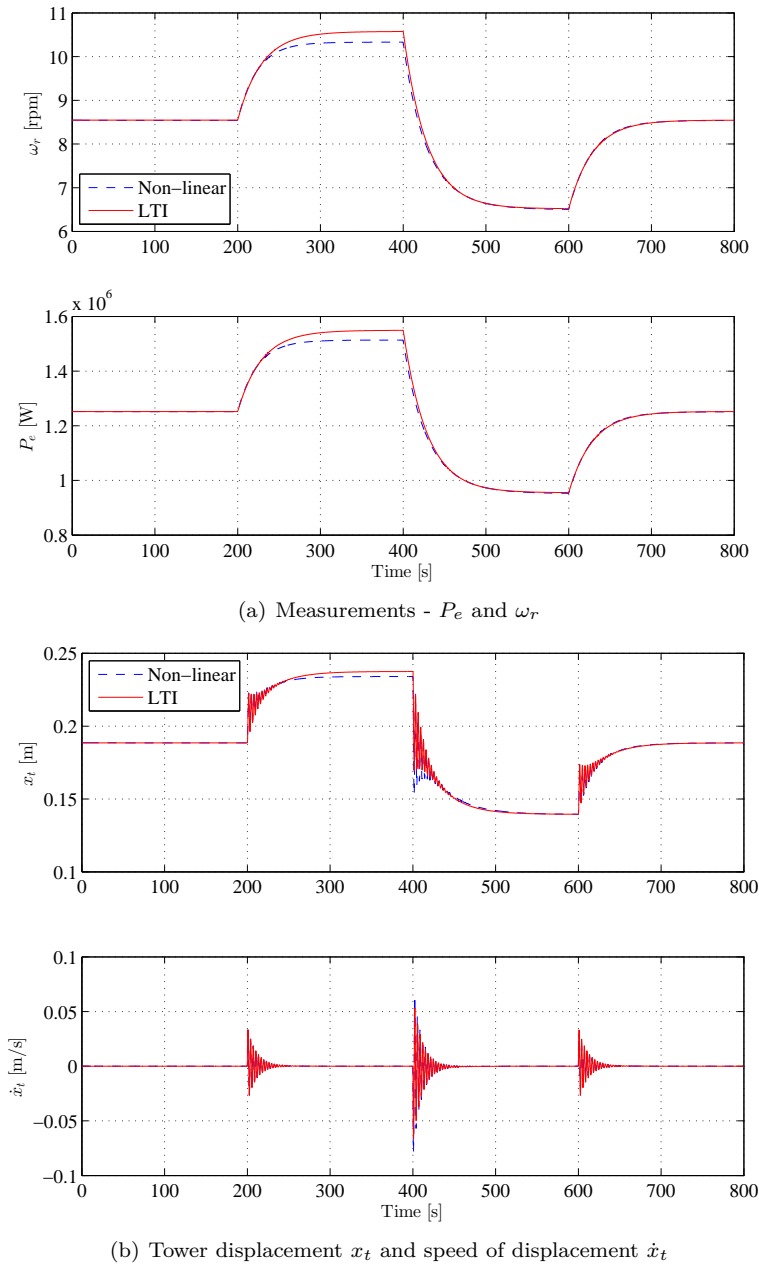(b) Tower displacement x_t and speed of displacement $\dot{x}_t$

Figure 2.23: Response to step changed in wind speed (fig. 2.21)

2.5.2   Full Load Case

At first step changes are considered in pitch input. Profile applied into system is shown on figure 2.24. Other inputs are naturally kept at their respective steady state values. Resulting responses are shown in figure 2.25. Contrary to the partial load case, when partial derivative of c_p with respect to pitch was zero, in full load, system is controllable by both control inputs (β and T_g).
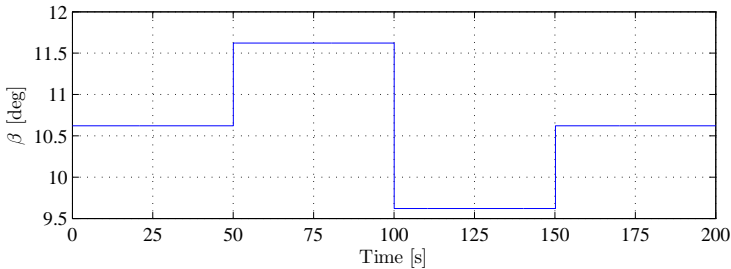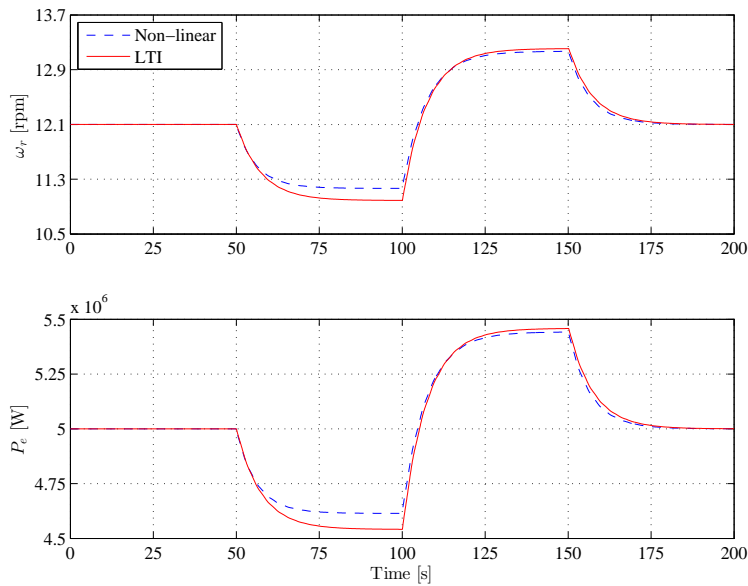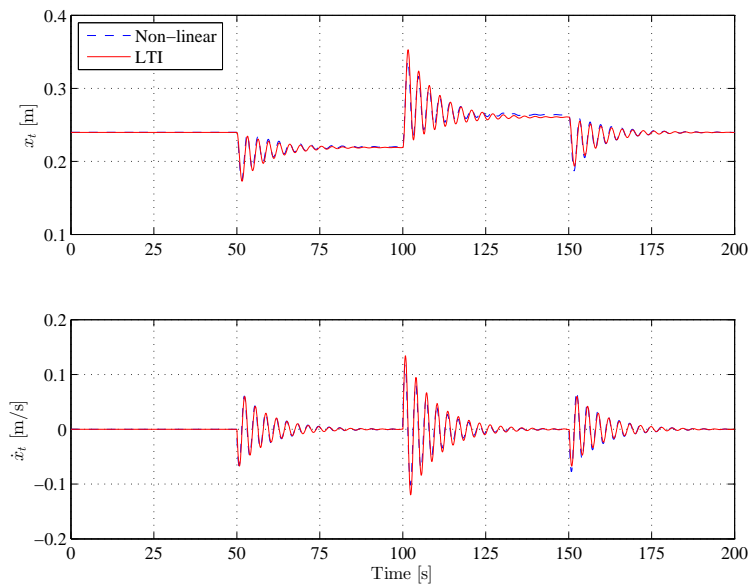

Figure 2.24: Step changes in pitch control action

Figure 2.25(a) shows the response of rotational speed and generated power. Notice that when making step change in positive way from stationary value, resulting difference in rotational, thus in power generation, speed between non-linear model and LTI model is larger (fig. 2.25(a)), compared when making step change in negative way. This behaviour is caused by non-linearities in $c_p(\lambda, \beta)$ curve.

Differences between LTI model and non-linear model in case of tower for-aft movement are very small (fig. 2.25(b)). This is expectable, because the model of tower for-aft movement is made linear. Only non-linearities in tower for-aft movement model arise from the thrust force F_t. But $c_t(\lambda, \beta)$ curve does not change rapidly in top region, which justify small differences between non-linear model and linear model in case of tower for-aft movement.

(a) Measurements - P_e and ω_r

(b) Tower displacement x_t and speed of displacement $\dot{x}_t$

Figure 2.25: Response to change in pitch (β) control input (fig. 2.24)

Second input taken into to consideration is generator torque. Step changes, which are applied to system are shown on figure 2.26. The relation between generator torque input and rotational speed is linear, so only small differences between non-linear model and LTI model are expected. Direct connection between generator torque input and power generator results in step response shown in figure 2.28(a). The tower for-aft movement is effected only by changes in the rotational speed, and by the generator torque directly, so small changes are occurring in tower for-aft displacement and speed of the displacement 2.28(b).
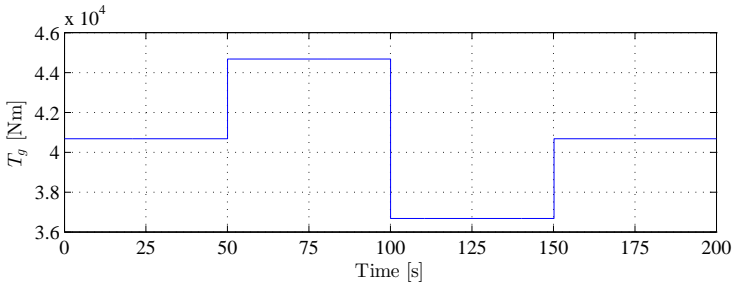

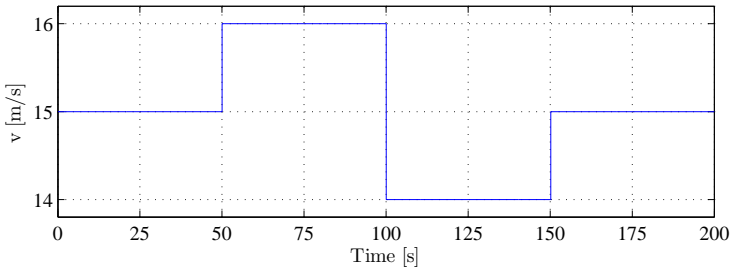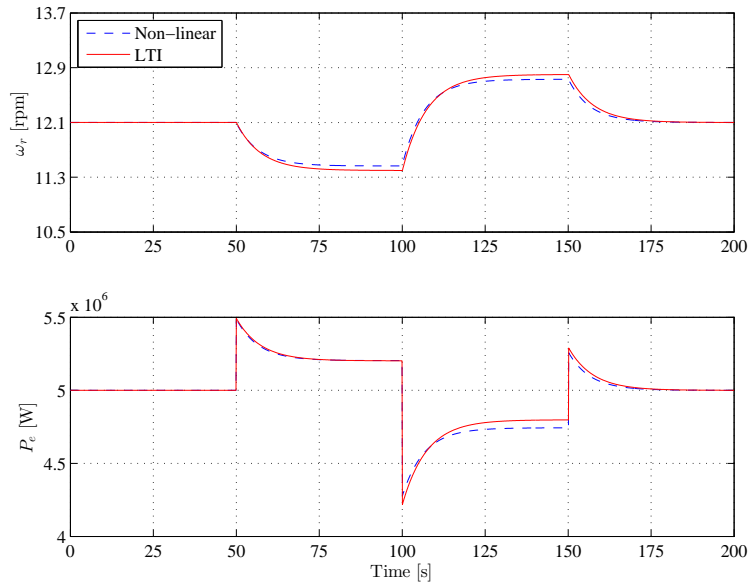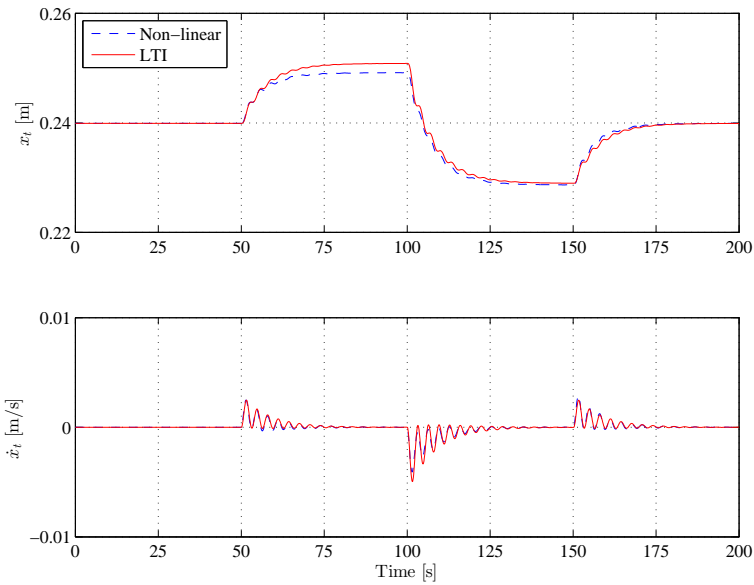**Figure 2.26:** Step changes in generator torque control action

Figure 2.27: Step changes in wind speed

Final set of figures shows the response to wind speed step change. The wind speed profile is shown in figure 2.27. Responses and displayed on figure 2.29.

(a) Measurements - P_e and ω_r

(b) Tower displacement x_t and speed of displacement $\dot{x}_t$

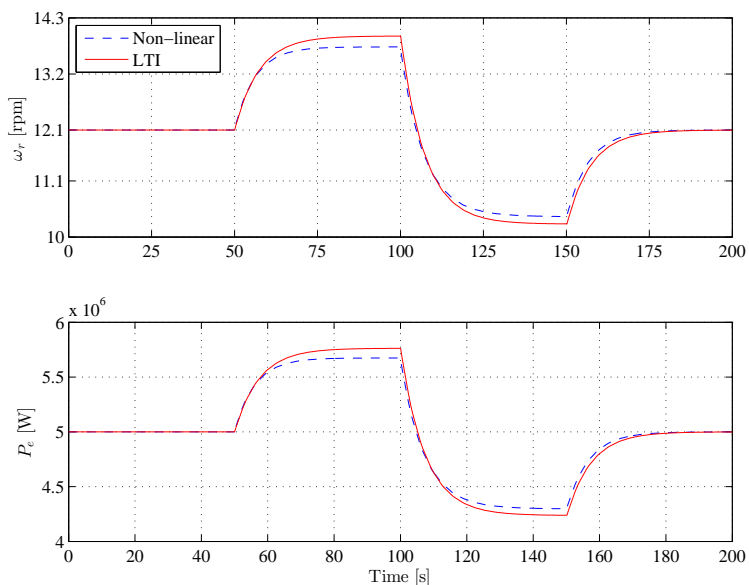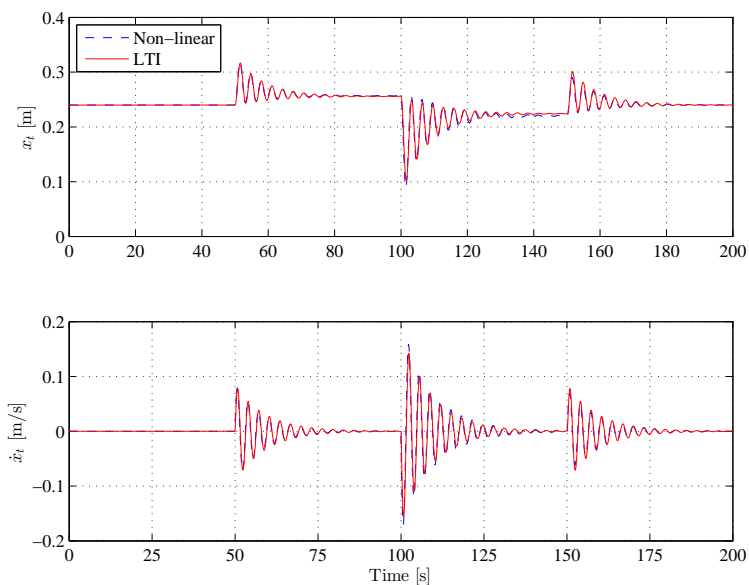**Figure 2.28:** Response to generator torque step change (fig. 2.26)

(a) Measurements - P_e and ω_r

(b) Tower displacement x_t and speed of displacement $\dot{x}_t$

Figure 2.29: Response to wind step changes (fig. 2.27)

Figure 2.30 shown the response of tower for-aft movement to step change in the
wind speed from 15 to 16 m/s. On this figure is compared structural damping
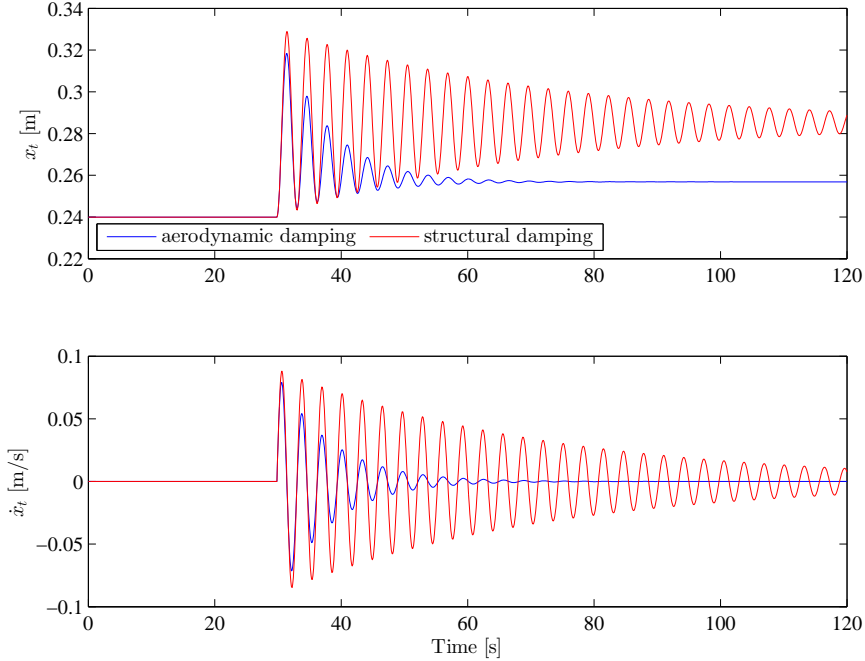of the tower together with aerodynamic damping.

**Figure 2.30:** Effect of aerodynamics to the tower for-aft movement

2.6 Frequency Responses

This thesis deals with design of frequency weighted MPC controller, for that
reason some frequency responses of the system are evaluated. Transfer function
from all inputs to all outputs and states are considered. Specifically from control
inputs β, T_g and from wind speed v to output P_e and states ω_r, x_t, $\dot{x}_t$. Notice,
that all responses have characteristics of low-pass filter except responses of the
transfer function $G_{T_g,P_e}(j\omega)$, which has high-pass characteristic. This is caused
by non-zero D matrix, in state space model.

More detailed frequency responses at all wind speeds can be found in appendix
B, in which 3D bode plots are made.
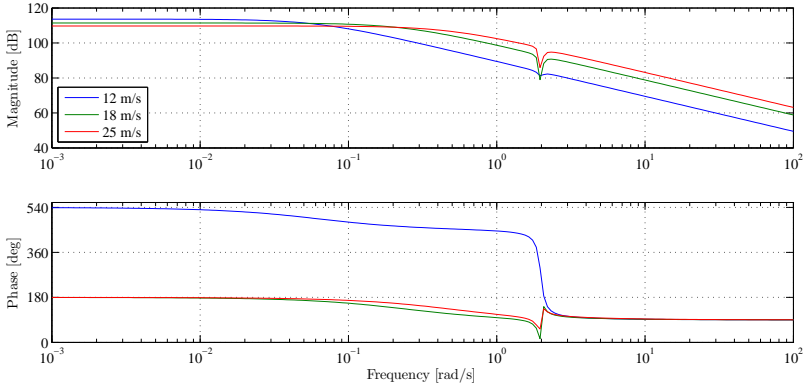
(a) $G_{\beta, P_e}(j\omega)$
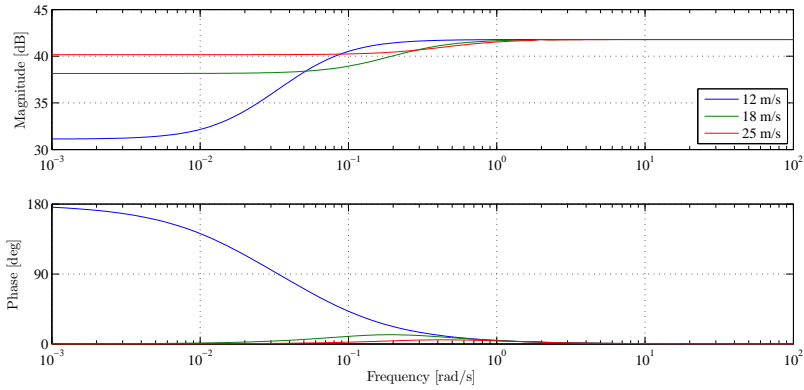
(b) $G_{T_g, P_e}(j\omega)$
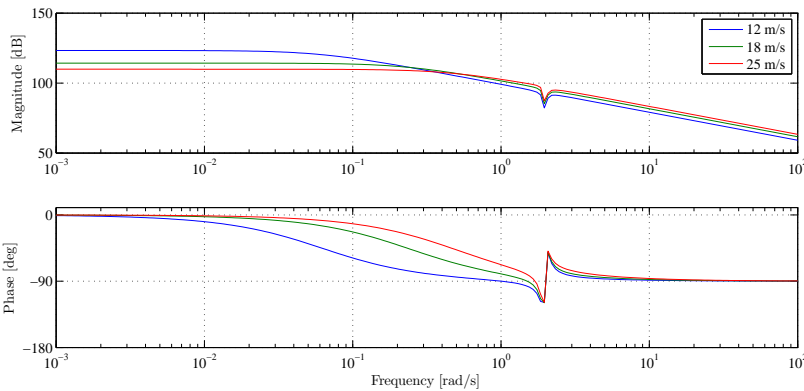
(c) $G_{v, P_e}(j\omega)$

Figure 2.31: Frequency response from inputs to generated power

(a) $G_{\beta,\omega_r}(j\omega)$

(b) $G_{T_g,\omega_r}(j\omega)$

(c) $G_{v,\omega_r}(j\omega)$

Figure 2.32: Frequency response from inputs to rotational speed
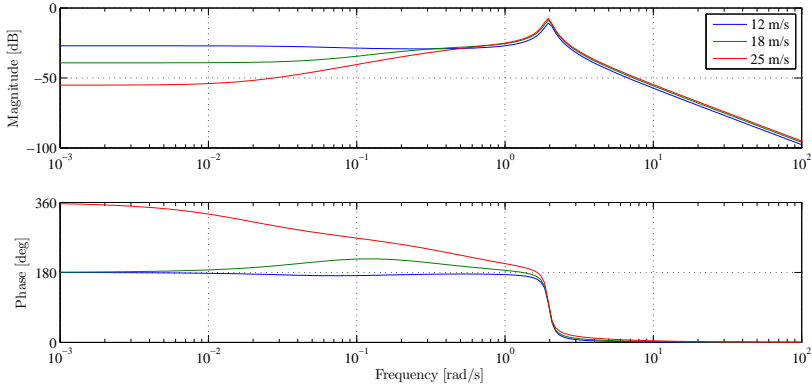
(a) $G_{\beta, x_t}(j\omega)$
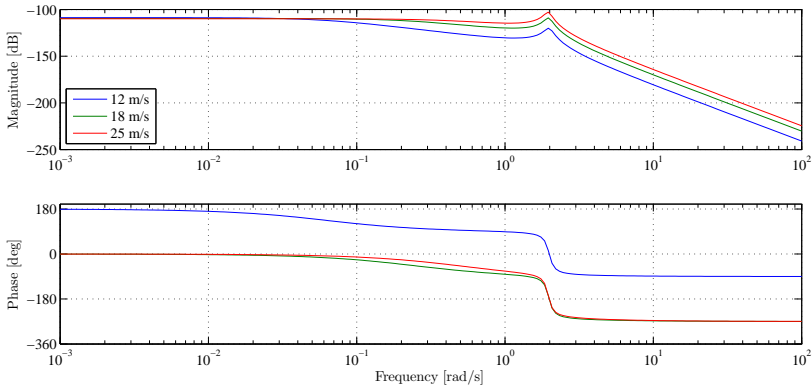
(b) $G_{T_g, x_t}(j\omega)$

(c) $G_{v, x_t}(j\omega)$

Figure 2.33: Frequency response from inputs to tower for-aft displacement
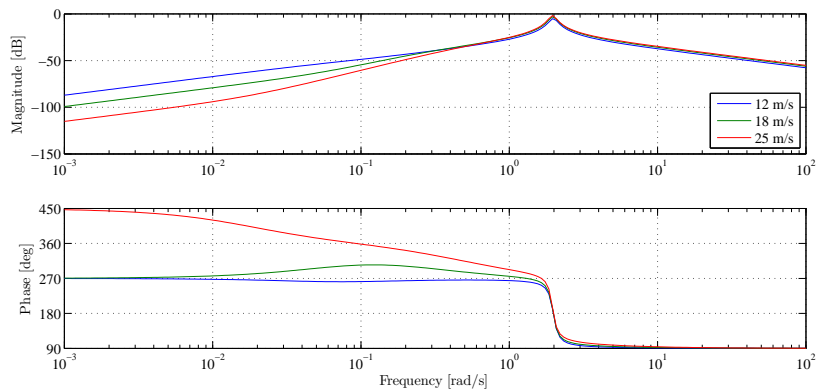
(a) $G_{\beta, \dot{x}_t}(j\omega)$
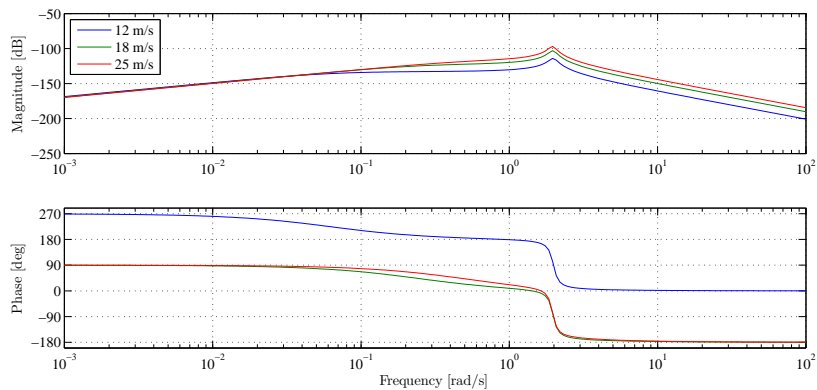
(b) $G_{T_g, \dot{x}_t}(j\omega)$
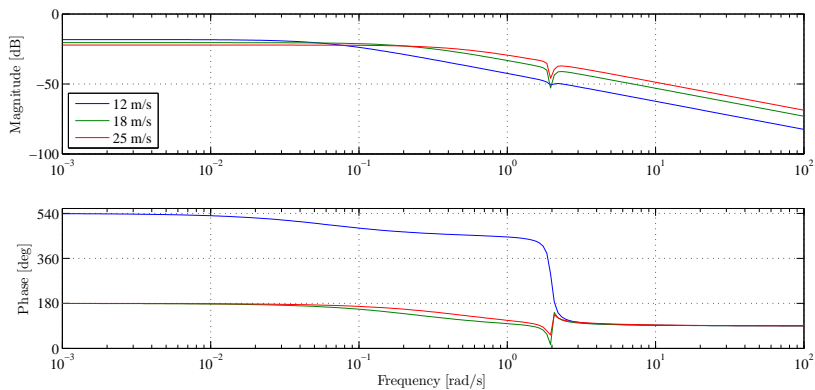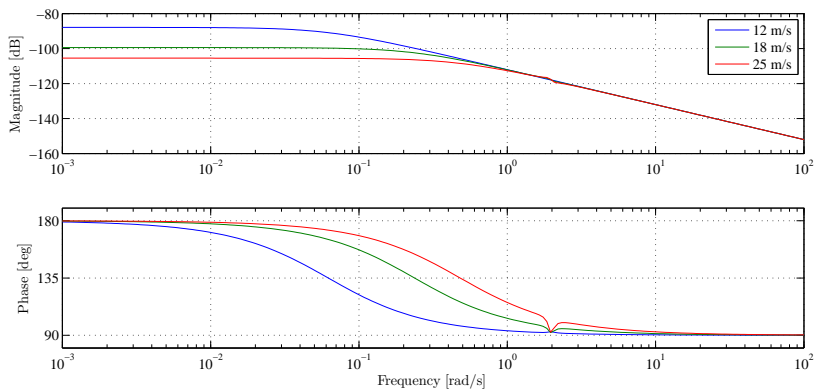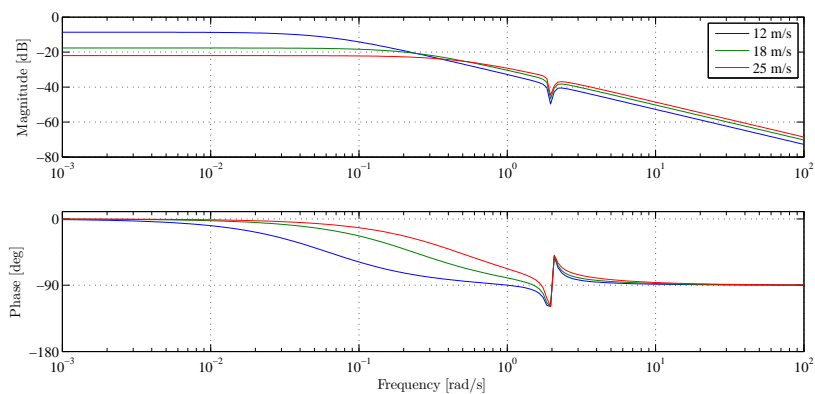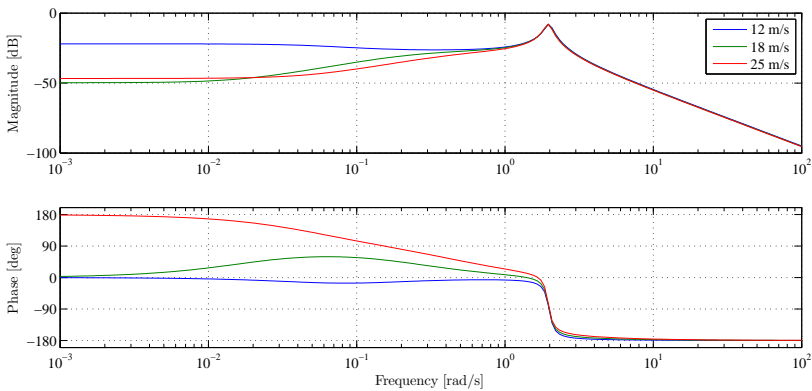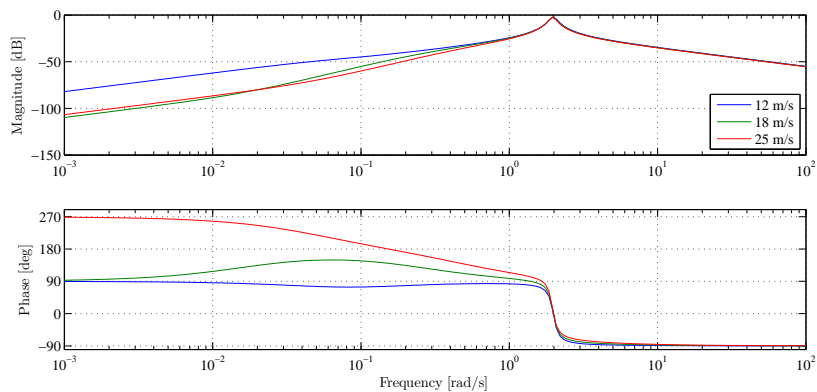

(c) $G_{v, \dot{x}_t}(j\omega)$

Figure 2.34: Frequency response from inputs to tower for-aft speed of displacement

CHAPTER 3

Wind Speed Estimation and Disturbance Modelling

Model Predictive Control is a state feedback control. This means, that estimation of the states is required. Since we are not measuring the wind speed, estimation of this quantity is required as well. Based on the estimation of the wind speed, linearisation point and system dynamics are changed. Last signals that needed to be estimated, are unmeasured input and output disturbances, so offset-free regulation is achieved.

3.1 Wind Speed Estimation

In real world application, where the wind speed is varying throughout rotor disc, it is difficult to measure reliably the wind speed. Due to this fact, the wind turbine itself serves as a measurement device of the wind speed. Several methods has been proposed how to achieve satisfactory wind speed estimation. Very common approach is to use stationary Kalman filter, like proposed in (Xin et al., 1997). Approach proposed by (Bourlis and Bleijs, 2010), demonstrates usage of adaptive Kalman filter. Another approach presented by (Østergaard et al., 2007) is to use Kalman filter to estimate rotor speed and aerodynamic torque, and using equation 3.1 to calculate λ. Once λ is known, wind speed can

be easily calculated. This concept proven to be working without any problems only in wind speed range from 10 to 14 m/s. At other wind speed numerical difficulties arise during solving equation 3.1 for λ, and also the fact, that c_p curve is concave, which means that for two different λ values, same c_p value is calculated.

$$Q_r \omega_R = \frac{1}{2} \rho \pi R^2 \frac{R^3 \omega_r^3}{\lambda^3} c_p(\lambda, \beta) \tag{3.1}$$

In this project very well known stationary predictive Kalman filter (Poulsen, 2007) has been used in order to estimate the wind speed. Satisfactory results have been obtain using this strategy.

3.2   Disturbance Modelling

Disturbance modelling has proven to be very effective in order to estimate unmeasured disturbances and mismatch between linear and non-linear model. Once these disturbances are estimated, MPC algorithm can be easily modified, so these disturbances are rejected (Pannocchia and Rawlings, 2003).

The main idea behind this approach, is to augment discrete time state space model (eq. 3.2) with number of integrating disturbances. Specially in our case we have to take to account the estimation of the wind speed as well. Based on this augmented system description predictive Kalman filter is designed.

Original state space description in discrete time:

$$x_{k+1} = Ax_k + Bu_k + B_v v_k + E_x d_k + \gamma_k \tag{3.2}$$
$$y_k = Cx_k + Du_k + E_y d_k + \eta_k \tag{3.3}$$

where x_k are the state variables at given sample k, u_k is the control input vector. v_k is the wind speed, d_k are unmeasured disturbances, γ and η are process and measurement noise.

Statistical characteristics of the noise variables are:

$$\gamma \in N_{iid}(0, Q_e) \qquad \eta \in N_{iid}(0, R_e) \tag{3.4}$$

Considered state variables in the augmented system (eq. 3.6) are, $\hat{x}$ denotes state variables of original system state space description, $\hat{x}_v$ are state variables linked to wind speed model, and $\hat{d}$ are estimated disturbances.

$$\begin{bmatrix} \hat{x} \\ \hat{x}_v \\ \hat{d} \end{bmatrix}_{k+1} = \begin{bmatrix} A & B_v & E_x \\ 0 & A_w & 0 \\ 0 & 0 & I \end{bmatrix} \begin{bmatrix} \hat{x} \\ \hat{x}_v \\ \hat{d} \end{bmatrix}_k + \begin{bmatrix} B \\ 0 \\ 0 \end{bmatrix} u_k + \gamma_k \tag{3.5a}$$

$$\hat{y}_k = \begin{bmatrix} C & 0 & E_y \end{bmatrix} \begin{bmatrix} \hat{x} \\ \hat{x}_v \\ \hat{d} \end{bmatrix}_k + Du_k + \eta_k \tag{3.5b}$$

yielding:

$$\hat{\mathbf{x}}_{k+1} = A_e \hat{\mathbf{x}}_k + B_e u_k + \gamma_k \tag{3.6a}$$
$$y = C_e \hat{\mathbf{x}}_k + Du_k + \eta_k \tag{3.6b}$$

The estimation takes place as follows:

$$\begin{bmatrix} \hat{x} \\ \hat{x}_v \\ \hat{d} \end{bmatrix}_{k|k} = \begin{bmatrix} \hat{x} \\ \hat{x}_v \\ \hat{d} \end{bmatrix}_{k|k-1} + \triangle \mathbf{x}^s + L \left(y_m - \hat{y}_{k|k-1} \right) \tag{3.7}$$

where $\triangle \mathbf{x}^s$ is the difference between steady state values of the states 3.8. Value of $\triangle \mathbf{x}^s$ will remain zero, when the linearisation point does not change. In the case of steady values of wind speed model, only steady state value of the first state variable is non-zero. The steady state value of the second state in wind speed model as well as the disturbances has steady state values equal to zero.

$$\triangle \mathbf{x}^s = \begin{bmatrix} \begin{bmatrix} x_{k-1}^s - x_k^s \\ v_{m,k-1} - v_{m,k} \end{bmatrix} \\ 0 \\ 0 \end{bmatrix} \tag{3.8}$$

This correction has to be made, because the system dynamics together with linearisation point needs to be changed during control. This will ensure, that when the system dynamics changes, that the estimator will give the same result. Block diagram of the observer is shown on figure 3.1.

The prediction part of the estimator is described in following equation:

$$
\begin{bmatrix} \hat{x} \\ \hat{x}_v \\ \hat{d} \end{bmatrix}_{k+1|k} = \begin{bmatrix} A & B_v & E_x \\ 0 & A_w & 0 \\ 0 & 0 & I \end{bmatrix} \begin{bmatrix} \hat{x} \\ \hat{x}_v \\ \hat{d} \end{bmatrix}_{k|k} + \begin{bmatrix} B \\ 0 \\ 0 \end{bmatrix} u_{k|k} \tag{3.9a}
$$

$$
\hat{y}_k = \begin{bmatrix} C & 0 & E_y \end{bmatrix} \begin{bmatrix} \hat{x} \\ \hat{x}_v \\ \hat{d} \end{bmatrix}_{k|k} + Du_{k|k} \tag{3.9b}
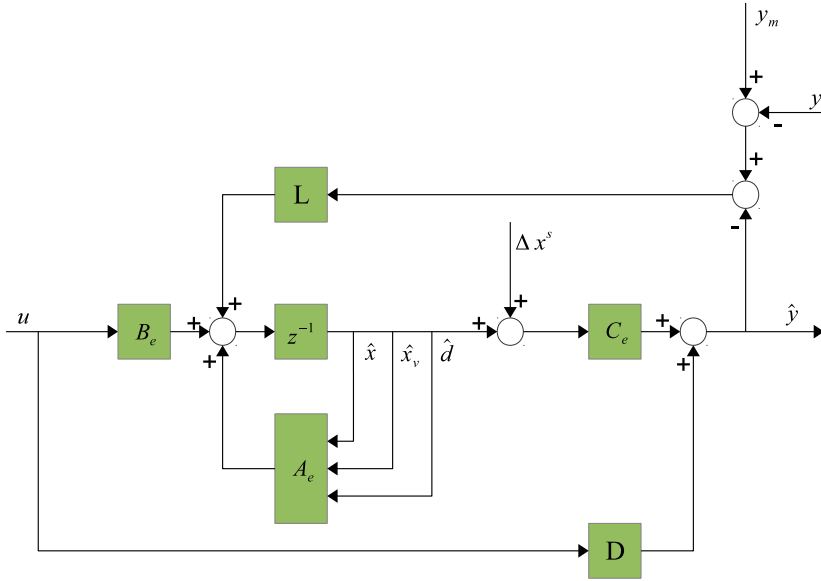$$

Figure 3.1: Structure of the linear observer

Predictor gain matrix is calculated from 3.10, which preceded by solving algebraic Riccati equation in discrete time 3.11.

$$
L = A_e \Sigma C^T (C \Sigma C^T + R)^{-1} \tag{3.10}
$$

$$
\Sigma = A_e \Sigma A_e^T + Q - A_e \Sigma C^T (C \Sigma C^T + R)^{-1} C \Sigma A_e^T \tag{3.11}
$$

CHAPTER 4

Model Predictive Control

4.1 Standard MPC

The core of MPC lies in solving quadratic objective function with linear constraints. Such mathematical problem is called quadratic programming (QP). In general, QP program can be expressed in following form (Boyd and Vandenberghe, 2009):

$$\text{minimize} \quad \frac{1}{2}v^T H v + g^T v + r \tag{4.1a}$$

$$\text{s. t.} \quad Cv \preceq d \tag{4.1b}$$

$$Av = b \tag{4.1c}$$

where $H \in \mathbb{S}^n$, $C \in \mathbb{R}^{m \times n}$, $A \in \mathbb{R}^{p \times n}$. In this section we will focus on formulating the control problem as a standard MPC problem, which we will translate into QP formulation.

Writing the cost function with the constraints is big part of the MPC implementation. There are several ways how approach this problem and it also depend on the application. In this thesis output regulation with constraints is considered, and the optimizing variable will be the control input vector.

There are however several other approaches. Widely used is formulation, where

the optimization variable is control move ($\triangle u = u_k - u_{k-1}$) instead of absolute value of control signal (u_k) (Maciejowski, 2002; Camacho and Bordons, 2007; Gosk, 2011). Another formulation arise by directly looking at the basic formulation (equation 4.2a) and treat both state variables and control input variables as optimization variables (Kvasnica, 2009). This formulation has one drawback because we increase the number of optimizing variables, but advantage could be sparsity of curvature matrix (matrix H from 4.1a), which in this case is diagonal. In previously mentioned approach, where the optimization variable is control input vector, or control move vector, the curvature matrix is dense. This may increase the time needed for calculation, due to the fact, that during solving QP problem this matrix must be inverted. Another formulation which is currently being researched, is that the control input vector is eliminated from the cost function and only state variables are considered as optimizing variables (Mancuso and Kerrigan, 2011).

General formulation of standard MPC problem with linear constraints is shown in eq. 4.2a. State space model represents the equality constraints. Bounds on control inputs together with bounds on states represent the inequality constraints.

$$\Phi \qquad = \min \sum_{k=1}^{N} x^T Q x + \sum_{k=1}^{N-1} u^T R u \qquad (4.2a)$$

$$s.t. \qquad x_{k+1} = A x_k + B u_k \qquad (4.2b)$$

$$x \in \mathbb{X} \qquad (4.2c)$$

$$u \in \mathbb{U} \qquad (4.2d)$$

where N is prediction horizon, $Q \in \mathbb{R}^{n_x \times n_x}, R \in \mathbb{R}^{n_u \times n_u}$ are weighting matrices. Presented formulation has several drawbacks, and it is not suited for great portion of applications. The main issue is, that using cost function written in 4.2a deviations of x, u from zero is penalized. This cannot be used for offset free control unless changes are made. One of many possibilities is to introduce target variables (Muske and Rawlings, 1993), so the cost function will be changed in following manner:

$$\Phi = \min \sum_{k=1}^{N} (x - x_s)^T Q (x - x_s) + \sum_{k=1}^{N-1} (u - u_s)^T R (u - u_s) \qquad (4.3)$$

Where x_s, u_s are steady state values. In the section (4.1.1) will be introduced another approach to handle offset free control along with QP formulation based on control vector as an optimization variable.

As it can be understood from the presented equations, by solving QP problem we calculate the optimal control inputs over the prediction horizon. Once these

inputs are applied to the plant, states of the plant are moved to different values. Such application resembles open-loop implementation. However for satisfactory results and offset free control, closed-loop implementation is chosen. In closed-loop application the optimization is performed at each sample, with new initial condition ($x_0 = x_k$). In most applications the length of the horizon is preserved. Such control strategy is known as *receding horizon control* (RHC). RHC implementation has been widely researched (e.g. (Maciejowski, 2002)) and used in various industrial implementation i.e. (Prasath et al., 2010).

Output regulation problem formulated in 4.4 together with disturbance modelling (previous chapter) will achieve offset free reference tracking.

$$\Phi = \frac{1}{2} \sum_{k=0}^{N} ||r_k - y_k||_Q^2 + \frac{1}{2} \sum_{k=0}^{N-1} ||\triangle u_k||_R^2 \qquad (4.4)$$

Where r_k is the reference value for the output and y_k is the measurement of the output. This objective function will suppress the changes in the control signal $\triangle u_k$. It will have no bearing on the difference between absolute value of the control input and zero like in formulation 4.2a.

4.1.1 Unconstrained MPC

In this section, unconstrained MPC controller will be presented. In order to solve optimization problem expressed in 4.4, this objective function must be rewritten into form presented in 4.1a. As it was mentioned in begging of this chapter, the optimization variable will be the control inputs U over the chosen prediction horizon.

For the purpose of rewriting the MPC cost function into standard QP problem, relation between the outputs y_k and inputs u_k must be known. Evolution based in state space model will be used (eq. 4.5).

$$
\begin{align}
x_{k+1} &= Ax_k + Bu_k + E_x d_k & k = 0..N \qquad &(4.5a) \\
y_k &= Cx_k + Du_k + E_y d_k & k = 0..N \qquad &(4.5b)
\end{align}
$$

Contrary to the suggested set-up in e.g. (Maciejowski, 2002), D matrix must be considered in MPC design for wind turbines as well.

QP problem which is formulated can be expressed as a weighted least square quadratic optimization problem 4.6, in which $U^\star$ is the optimal solution to the problem. In this case weighting matrix is related to outputs; $Q \in \mathbb{R}^{n_y \times n_y}$

$$U^\star = \min \quad \frac{1}{2}||Y - R||_Q^2 + \frac{1}{2}||\triangle U||_R^2 \tag{4.6}$$

This cost function can be then translated into standard QP problem shown in 4.7 by exploiting the evolution of the outputs over the prediction horizon based on state space model (eq. 4.8 through 4.13). Model without disturbances d is considered first.

$$U^\star = \min \quad \frac{1}{2}U^T H U + g^T U + r \tag{4.7}$$

State space evolution for sample $k = 1$:

$$x_{k+1} = Ax_k + Bu_k \tag{4.8}$$
$$y_k = Cx_k + Du_k \tag{4.9}$$

State space evolution for sample $k = 2$:

$$\begin{aligned} x_{k+2} &= Ax_{k+1} + Bu_{k+1} \\ &= A(Ax_k + Bu_k) + Bu_{k+1} \\ &= A^2 x_k + ABu_k + Bu_{k+1} \end{aligned} \tag{4.10}$$

$$\begin{aligned} y_{k+1} &= Cx_{k+1} + Du_{k+1} \\ &= C(Ax_k + Bu_k) + Du_{k+1} \\ &= CAx_k + CBu_k + Du_{k+1} \end{aligned} \tag{4.11}$$

State space evolution for sample $k = 3$:

$$\begin{aligned} x_{k+3} &= Ax_{k+2} + Bu_{k+2} \\ &= A(A^2 x_k + ABu_k + Bu_{k+1}) + Bu_{k+1} \\ &= A^3 x_k + A^2 Bu_k + ABu_{k+1} + Bu_{k+2} \end{aligned} \tag{4.12}$$

$$\begin{aligned} y_{k+2} &= Cx_{k+2} + Du_{k+2} \\ &= C(A^2 x_k + ABu_k + Bu_{k+1}) + Du_{k+2} \\ &= CA^2 x_k + CABu_k + CBu_{k+1} + Du_{k+2} \end{aligned} \tag{4.13}$$

Based on equations 4.8, 4.11 and 4.13 matrix form of prediction equation is expressed (eq. 4.14).

$$Y = \Psi x_k + \Gamma U \tag{4.14}$$

in which:

$$U = \begin{bmatrix} u_k \\ u_{k+1} \\ u_{k+2} \\ u_{k+3} \\ \vdots \\ u_{k+N-1} \end{bmatrix} \qquad Y = \begin{bmatrix} y_k \\ y_{k+1} \\ y_{k+2} \\ y_{k+3} \\ \vdots \\ y_{k+N-1} \end{bmatrix} \tag{4.15}$$

$$\Psi = \begin{bmatrix} C \\ CA \\ CA^2 \\ CA^3 \\ \vdots \\ CA^{N-1} \end{bmatrix} \tag{4.16}$$

$$\Gamma = \begin{bmatrix} D & 0 & 0 & 0 & \cdots & 0 \\ CB & D & 0 & 0 & \cdots & 0 \\ CAB & CB & D & 0 & \cdots & 0 \\ CA^2B & CAB & CB & D & \ddots & 0 \\ \vdots & \ddots & \ddots & \ddots & \ddots & 0 \\ CA^{N-2}B & CA^{N-3}B & CA^{N-4}B & \cdots & CAB & D \end{bmatrix} \tag{4.17}$$

Where $\Psi \in \mathbb{R}^{Nn_u \times n_x}$

Control moves are defined as was previously mentioned as $\triangle u_k = u_k - u_{k-1}$. Using this definition, vector form of control moves over the control horizon is written:

$$\begin{bmatrix} \triangle u_k \\ \triangle u_{k+1} \\ \triangle u_{k+2} \\ \vdots \\ \triangle u_{k+N-1} \end{bmatrix} = \begin{bmatrix} u_k - u_{k-1} \\ u_{k+1} - u_k \\ u_{k+2} - u_{k+1} \\ \vdots \\ u_{k+N-1} - u_{k+N-2} \end{bmatrix} \tag{4.18}$$

$$
\begin{bmatrix}
\triangle u_k \\
\triangle u_{k+1} \\
\triangle u_{k+2} \\
\vdots \\
\triangle u_{k+N-1}
\end{bmatrix}
=
\begin{bmatrix}
I_u & 0 & 0 & 0 & 0 \\
-I_u & I_u & 0 & 0 & 0 \\
0 & -I_u & I_u & 0 & 0 \\
0 & 0 & \ddots & \ddots & 0 \\
0 & 0 & 0 & -I_u & I_u
\end{bmatrix}
\begin{bmatrix}
u_k \\
u_{k+1} \\
u_{k+2} \\
\vdots \\
u_{k+N-1}
\end{bmatrix}
-
\begin{bmatrix}
I_u \\
0 \\
0 \\
\vdots \\
0
\end{bmatrix}
u_{k-1}
\quad (4.19)
$$

where $I_u \in \mathbb{I}^{n_u \times n_u}$.

$$
\triangle U = \Lambda U - I_{1,u} u_{k-1} \tag{4.20}
$$

By determining all matrices and vector, standard QP problem is formulated as it was suggested in (Jørgensen, 2011; Muske and Rawlings, 1993). For the purpose of simplifying notation we will write:

$$
U^\star = \min \ \left(\frac{1}{2}||R - Y||_Q^2 + \frac{1}{2}||\triangle U||_R^2 \right) = \min \ (\Phi_Y + \Phi_U) \tag{4.21}
$$

$$
Y - R = (\Gamma U + \Phi x_k) - R = \Gamma U - (R - \Phi x_k) = \Gamma U - c \tag{4.22}
$$

$$
\begin{aligned}
\Phi_Y &= \frac{1}{2}||Y - R||_Q^2 = \\
&= \frac{1}{2}||\Gamma U - c||_Q^2 = \\
&= \frac{1}{2}(\Gamma U - c)^T Q (\Gamma U - c) = \\
&= \frac{1}{2}U^T \Gamma^T Q \Gamma U - (\Gamma^T Q c)^T U + \frac{1}{2}c^T Q c
\end{aligned} \tag{4.23}
$$

$$
\begin{aligned}
\Phi_U &= \frac{1}{2}||\triangle U||_R^2 = \\
&= \frac{1}{2}||\Lambda U - I_{1,u} u_{k-1}||_R^2 = \\
&= \frac{1}{2}(\Lambda U - I_{1,u} u_{k-1})^T Q (\Lambda U - I_{1,u} u_{k-1}) = \\
&= \frac{1}{2}U^T \Lambda^T R \Lambda U - (\Lambda^T R I_{1,u} u_{k-1})^T U
\end{aligned} \tag{4.24}
$$

$$H = \Gamma^T Q \Gamma + \Lambda^T R \Lambda \tag{4.25}$$

$$\begin{aligned} g &= -\Gamma^T Q c - \Lambda^T R I_{1,u} u_{k-1} = \\ &= -\Gamma^T Q (R - \Phi x_k) - \Lambda^T R I_{1,u} u_{k-1} = \\ &= \Gamma^T Q R + \Gamma^T \Phi x_k - \Lambda^T R I_{1,u} u_{k-1} \end{aligned} \tag{4.26}$$

Equations 4.25 and 4.26 define curvature matrix H and first order coefficient vector g. In order to achieve offset free control, disturbances must be taken into account. In order to this, relation between outputs y and disturbances d is found. This is done similarly to finding relation between outputs and inputs. Equation 4.28 shows the matrix form of prediction equation, in which are included states, control inputs and disturbances.

$$\Gamma_D = \begin{bmatrix} E_y & 0 & 0 & 0 & \cdots & 0 \\ CE_x & E_y & 0 & 0 & \cdots & 0 \\ CAE_x & CE_x & E_y & 0 & \cdots & 0 \\ CA^2 E_x & CAE_x & CE_x & E_y & \ddots & 0 \\ \vdots & \ddots & \ddots & \ddots & \ddots & 0 \\ CA^{N-2} E_x & CA^{N-3} E_x & CA^{N-4} E_x & \cdots & CAE_x & E_y \end{bmatrix} \tag{4.27}$$

$$Y = \Psi x_k + \Gamma U + \Gamma_D D \tag{4.28}$$

This equation is then inserted into equation 4.22, yielding equation 4.29. By continuing derivation like it was presented in eq. 4.24 through 4.26. The curvature matrix H will remain unchanged, but the g vector will be change accordingly (eq. 4.30).

$$Y - R = (\Psi x_k + \Gamma U + \Gamma_D D) - R = \Gamma U - (R - \Phi x_k - \Gamma_D D) = \Gamma U - c \tag{4.29}$$

$$g = \Gamma^T Q R + \Gamma^T Q \Phi x_k - \Lambda^T R I_{1,u} u_{k-1} + \Gamma^T Q \Gamma_D D \tag{4.30}$$

For the purpose of simplifying notation, equation 4.30 is rewritten into:

$$g = M_R R + M_x x_k + M_u u_{k-1} + M_D D \qquad (4.31)$$

Final formulation presented in eq. 4.32 can be solved by numerous algorithms e.g. active-set algorithms (Nocedal and Wright, 1999). The tools solving QP problems used in this project were namely `quadprog()` in MATLAB and faster version of QP solver `qpas()` (Wills, 2007).

$$U^{star} = \min \quad \frac{1}{2} U^T H U + g^T U \qquad (4.32)$$

4.1.2 Hard Constraints

The main advantage of MPC is to handle constraints. Incorporating constraints into main QP problem is done as it is suggested in 4.1a. These constraints have form of linear inequality equations 4.33. In this section we will present the formulation of hard constraints on control inputs u, control moves $\triangle u$ and outputs y. Since we are dealing with stable system, constraints on system states may not be considered. However, if MPC is used on unstable process, then constraints on states should be considered.

$$
\begin{array}{ccccccl}
u_{min} & \leq & u_k & \leq & u_{max} & \qquad k = 0..N-1 \\
\triangle u_{min} & \leq & \triangle u_k & \leq & \triangle u_{max} & \qquad k = 0..N-1 \\
y_{min} & \leq & y_k & \leq & y_{max} & \qquad k = 0..N
\end{array} \qquad (4.33)
$$

Constraints presented in 4.33 must be rewritten into matrix form. The bounds on control signal are just stacked like in 4.34. Using definition of Λ matrix from eq. 4.20, matrix form of inequality constraints for control moves are expressed in eq. 4.35 yielding 4.36.

$$
U_{\min} = \begin{bmatrix} u_{\min} \\ u_{\min} \\ \vdots \\ u_{\min} \end{bmatrix}
\qquad\qquad
U_{\max} = \begin{bmatrix} u_{\max} \\ u_{\max} \\ \vdots \\ u_{\max} \end{bmatrix}
\qquad (4.34)
$$

$$
\begin{bmatrix} \triangle u_{\min} + u_{k-1} \\ \triangle u_{\min} \\ \vdots \\ \triangle u_{\min} \end{bmatrix} \leq \Lambda U \leq \begin{bmatrix} \triangle u_{\max} + u_{k-1} \\ \triangle u_{\max} \\ \vdots \\ \triangle u_{\max} \end{bmatrix} \tag{4.35}
$$

$$
\triangle U_{\min} + I_{1,u} u_{k-1} \leq \Lambda U \leq \triangle U_{\max} + I_{1,u} u_{k-1} \tag{4.36}
$$

Next formulation of output constraints is going to take place (eq. 4.37 and 4.38). Relation between matrix form of output and control inputs is used (eq. 4.28). Bounds on outputs $Y_{\min}$ and $Y_{\max}$ are created similarly as bound on inputs (eq. 4.34).

$$
Y_{\min} \leq \Psi x_k + \Gamma U + \Gamma_D D \leq Y_{\max} \tag{4.37}
$$

$$
Y_{\min} - (\Psi x_k + \Gamma_D D) \leq \Gamma U \leq Y_{\max} - (\Psi x_k + \Gamma_D D) \tag{4.38}
$$

Constraints defined in equations 4.36 and 4.38 can be put together resulting in 4.39.

$$
\begin{bmatrix} \triangle U_{\min} + I_{1,u} u_{k-1} \\ Y_{\min} - (\Psi x_k + \Gamma_D D) \end{bmatrix} \leq \begin{bmatrix} \Lambda \\ \Gamma \end{bmatrix} U \leq \begin{bmatrix} \triangle U_{\max} + I_{1,u} u_{k-1} \\ Y_{\max} - (\Psi x_k + \Gamma_D D) \end{bmatrix} \tag{4.39}
$$

Most of the already mentioned solvers require formulation like presented in 4.1a, so 4.39 must be reformulated as shown in 4.40.

$$
\begin{bmatrix} \Lambda \\ \Gamma \\ -\Lambda \\ -\Gamma \end{bmatrix} U \leq \begin{bmatrix} \triangle U_{\max} + I_{1,u} u_{k-1} \\ Y_{\max} - (\Psi x_k + \Gamma_D D) \\ -\triangle U_{\min} + I_{1,u} u_{k-1} \\ -(Y_{\min} - (\Psi x_k + \Gamma_D D)) \end{bmatrix} \tag{4.40}
$$

4.1.3 Soft Constraints

In general, hard constraints on output should be avoided due to the infeasibility issues, which may arise. It is strongly recommended to implement soft

constraints at least on the outputs, so the QP problem has always a solution (Prasath and Jørgensen, 2009; Zeilinger et al., 2010). Having hard constraints on control inputs, or control moves do not create the risk of running into infeasibility. These infeasibility issues arise mainly if we consider stochastic influences on the process, measurements can easily cross the hard limit we set in the constraints (Primbs, 2007). It is also a good practise to introduce soft constraints on inputs as well, so if it is necessary to ensure reference tracking, or in case of wind turbine disturbance rejection, MPC controller can achieve better performance.

Implementing soft constraints into QP problem has, however significant drawback. The soft margins (slack variables), we are introducing on outputs or inputs are becoming optimization variables as well. Objective function which needs to be minimized is shown in 4.41. It is clear, that increased complexity of the QP problem, may prolong the calculation time. In the new objective function, matrices S_u and S_y are weighting matrices related to the slack variables.

$$\Phi = \frac{1}{2}\sum_{k=0}^{N}||r_k - y_k||_Q^2 + \frac{1}{2}\sum_{k=0}^{N}||w_{y,k}||_{S_y}^2 + \frac{1}{2}\sum_{k=0}^{N-1}||\triangle u_k||_R^2 + \frac{1}{2}\sum_{k=0}^{N-1}||w_{u,k}||_{S_u}^2 \tag{4.41}$$

First, soft constraints on inputs is being considered 4.42. By introducing the slack variable $w_{u,k}$ we allow crossing the limit $\triangle u_{\min}$ and $\triangle u_{\max}$. As it was already mentioned, this slack variable will become optimization variable like U, so different and very high penalty is going to be applied for the soft margin, so the MPC controller will be "reluctant" to cross the limit.

$$\triangle u_{\min} - w_{u,k} \leq \triangle u_k \leq \triangle u_{\max} + w_{u,k} \tag{4.42}$$

$$\triangle U_{\min} - W_u \leq \triangle U \leq \triangle U_{\max} + W_u \tag{4.43}$$

Soft input constraints (eq. 4.43) must be rewritten into matrix form, which is suitable for most of the QP solvers 4.44. This has been already presented in eq. 4.40.

$$\begin{bmatrix} \Lambda & -I_{u,N} \\ -\Lambda & -I_{u,N} \end{bmatrix} \begin{bmatrix} U \\ W_u \end{bmatrix} \leq \begin{bmatrix} \triangle U_{\max} \\ -\triangle U_{\min} \end{bmatrix} \tag{4.44}$$

Where $I_{u,N} \in \mathbb{I}^{(N-1)n_u \times (N-1)n_u}$. Similar procedure is done for the output constraints (eq. 4.45). Again slack variables $w_{y,k}$ are being introduced to the inequality constraints. Matrix form is presented in 4.46. In case of the output constraints, output vector Y must substituted by the prediction equation 4.28, resulting 4.47.

$$y_{\min} - w_{y,k} \leq y_k \leq y_{\max} + w_{y,k} \tag{4.45}$$

$$Y_{\min} - W_y \leq Y \leq Y_{\max} + W_y \tag{4.46}$$

$$Y_{\min} - W_y \leq \Psi x_0 + \Gamma U + \Gamma_D D \leq Y_{\max} + W_y \tag{4.47}$$

By reformulating equation 4.47 and treating slack variable vector W_y as an optimization variable, we obtain following equation (similar to 4.44):

$$\begin{bmatrix} \Gamma & -I_{y,N} \\ -\Gamma & -I_{y,N} \end{bmatrix} \begin{bmatrix} U \\ W_y \end{bmatrix} \leq \begin{bmatrix} Y_{\max} - (\Psi x_k + \Gamma_D D) \\ -(Y_{\min} - (\Psi x_k + \Gamma_D D)) \end{bmatrix} \tag{4.48}$$

Where $I_{y,N} \in \mathbb{I}^{Nn_y \times Nn_y}$. Equations 4.48 and 4.44 can be merged together resulting complete matrix formulation (eq. 4.49), which describes the inequality soft constraints, as a part of the QP problem.

$$\mathcal{F}\mathcal{U} \leq b \tag{4.49}$$

where:

$$\mathcal{F} = \begin{bmatrix} \Lambda & -I_{u,N} & 0 \\ -\Lambda & -I_{u,N} & 0 \\ \Gamma & 0 & -I_{y,N} \\ -\Gamma & 0 & -I_{y,N} \end{bmatrix} \tag{4.50}$$

$$\mathcal{U} = \begin{bmatrix} U \\ W_u \\ W_y \end{bmatrix} \tag{4.51}$$

$$b = \begin{bmatrix} \triangle U_{\max} \\ -\triangle U_{\min} \\ Y_{\max} - (\Psi x_k + \Gamma_D D) \\ -(Y_{\min} - (\Psi x_k + \Gamma_D D)) \end{bmatrix} \tag{4.52}$$

Finally curvature matrix H must be expanded as well as vector g from equation 4.32. Extended curvature matrix $\mathcal{H}$ is defined as follows:

$$\mathcal{H} = \begin{bmatrix} H & & \\ & H_u & \\ & & H_y \end{bmatrix} \tag{4.53}$$

definition of H_u and H_y follows:

$$H_u = I_{N-1} \otimes S_u \tag{4.54}$$

$$H_y = I_N \otimes S_y \tag{4.55}$$

where $I_N \in \mathbb{I}^{N \times N}$, $I_{N-1} \in \mathbb{I}^{(N-1) \times (N-1)}$

Since there is no connection between slack variables and control input itself, $\mathcal{G}$ vector will have this form:

$$\mathcal{G} = \begin{bmatrix} g \\ 0 \\ 0 \end{bmatrix} \tag{4.56}$$

Once all the matrices and vector are derived, we can formulate overall QP problem:

$$\min \quad \frac{1}{2}\mathcal{U}^T H \mathcal{U} + \mathcal{G}^T \mathcal{U} \tag{4.57a}$$

$$\text{s. t.} \quad \mathcal{F}\mathcal{U} \preceq b \tag{4.57b}$$

$$\mathcal{U}_{\min} \leq \mathcal{U} \leq \mathcal{U}_{\max} \tag{4.57c}$$

Bounds on the $\mathcal{U}$ can be formulated as follows:

$$\mathcal{U}_{\min} = \begin{bmatrix} U_{\min} \\ W_{u,min} \\ W_{y,min} \end{bmatrix} \qquad \mathcal{U}_{\max} = \begin{bmatrix} U_{\max} \\ W_{u,max} \\ W_{y,max} \end{bmatrix} \tag{4.58}$$

Where $W_{u,y,\min}$ is set to zero, and $W_{u,y,\max}$ is usually set to certain number, which is called soft margin. Slightly different approach to soft constraints is proposed by (Prasath and Jørgensen, 2009), where vector $W_{u,y,\max}$ is set to infinity. This however means, that at certain circumstances (i.e. bad tuning) the controller can use control action of arbitrary magnitude.

4.2   Frequency Weighted MPC

Frequency weighted MPC (FMPC) control combines the advantages of model predictive control together with frequency weighting trough introducing filters into control loop (Poulsen, 2007). By introducing these filters into control system, tuning of the controller is shifted from standard weighting matrices (e.g. Q and R from previous section) to specifying the filters. Introducing filters into control system allows us to penalize certain frequency content on each signal separately. In case of wind turbine control, is desirable for example to penalize certain frequencies of the tower for-aft movement. However different frequency content is penalized in case of control inputs. As it was indicated, these filters are being put on control inputs, states and outputs as well, like shown in eq. 4.59.

$$
\begin{bmatrix} x_1^f \\ \vdots \\ x_n^f \end{bmatrix} = \begin{bmatrix} G_{x,1}(s) & & \\ & \ddots & \\ & & G_{x,n}(s) \end{bmatrix} \begin{bmatrix} x_1 \\ \vdots \\ x_n \end{bmatrix} \tag{4.59a}
$$

$$
\begin{bmatrix} y_1^f \\ \vdots \\ y_m^f \end{bmatrix} = \begin{bmatrix} G_{y,1}(s) & & \\ & \ddots & \\ & & G_{x,m}(s) \end{bmatrix} \begin{bmatrix} y_1 \\ \vdots \\ y_m \end{bmatrix} \tag{4.59b}
$$

$$
\begin{bmatrix} u_1^f \\ \vdots \\ u_i^f \end{bmatrix} = \begin{bmatrix} G_{u,1}(s) & & \\ & \ddots & \\ & & G_{u,i}(s) \end{bmatrix} \begin{bmatrix} u_1 \\ \vdots \\ u_i \end{bmatrix} \tag{4.59c}
$$

This transfer function matrices can be very easily represented in state space form.

$$\begin{bmatrix} \dot{x}_1^f \\ \vdots \\ \dot{x}_n^f \end{bmatrix} = \begin{bmatrix} A_{x,1}^f & & \\ & \ddots & \\ & & A_{x,n}^f \end{bmatrix} \begin{bmatrix} x_1^f \\ \vdots \\ x_n^f \end{bmatrix} + \begin{bmatrix} B_{x,1}^f & & \\ & \ddots & \\ & & B_{x,n}^f \end{bmatrix} \begin{bmatrix} x_1 \\ \vdots \\ x_n \end{bmatrix} \tag{4.60}$$

$$\begin{bmatrix} y_{x,1}^f \\ \vdots \\ y_{x,n}^f \end{bmatrix} = \begin{bmatrix} C_{x,1}^f & & \\ & \ddots & \\ & & C_{x,n}^f \end{bmatrix} \begin{bmatrix} x_1^f \\ \vdots \\ x_n^f \end{bmatrix} + \begin{bmatrix} D_{x,1}^f & & \\ & \ddots & \\ & & D_{x,n}^f \end{bmatrix} \begin{bmatrix} x_1 \\ \vdots \\ x_n \end{bmatrix} \tag{4.61}$$

Where $A_{x,1}^f$, $B_{x,1}^f$, $C_{x,1}^f$, $D_{x,1}^f$ is state space representing the transfer function $G_{x,1}(s)$. Equation presented above is being simplified and resulting in 4.62. Same rules are applied on input and output filters obtaining state space formulation for input filters (eq. 4.63) and output filters (eq. 4.64).

$$\dot{\mathbf{x}}^{\mathbf{f}} = \mathbf{A_x^f x^f} + \mathbf{B_x^f} x \tag{4.62a}$$

$$\mathbf{y_x^f} = \mathbf{C_x^f x^f} + \mathbf{D_x^f} x \tag{4.62b}$$

$$\dot{\mathbf{u}}^{\mathbf{f}} = \mathbf{A_u^f u^f} + \mathbf{B_u^f} u \tag{4.63a}$$

$$\mathbf{y_u^f} = \mathbf{C_u^f u^f} + \mathbf{D_u^f} u \tag{4.63b}$$

$$\dot{\mathbf{y}}^{\mathbf{f}} = \mathbf{A_y^f y^f} + \mathbf{B_y^f} y \tag{4.64a}$$

$$\mathbf{y_y^f} = \mathbf{C_y^f y^f} + \mathbf{D_y^f} y \tag{4.64b}$$

In order to construct the overall state space model, equation 4.64 must be modified. Reason for this is, that original output vector y cannot be translated into overall state space model. To remedy this problem, in equation 4.64 output vector y will be substituted with output equation from original state space model.

$$\dot{\mathbf{y}}^{\mathbf{f}} = \mathbf{A_y^f y^f} + \mathbf{B_y^f}(Cx + Du) = \mathbf{A_y^f y^f} + \mathbf{B_y^f} Cx + \mathbf{B_y^f} Du \tag{4.65a}$$

$$\mathbf{y_y^f} = \mathbf{C_y^f y^f} + \mathbf{D_y^f}(Cx + Du) = \mathbf{C_y^f y^f} + \mathbf{D_y^f} Cx + \mathbf{D_y^f} Du \tag{4.65b}$$

By combination of presented state space representations, complete state space model together with original state space description is constructed:

$$
\begin{bmatrix} \dot{x} \\ \dot{\mathbf{x}}^{\mathbf{f}} \\ \dot{\mathbf{y}}^{\mathbf{f}} \\ \dot{\mathbf{u}}^{\mathbf{f}} \end{bmatrix} = \begin{bmatrix} A & & & \\ \mathbf{B^f_x} & \mathbf{A^f_x} & & \\ \mathbf{B^f_y}C & & \mathbf{A^f_y} & \\ & & & \mathbf{A^f_u} \end{bmatrix} \begin{bmatrix} x \\ \mathbf{x^f} \\ \mathbf{y^f} \\ \mathbf{u^f} \end{bmatrix} + \begin{bmatrix} B \\ \\ \\ \mathbf{B^f_u} \end{bmatrix} u \qquad (4.66a)
$$

$$
\begin{bmatrix} \mathbf{y^f_x} \\ \mathbf{y^f_y} \\ \mathbf{y^f_u} \end{bmatrix} = \begin{bmatrix} \mathbf{D^f_x} & \mathbf{C^f_x} & & \\ \mathbf{D^f_y}C & & \mathbf{C^f_y} & \\ & & & \mathbf{C^f_u} \end{bmatrix} \begin{bmatrix} x \\ \mathbf{x^f} \\ \mathbf{y^f} \\ \mathbf{u^f} \end{bmatrix} + \begin{bmatrix} \\ \\ \mathbf{D^f_u} \end{bmatrix} u \qquad (4.66b)
$$

States and outputs considered are:

$$
\mathbf{x} = \begin{bmatrix} x \\ x^f \\ u^f \\ y^f \end{bmatrix} \qquad \mathbf{y} = \begin{bmatrix} x^f \\ u^f \\ y^f \end{bmatrix} \qquad (4.67)
$$

Number of control inputs is the same. State space model presented in 4.66 with state and output definition from 4.67, must be descretized yielding following formulation:

$$
\dot{\mathbf{x}^f}_k = \mathbf{A^f}\mathbf{x}_k\mathbf{B^f}u_k \qquad (4.68a)
$$

$$
\mathbf{y^f}_k = \mathbf{C^f}\mathbf{x}_k\mathbf{D^f}u_k \qquad (4.68b)
$$

The cost function formulated for frequency weighted MPC is expressed in 4.69. Notice, that inputs are not penalized separately, but are included in vector **y**. Rules presented in previous section are used in order to construct necessary matrices for the QP optimization problem.

$$
\Phi \quad = \min \sum_{k=1}^{N} y^T Q y \qquad (4.69a)
$$

$$
s.t. \quad \mathbf{x}_{k+1} = \mathbf{A^f}\mathbf{x}_k + \mathbf{A^f}u_k \qquad (4.69b)
$$

$$
\mathbf{y} = \mathbf{C^f}\mathbf{x}_k + \mathbf{D^f}u_k \qquad (4.69c)
$$

$$
u \in \mathbb{U} \qquad (4.69d)
$$

$$
x \in \mathbb{X} \qquad (4.69e)
$$

$$
y \in \mathbb{Y} \qquad (4.69f)
$$

General rule for the frequency tuning says, that high-pass filter should be considered on inputs, and low pass filters on states and outputs (Skogestad and Postlethwaite, 2005). The main reason for using high-pass filters on inputs is penalizing high frequency activity of the controller. Implementing low-pass filter on inputs its may move eigenvalues of the closed loop system closer to stability margin. In case of wind turbine and tower for-aft movement, high-pass or rather band-pass filters are implemented, because tower oscillations should be dampened. This tuning will be explained in detail in chapter 5.

CHAPTER 5

Model Predictive Control Design for HAWT

5.1 Main Design

In this chapter, tuning of the MPC strategies and the estimator will be discussed. Control objective in partial load is to maximize the power. Due to the fact, that the linear model is not controllable by pitch action in partial load, only generator torque is considered as control input. Pitch action in partial load is calculated in order to maximize c_p value for given TSR. TSR is given by the estimate of the wind speed and measurement of the rotational speed. Based on this fact, two consequences arise:

1. Oscillations in tower for-aft movement can not by damped actively, because the link between generator torque action and tower for-aft movement is extremely week (step responses section 2.5)

2. Introducing filters and using FMPC is not relevant in partial load. Since the primary objective is to maximize the power, all available control activity of generator torque must be put into fulfilling this task

In top region, both control inputs are considered. Primary objective of the controller would be to keep rotational speed and power output at its respective nominal values. In this case introducing filters and using FMPC proves to be a relevant step, because it allows us to minimize the stress effecting the plant even further than the standard MPC.

In case of standard MPC approach, state space matrices already presented in modelling section are used in order to design the MPC Controller. Rules mentioned in section 4.1 are applied, and QP is formulated. However, in case of FMPC, state space model must be first introduced. After deriving the state space model for original model and filters, QP problem can be formulated.

5.1.1 Model Scaling

In order to avoid numerical problems during solving quadratic programming, state space model has been scaled. Scaling took place on the inputs as well as on the outputs. Since there are huge differences in magnitude of inputs signals:

$$\beta_0 \in < -1.56; \ 23.35 > deg \qquad T_g \in < 0.73; \ 40.68 > kNm \qquad (5.1)$$

scaling factor for pitch input has been chosen as $f_\beta = 22 \ deg$. Scaling factor for generator torque action has been chosen as $f_{T_g} = 45 \ kNm$. Stationary values of inputs signals will belong to the intervals expressed in 5.2. After applying such scaling to the state space model, values of B matrix will be levelled-up (eq. 5.3).

$$\bar{\beta}_0 \in < -0.07; \ 1.06 > \qquad \bar{T}_g \in < 0.02; \ 0.90 > \qquad (5.2)$$

$$B = \begin{bmatrix} -0.0158 & -2.5021 \cdot 10^{-6} \\ 0 & 0 \\ -0.1490 & 0 \end{bmatrix} \qquad \bar{B} = \begin{bmatrix} -0.3484 & -0.1126 \\ 0 & 0 \\ -3.2781 & 0 \end{bmatrix} \qquad (5.3)$$

Similar scaling is done for the power output, where the unscaled C and D

matrices have this shape:

$$
C = \begin{bmatrix} 3945990 & 0 & 0 \\ 1 & 0 & 0 \\ 0 & 0 & 1 \end{bmatrix} \qquad D = \begin{bmatrix} 0 & 122.9096 \\ 0 & 0 \\ 0 & 0 \end{bmatrix} \tag{5.4}
$$

After applying scaling factor f_{T_g} on generator torque action, values in C matrix will still have different order of magnitude. First row of output equation is divided by gear coefficient $N_g = 97$ yielding:

$$
C = \begin{bmatrix} 0.9040 & 0 & 0 \\ 1 & 0 & 0 \\ 0 & 0 & 1 \end{bmatrix} \qquad D = \begin{bmatrix} 0 & 1.2671 \\ 0 & 0 \\ 0 & 0 \end{bmatrix} \tag{5.5}
$$

Note, that these scaling factors can be chosen differently. These scaling factors prove to result in better levelled curvature matrix H. These examples of matrices have been given for wind speed equal to 15 m/s. The entire state space model, in C-Time is presented in A.

5.1.2 Standard MPC

Table 5.1 shows the tuning parameters of MPC controller in all four regions, and table 5.2. Satisfactory results in simulations were obtained using only one set of weighting matrices in each region. The order of state variables, control inputs and system outputs is:

$$
x = \begin{bmatrix} \omega_r \\ x_t \\ \dot{x}_t \end{bmatrix} \qquad u = \begin{bmatrix} \beta \\ T_g \end{bmatrix} \qquad y = \begin{bmatrix} P_e \\ \omega_r \\ \dot{x}_t \end{bmatrix} \tag{5.6}
$$

except partial load, when only generator torque is considered as control input.

Order of the states in disturbance model is:

$$
\hat{\mathbf{x}} = \begin{bmatrix} \omega_r & x_t & \dot{x}_t & v & \dot{v} & d \end{bmatrix}^T \tag{5.7}
$$

Table 5.1: Tuning parameters for standard MPC controller

	Region 1	Region 2	Region 3	Region 4
R	1e-2	1e-3	1e0	[1e1 1e-1]
Q	[1e-1, 1e1, 1e-1]	[1e-1, 1e1, 1e0]		[1e0, 1e0, 1e0]
S_u	1e3			[1e3, 1e3]
S_y	[1e5, 1e5, 1e5]			

In table 5.2, there are three sets of matrices. Input covariance matrix Q_e is split into two separate matrices $Q_{e,x}$ and $Q_{e,d}$. While the matrix $Q_{e,x}$ indicate setting of covariance matrix for state estimation, covariance matrix $Q_{e,d}$ shows the tuning for wind speed estimation, and additional disturbances. These matrices should be then place together as it is stated in eq. 5.21.

$$Q_e = \begin{bmatrix} Q_{e,x} & \\ & Q_{e,d} \end{bmatrix} \tag{5.8}$$

Table 5.2: Tuning parameters for stationary predictive Kalman filter

	Region 1	Region 2
$Q_{e,x}$	[1e-3, 1e0, 1e0]	[1e-3, 1e1, 1e0]
$Q_{e,d}$	[1e1, 1e1, 1e1]	[1e1, 1e1, 1e-5]
R_e	[1e-3, 1e-3, 1e-3]	[1e-1, 1e-3, 1e-3]

	Region 3	Region 4
$Q_{e,x}$	[1e-3, 1e0, 1e0]	[1e-3, 1e1, 1e0]
$Q_{e,d}$	[1e2, 1e2, 1e-2]	[1e1, 1e1, 1e0, 1e0]
R_e	[1e-3, 1e-3, 1e-3]	[1e-3, 1e-3, 1e-3]

In partial load only one output disturbance is considered, and namely only on rotational speed. In full load, two output disturbances are considered, specifically output disturbances on generated power and on rotational speed.

In partial load, disturbances matrices has this form:

$$E_x = \begin{bmatrix} 0 \\ 0 \\ 0 \end{bmatrix} \qquad E_y = \begin{bmatrix} 0 \\ 1 \\ 0 \end{bmatrix} \tag{5.9}$$

Putting disturbances on input should be avoided. Since predictive Kalman filter is used also on wind speed estimation, which is considered as input disturbance,

putting additional disturbances will worsen the wind speed estimation. Since the primary objective is to maximize the power, through controlling the rotational speed, putting only one output disturbance proven to be enough.

If one would be considering disturbances on the input, values in E_x matrix plays huge role. Numbers in E_x matrix must not be greater than the maximum number for given row in B_v matrix. In opposite case, wind speed estimation will degrade, even when low coefficient in $Q_{e,d}$ matrix is placed.

Same goes for estimation in full load. Considered disturbances on power generation and rotational speed (eq. 5.10) proven to yield satisfactory results.

$$E_x = \begin{bmatrix} 0 & 0 \\ 0 & 0 \\ 0 & 0 \end{bmatrix} \qquad E_y = \begin{bmatrix} 1 & 0 \\ 0 & 1 \\ 0 & 0 \end{bmatrix} \tag{5.10}$$

Gain of the predictive Kalman filter L is then calculated using `dlqe` command in MATLAB .

It must be also noted, that these simulations were performed on model mention in modelling section (section 2.1). If such controller will be implemented on more complex model e.g. FAST (Jonkman and Buhl Jr., 2005), different settings of disturbances should be considered.

Prediction horizons considered in standard MPC are:

$$N = 3s = 30 \text{ samples}$$

5.1.3 Frequency Weighted MPC

In this subsection tuning parameters for frequency weighted MPC will be discussed. First, order of considered states variables is presented:

$$\mathbf{x} = \begin{bmatrix} \omega_r & x_t & \dot{x}_t & \omega_r^f & x_t^f & \dot{x}_t^f & P_e^f & u_1^f & u_2^f \end{bmatrix}^T \tag{5.11}$$

Order of outputs variables considered in FMPC design:

$$\mathbf{y^f} = \begin{bmatrix} \omega_r^f & x_t^f & \dot{x}_t^f & P_e^f & u_1^f & u_2^f \end{bmatrix}^T \tag{5.12}$$

As mentioned in previous chapter in FMPC tuning, is shifted from weighting matrices Q and R, into transfer function design. However, tuning matrix Q is present in this design as well, but it is set to identity matrix, except coefficients related to control inputs, which has been lowered (eq. 5.13). In such case, controller has more "freedom" to move from steady state point.

$$Q = diag([1, 1, 1, 1, 10^{-2}, 10^{-2}]) \tag{5.13}$$

Filters placed on the control inputs have high-pass characteristic:

$$H_\beta(s) = \frac{40s + 1}{10s + 1} \tag{5.14a}$$

$$H_{T_g}(s) = \frac{100s + 1}{4s + 1} \tag{5.14b}$$

Filter placed on the the rotational speed is characterised as low-pass filter and on the states related to tower movement, has type of band-pass filter:

$$H_{\omega_r} = \frac{0.25s + 1}{0.5s + 1} \tag{5.15a}$$

$$H_{x_t} = \frac{s^2 + 3s + 1}{s^2 + s + 1} \tag{5.15b}$$

$$H_{\dot{x}_t} = \frac{s^2 + 6s + 1}{s^2 + s + 1} \tag{5.15c}$$

Filter placed on power output has also low-pass characteristics:

$$H_{P_e}(s) = \frac{0.1s + 1}{2s + 1} \tag{5.16}$$

Due to the fact, that rotational speed and speed of the tower are directly measured states, filters on these outputs are not placed. Frequency responses of presented filters are shown on figures 5.1, 5.2 and 5.3.

For FMPC linear observer in form of stationary predictive Kalman filter has been designed as well. Considered order of state variables is:

$$\hat{\mathbf{x}} = \begin{bmatrix} \mathbf{x} & v & \dot{v} & d \end{bmatrix}^T \tag{5.17}$$
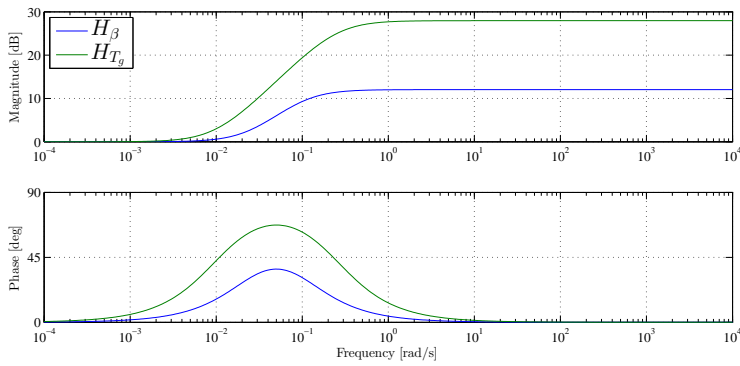
Figure 5.1: Frequency responses of the input filters
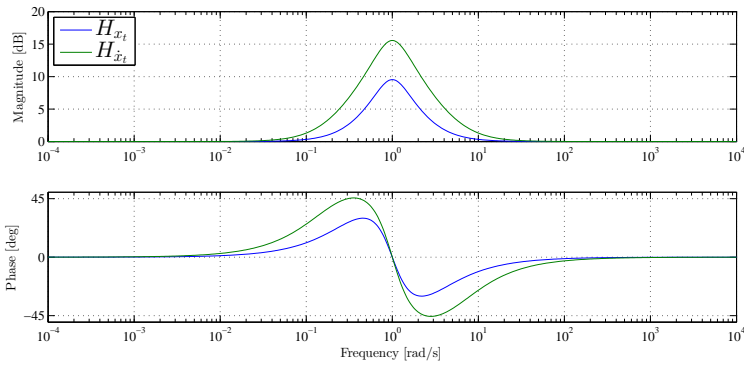
Figure 5.2: Frequency responses of filters related to tower for-aft movement
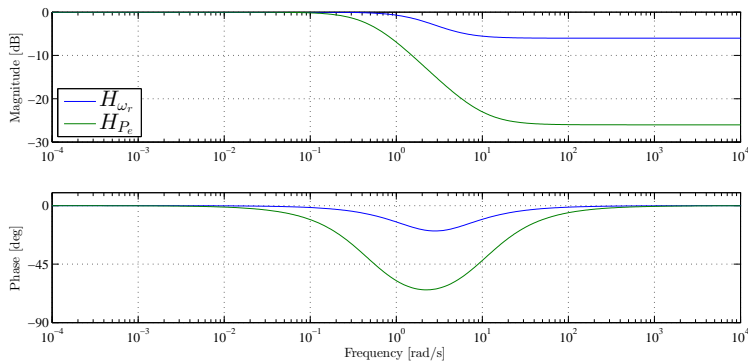
Figure 5.3: Frequency responses of the output filter and filter on rotational speed

Outputs considered in predictive Kalman filter:

$$\mathbf{y} = \begin{bmatrix} P_e & \omega_r & \dot{x}_t & \mathbf{y^f} \end{bmatrix}^T \tag{5.18}$$

Two disturbances are considered similarly to standard MPC design. They are placed on outputs, on filtered measurement of generated power and on the filtered measurement of rotational speed. Output disturbance matrix has following structure:

$$E_y = \begin{bmatrix} 0 & 1 \\ 0 & 0 \\ 0 & 0 \\ 1 & 0 \\ 0 & 0 \\ 0 & 0 \end{bmatrix} \tag{5.19}$$

Input disturbance matrix E_x is set to zero matrix with appropriate size.

Tuning of the Kalman filter state covariance matrix is:

$$Q_{e,x} = diag([10^{-3}, 10, 1]) \tag{5.20a}$$

$$Q_{e,xf} = diag([10^{-3}, 10^{-3}, 10^{-3}, 10^{-3}, 10^{-3}, 10^{-3}]) \tag{5.20b}$$

$$Q_{e,d} = diag([10, 10, 1, 1]) \tag{5.20c}$$

Where Q_x is diagonal matrix related to original states, Q_{xf} is diagonal matrix related to filtered states and Q_d is diagonal matrix related to wind speed model and additional disturbances. Notice, that Q_x and Q_d is the same, like in case of Kalman filter for standard MPC in top region. State covariance matrix Q_e, upon which is Kalman filter design based is:

$$Q_e = \begin{bmatrix} Q_{e,x} & & \\ & Q_{e,xf} & \\ & & Q_{e,d} \end{bmatrix} \tag{5.21}$$

Output covariance matrix is constructed in same way, but following tuning:

$$R_{e,y} = diag([10^{-3}, 10^{-3}, 10^{-3}]) \tag{5.22a}$$

$$R_{e,y^f} = diag([10^{-1}, 10^{-1}, 10^{-1}, 10^{-1}, 10^{-1}, 10^{-1}]) \tag{5.22b}$$

$$\tag{5.22c}$$

It may seem, that too much state variables are estimated, or too much measurements is used, but MATLAB implementation was straight forward in this way. Also we should keep in mind, when this controller is going to be used on more complex models, disturbance placement may need to be revisited.

Prediction horizons considered in frequency weighted MPC are:

$$N = 3s = 30 \text{ samples}$$

These horizons prove to be the minimum prediction horizon, when satisfactory performance of the controller has been achieved. Prolonging the horizon did not yield significantly better performance, but it has decreased the computational time. It must be noted, when actuators are implemented, setting for prediction horizon should be revisited.

5.2 Operational Constraints

Operational constraints implemented in MPC controllers are stated in table 5.3. Scaled and sampled values are presented as well. Sampling frequency of 10 Hz is used in simulations.

Table 5.3: Operational Constraints

	Nominal		Scaled		Scaled Sampled	
$\beta_{\max}$	30	[deg]	1.3636	[deg]	1.3636	[deg]
$\beta_{\min}$	-5	[deg]	-0.2273	[deg]	-0.2273	[deg]
$\triangle\beta_{\max}$	8	[deg/s]	0.3636	[deg/s]	0.0364	[deg per sample]
$\triangle\beta_{\min}$	-8	[deg/s]	-0.3636	[deg/s]	-0.0364	[deg per sample]
$T_{g,\max}$	47403	[Nm]	1.0534	[Nm]	1.0534	[Nm]
$T_{g,\min}$	0	[Nm]	0	[Nm]	0	[Nm]
$\triangle T_{g,\max}$	15000	[Nm/s]	0.3333	[Nm/s]	0.0333	[Nm per sample]
$\triangle T_{g,\min}$	-15000	[Nm/s]	-0.3333	[Nm/s]	-0.0333	[Nm per sample]

Constraints on rotational speed was originally put as 5 to 10% above or below maximum and minimum values, but it proves to be not necessary, because these constraints were never active. Same goes for generated power. However, this could be only case, that fairly simple model of turbine has been used on which simulations were performed.

Soft margin on pitch rate was set to additional 2 deg/s, soft margin for generator torque rate was set to 5000 Nm/s.

5.3 Simulations

All simulations were performed in such way, that first wind speed profile was generated. Then system dynamics matrices, optimization matrices and Kalman gains were calculated for every 0.1 m/s in the wind speed interval from 3 to 25 m/s. This setting is sufficient due to the slow changes in dynamics of the system in the partial load. On the other hand in the full load, dynamics of the system change rather rapidly with increasing wind speed, calculation of the matrices at specific wind speed has been taken into consideration. Specifically the element in B matrix linking pitch angle and rotational speed is changing rapidly. To improve the performance matrices were calculated at every wind speed over 11.2 m/s. This however has significant drawback, because it increases the calculation time of the simulation by approximately 40%. To remedy this problem, interpolation procedure has been implemented, but still there was increase in calculation time by approximately by 20%.

Block diagram of the simulations are shown in figure 5.4(a). Figure 5.4(b) shows block diagram of frequency weighted MPC controller. Keep in mind, that same procedure with changing dynamics is also applied in case of FMPC simulations.
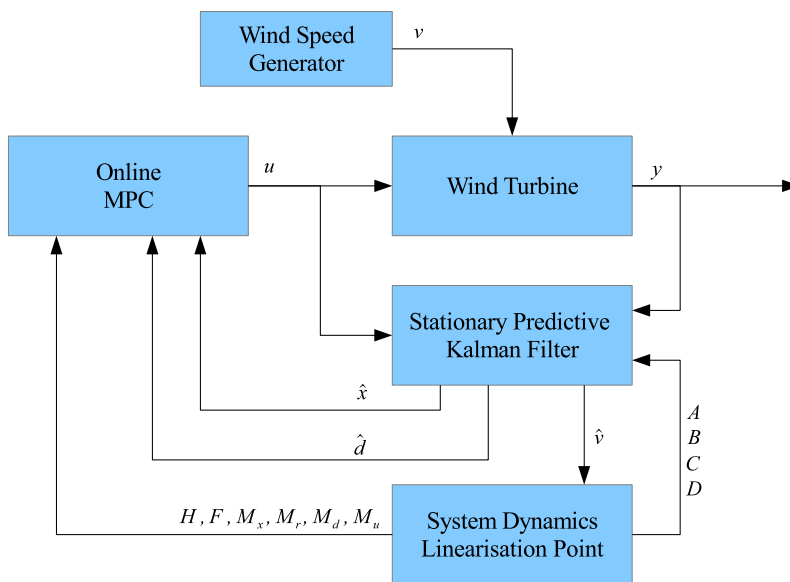
(a) Standard MPC
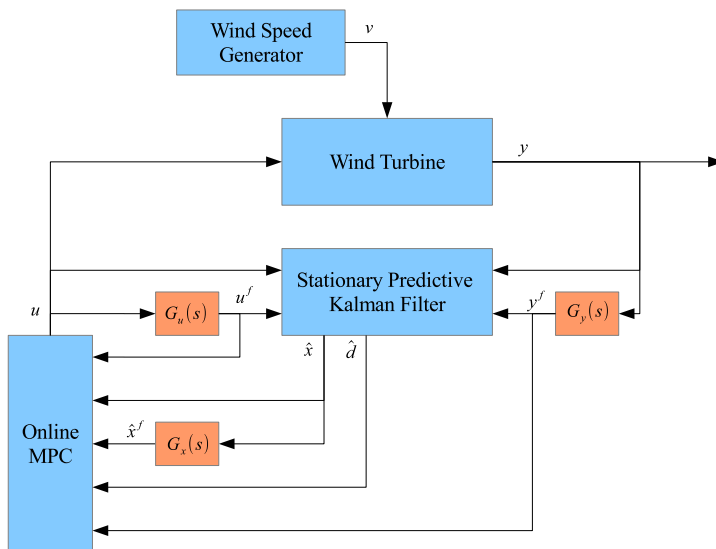
(b) Frequency weighted MPC

Figure 5.4: Block diagrams

CHAPTER 6

Full Load Simulations

The first set of simulation shows the performance of the controllers in the top region. Partial load simulations will follow in the next chapter, where will be also shown an overall simulation, throughout entire wind speed operation interval.

Objective of the controller in the full load is to maintain the power output and rotational speed at theirs respective nominal values ($P_{nom} = 5\ MW$ and $\omega_{r,nom} = 12.1\ rpm$). Secondary objective of the controller is to minimize the physical stress on the device itself.

In full load case two MPC controllers have been tested; standard MPC and frequency weighted MPC controllers. Both deterministic and stochastic simulations are performed. Performance of the standard MPC controller will be compared with FMPC. When applied deterministic wind speed profiles, effects of different tunings of the filters will be explored. Simulations with stochastic wind speed profile will be shown as well. Mean values and standard deviation of the signals will be compared as well.

6.1 Standard MPC

Tuning of MPC controllers was presented in chapter 5. First shown simulation is for deterministic wind speed profile. Wind speed profile is shown n figure 6.1. Estimation od the wind speed is shown as well. Notice slight estimation error when step change is made from 17 to 15 m/s. This can be easily neglected, because the system dynamics does not change significantly when wind speed changes by 0.05 m/s. Also implemented disturbance modelling takes care of slight mismatch in estimation.
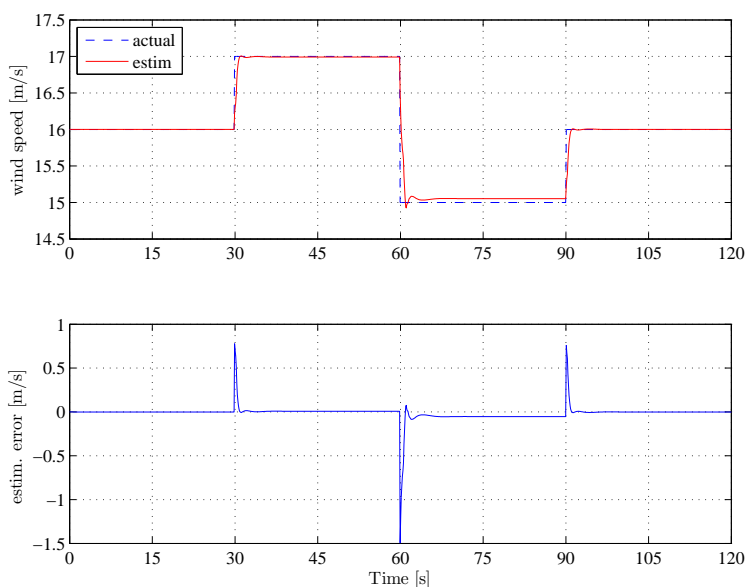
Figure 6.1: Deterministic wind speed profile

Contrary to the partial load simulations, less only 3 step changes were applied to the system, so the transients especially in states related to tower movement can be seen better. This deterministic wind speed profile is used throughout this entire chapter, same goes for later presented stochastic wind speed profile. Measurements of power and rotational speed are shown on figure 6.2. States related to tower for-aft movement are displayed on figure 6.3. Control actions are shown on figures 6.4 and 6.5. Constraints are active only on pitch rate. This deterministic simulation will serve as a basis for comparison with frequency weighted MPC (section 6.2). Deterministic simulation is followed by stochastic simulation.
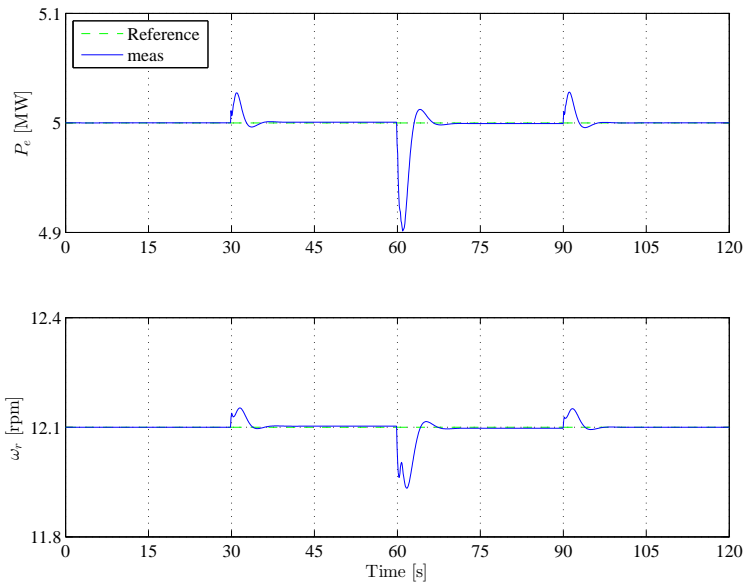
Figure 6.2: Measurements - P_e and ω_r
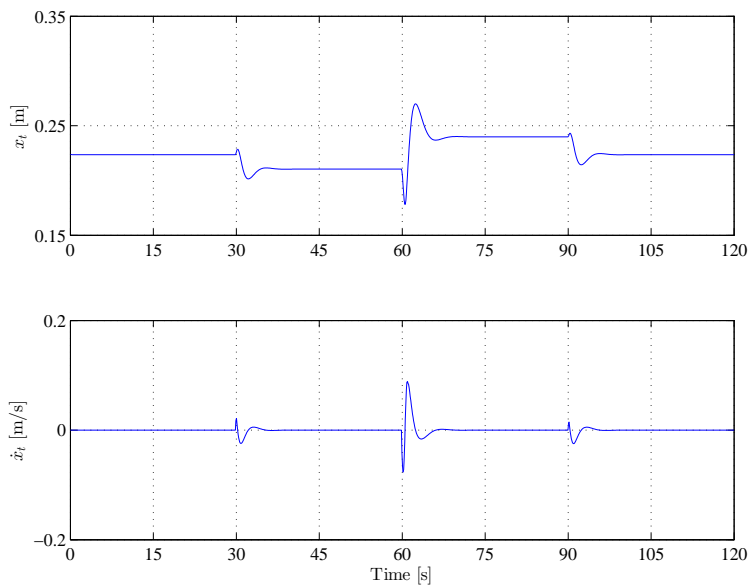
Figure 6.3: Tower for-aft movement
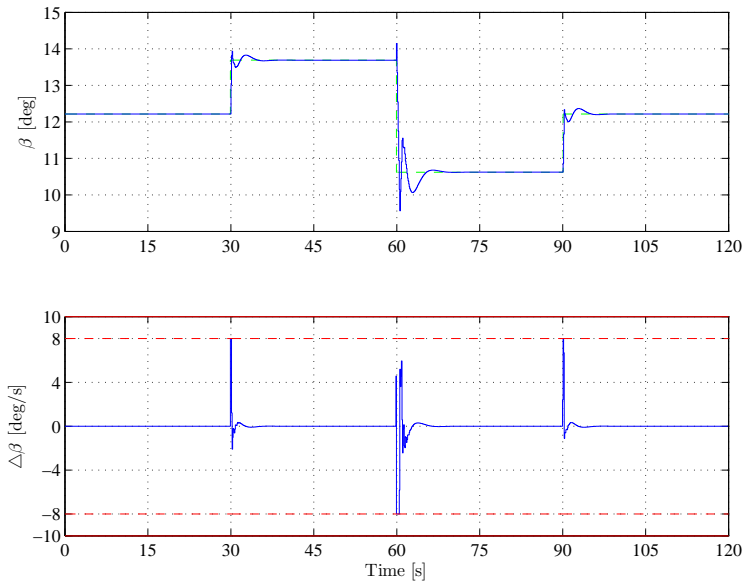
Figure 6.4: Pitch control action
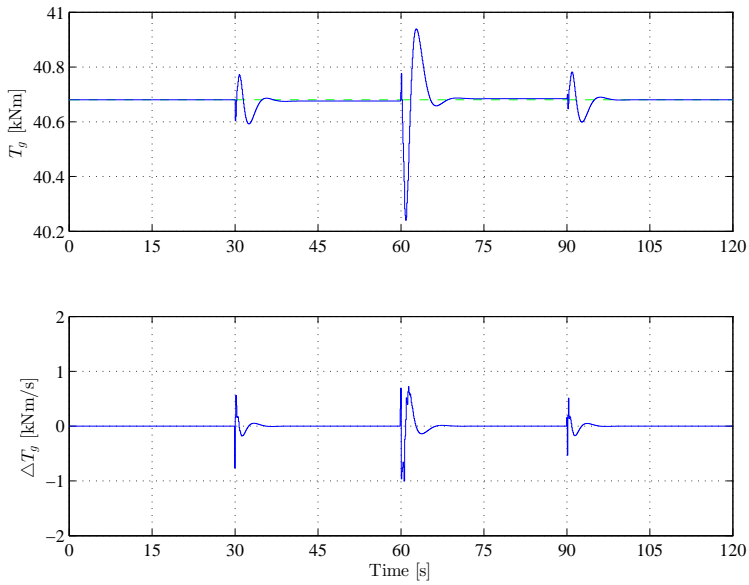
Figure 6.5: Generator torque control action

Stochastic wind profile, which is applied to the system is shown on figure 6.6. Estimation together with estimation error is shown as well. Notice that estimation error is reaching almost 0.4 m/s in absolute value. This is by limitations of the stationary predictive Kalman filter, but the overall performance will not be affected much. We must realize, that the wind speed variations change much faster than system can react to the changes. Due to this observation we can neglect this estimation error. However it must be noted, that using this kind of estimation procedure may not be satisfactory when combined with more complex models, or on simulations with FAST.
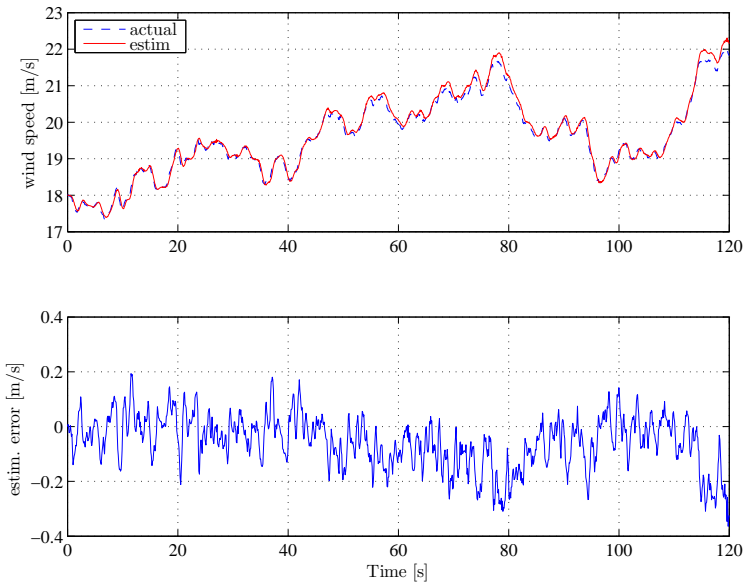
Figure 6.6: Stochastic wind speed profile

Resulting power output measurement with rotational speed is shown on figure 6.7. States related to to tower for-aft movement are shown on figure 6.8. Constraints on control inputs are not active (fig. 6.9 and 6.10).
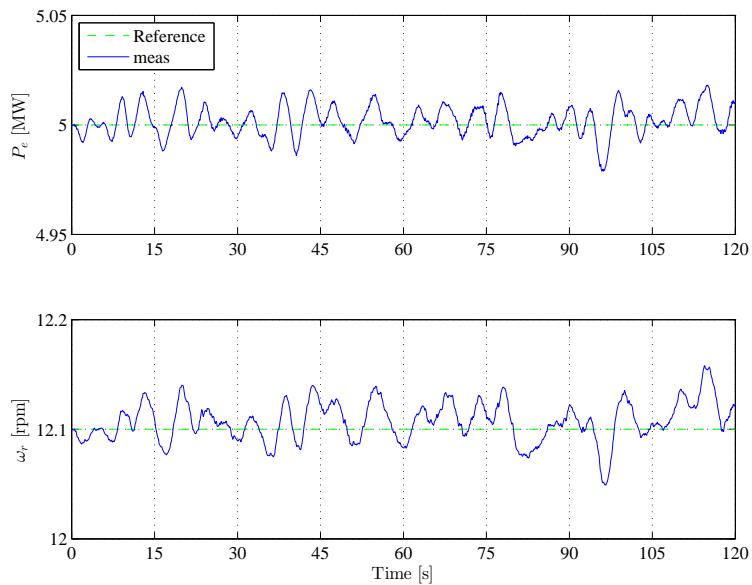
Figure 6.7: Measurements - P_e and ω_r
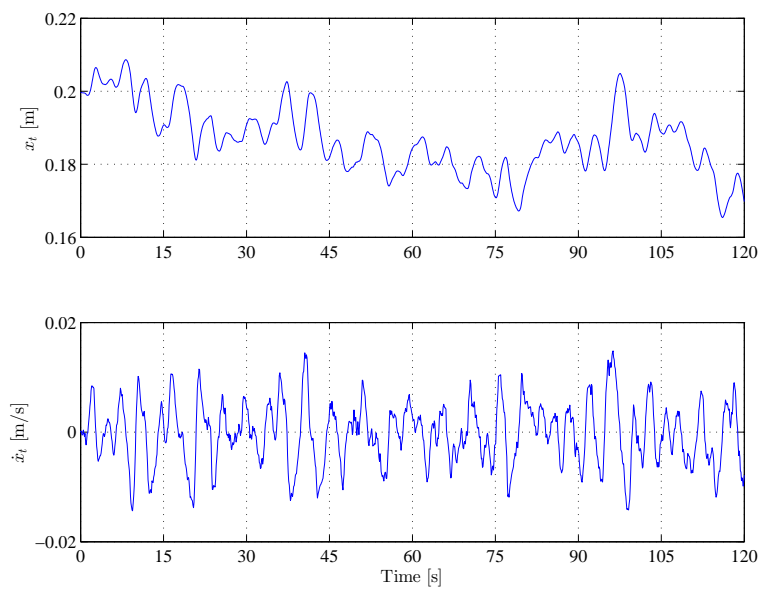
Figure 6.8: Tower for-aft movement
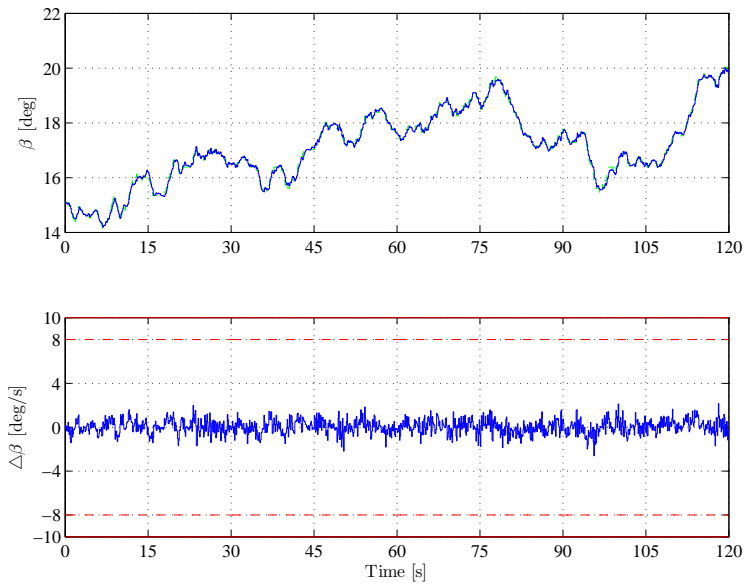
Figure 6.9: Pitch control action
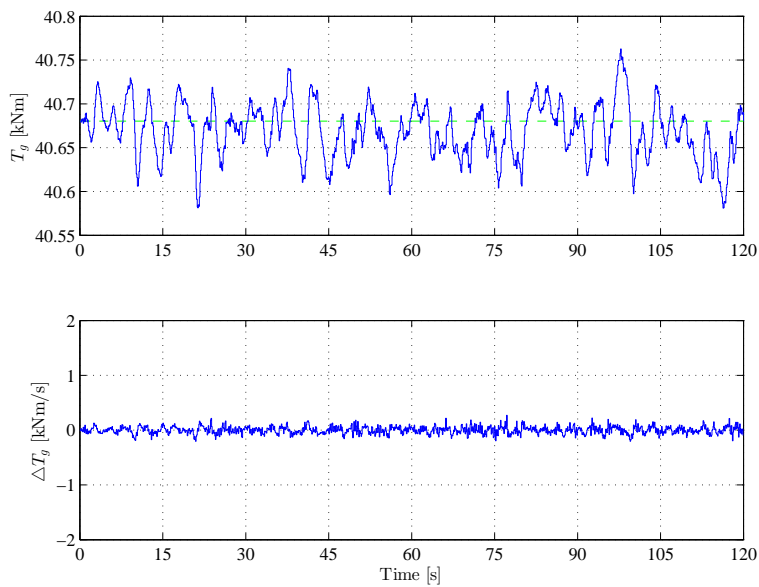
Figure 6.10: Generator torque control action

6.2 Frequency weighted MPC

In following section simulations with frequency weighted MPC will be shown. First effects of various filters on the performance will be explored. For this purpose deterministic wind speed profile, shown in previous section, is applied to the system. Comparison between FMPC and MPC is also shown.

6.2.1 Filters on control inputs

In general on inputs high-pass filters are considered. The argument for this is to penalize high frequencies at control activity. We also should have in mind, that introducing low-pass filter on input may move the closed loop system closer to stability margin, due to allowing high controller activity. As an example same low-pass and same high-pass filter is considered on pitch and also on generator torque.

(a) Low-pass filter   (b) High-pass filter
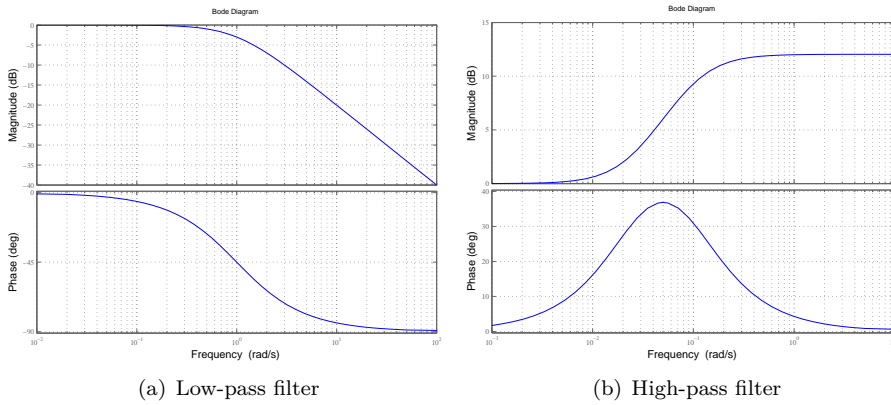
Figure 6.11: Frequency response of considered filters

Low-pass filter, with frequency response shown on figure 6.11(a):

$$H_{LP}(s) = \frac{1}{4s+1} \tag{6.1}$$

High-pass filter, with frequency response shown on figure 6.11(b):

$$H_{HP}(s) = \frac{20s+1}{4s+1} \tag{6.2}$$

Next set of figures shows the comparison of FMPC with low-pass and high-pass filters and with standard MPC controller. It must be noted, that filters only on inputs are considered so the tower oscillations are not damped. On figure 6.12 are shown measurements. Tower related states are shown in figure 6.13. Cyan color is used to show performance of the FMPC with low-pass filter on control inputs. Simulation of FMPC with high-pass filter is shown using magenta lines. Figures 6.14 and 6.15 shows the control inputs. By blue lines is shown the performance of the standard MPC controller. The differences of low-pass and high-pass filters are obvious. It must be noted, that no filter is considered for tower for-aft movement. Naturally this will poorly reflect on the overall result. But purpose of these simulations is to show the effects of different filters on inputs signals.
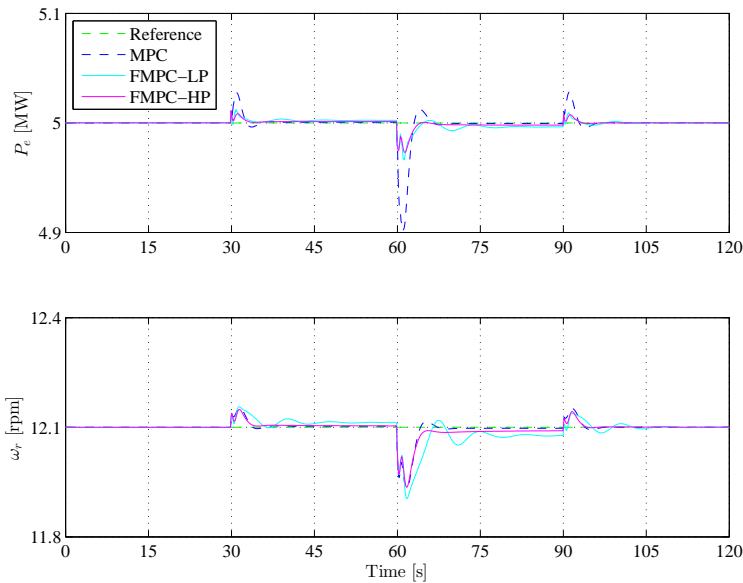
(a) Measurements - P_e and ω_r

Figure 6.12: Measurements - P_e and ω_r (low-pass and high-pass filter on inputs)
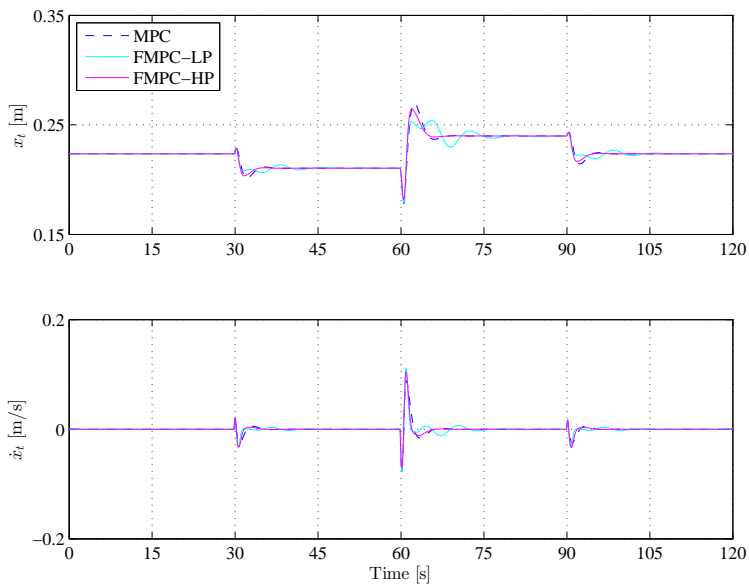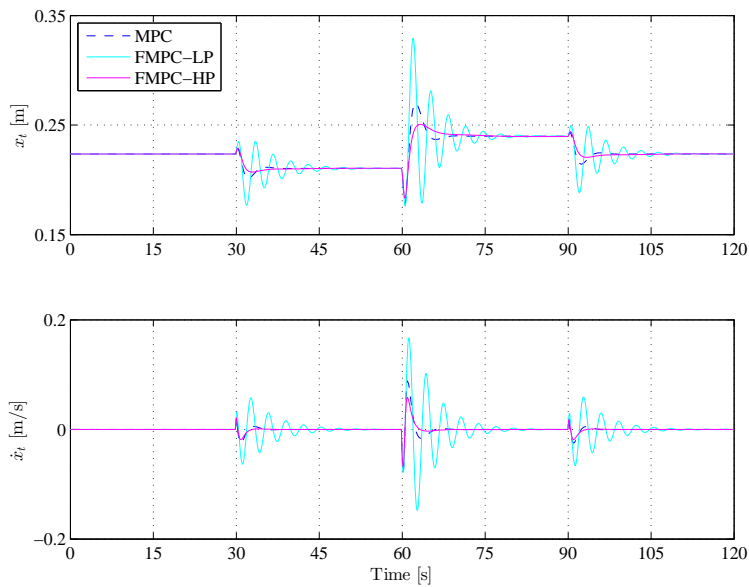
Figure 6.13: Tower for-aft movement (low-pass and high-pass filter on inputs)
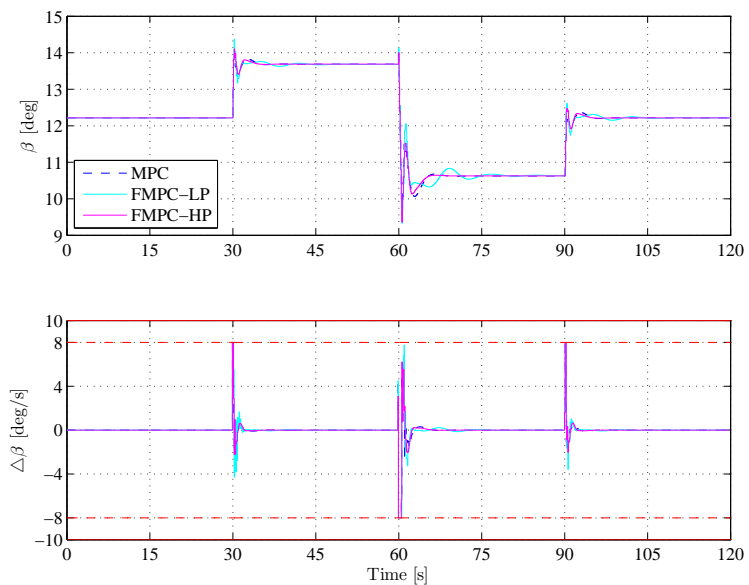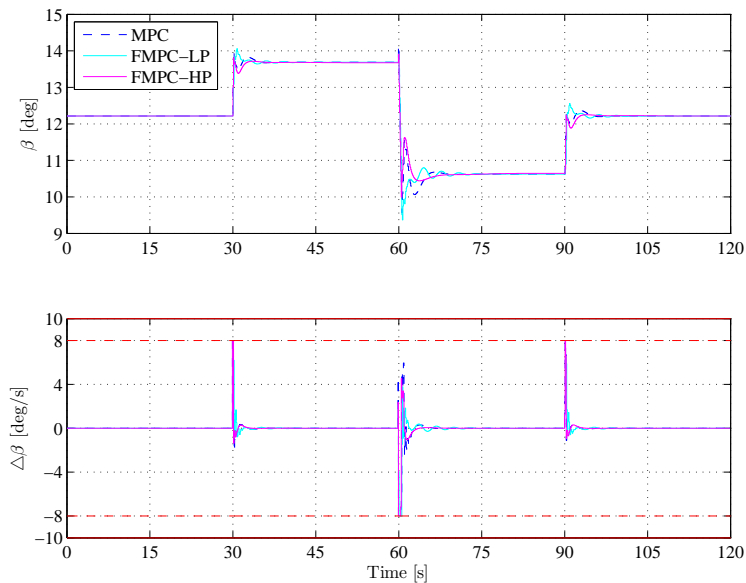

Figure 6.14: Pitch control inputs (low-pass and high-pass filter on inputs)
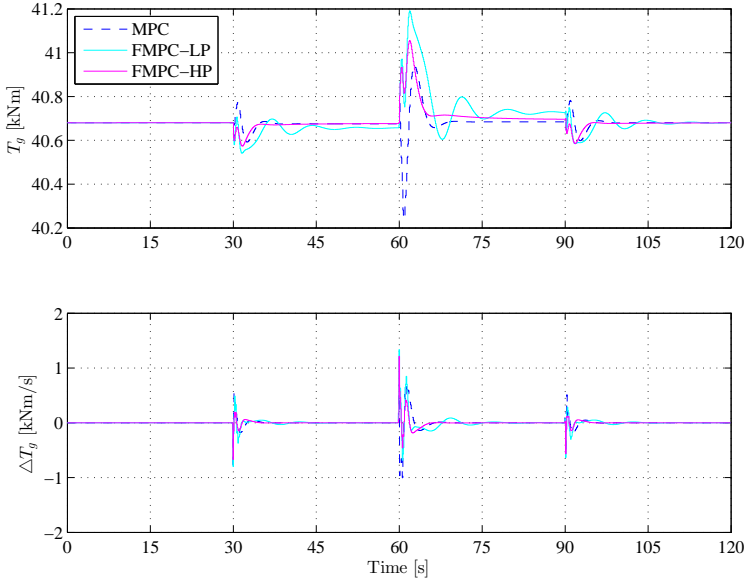
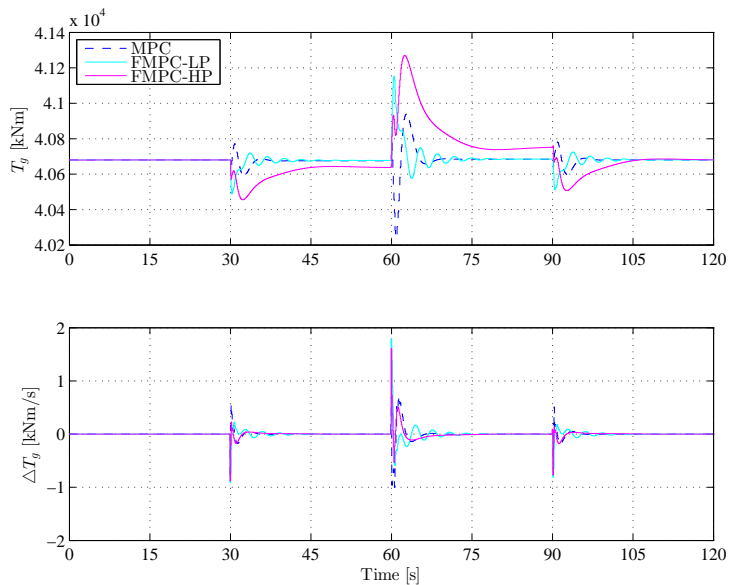**Figure 6.15:** Generator torque control input (low-pass and high-pass filter on inputs)

6.2.2   Filters on rotational speed and power

Effects of filters placed on rotational speed, or on the power output are barely noticeable in case of deterministic simulation. However in case of stochastic simulations, when all other filters are considered, low pass filters considered in case of rotational speed and power helped decrease the variance of the output by approximately 5 %. Due to this finding, low pass filters are considered in final tuning, as in was shown in chapter 5, which was devoted to tuning of the MPC controllers. One of the reason for this behaviour could be the simplicity of the model.

6.2.3   Filters on states related to tower movement

The main reason implementing frequency weighted MPC is to better handle the tower oscilations. For this purpose several types of filters are explored. Namely we consider low and high pass filters, but also band-stop and band-pass filters.

In the following set of simulations low-pass and high-pass filters on states related

to tower are considered (fig. 6.16). On the figure 6.17 we can see the effects on the measurements, and tower displacement. Comparison with standard MPC is also shown, so we can see the benefits of frequency tuning.

Low-pass filter, with frequency response shown on figure 6.16(a):

$$H_{LP}(s) = \frac{1}{4s + 1} \tag{6.3}$$

High-pass filter, with frequency response shown on figure 6.16(b):

$$H_{HP}(s) = \frac{8s + 1}{4s + 1} \tag{6.4}$$

(a) Low-pass filter   (b) High-pass filter
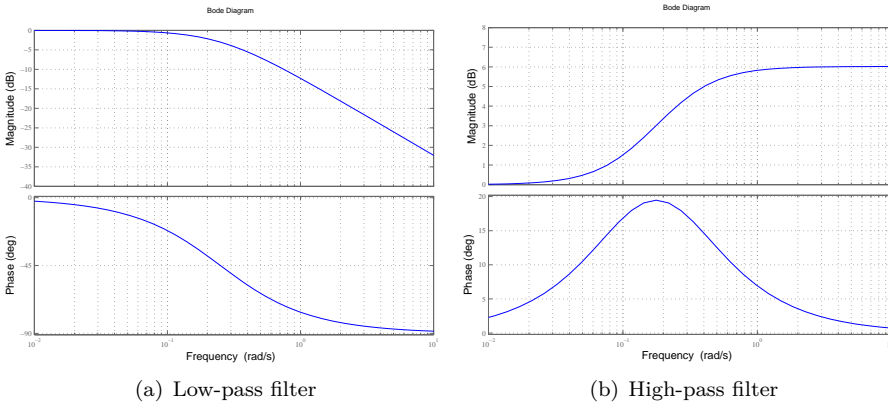
Figure 6.16: Frequency response of considered filters

Low-pass filter in this case has negative effect on the overall performance. Power and rotational speed is kept at theirs respective nominal values (fig. 6.17), while using low-pass filter, however the performance of the tower component is not satisfactory (fig. 6.18). Cyan lines are used to display performance with low-pass filter. On the other hand high pass filter introduce some minor offsets in measured power and speed of the turbine, but oscillations of the tower related states are significantly damped (magenta lines). The dashed (blue lines) shows performance using standard MPC control. Using FMPC with high-pass filter we can see improvement in contrast with MPC.Figures 6.19 and 6.20 shows the control inputs. We may notice, that in case of low-pass filter, oscillations occurs in the generator torque activity. This is cause by placing high weights in Q matrix for rotational speed and generated power in FMPC design. Constraints on pitch rate are active only when high pass filter is used. Generator torque rate is way below it's bounds in all cases. This is expectable, because the steady state values of generator torque does not change in top region.
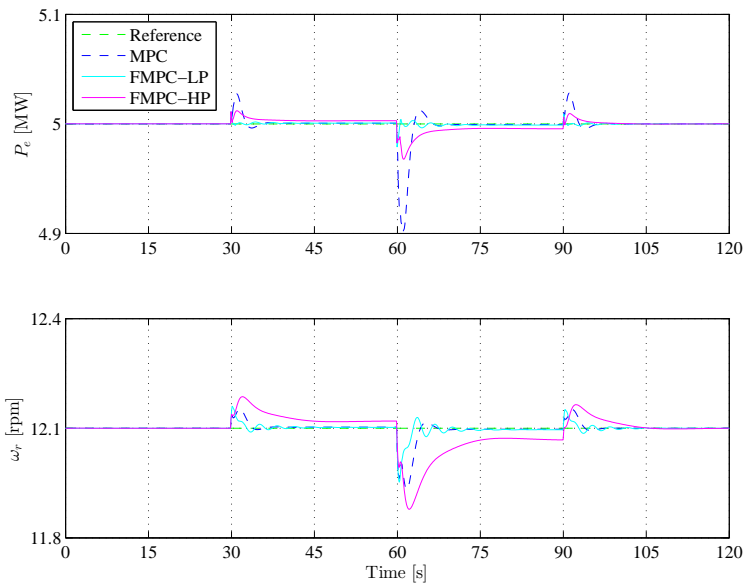
Figure 6.17: Measurements - P_e and ω_r (low-pass and high-pass filter on tower states)

Figure 6.18: Tower for-aft movement (low-pass and high-pass filter on tower states)

Figure 6.19: Pitch control inputs (low-pass and high-pass filter on tower states)

Figure 6.20: Generator torque control input (low-pass and high-pass filter on tower states)

Application of band-pass and band-stop filters with connection to the tower has been explored as well. Band-pass filter has similar effects as high-pass filter. Naturally band-stop filter will worsen the performance..

(a) Band-stop
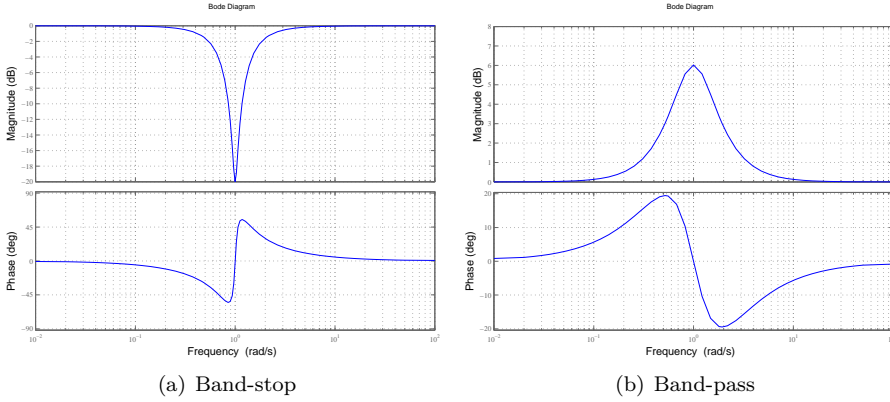
(b) Band-pass

Figure 6.21: Frequency response of considered filters

Band-stop filter, with frequency response shown on figure 6.21(a):

$$H_{BS}(s) = \frac{s^2 + 0.1s + 1}{s^2 + s + 1} \tag{6.5}$$

Band-pass filter, with frequency response shown on figure 6.21(b):

$$H_{BP}(s) = \frac{s^2 + 2s + 1}{s^2 + s + 1} \tag{6.6}$$

Introducing band-pass filter (magenta lines) managed to decrease the oscillations on the tower related states, however it also introduces minor offset in power and rotational speed (fig. 6.22 and 6.23). As it was indicated band-stop filter (cyan lines) did not damped the oscillations of the tower for-aft movement. Control activity is very similar, if not the same as using low-pass and high-pass filters instead of band-stop and band-pass filters (figures 6.24 and 6.25). It must be mentioned, that using higher order filters increases the complexity of the model, which may have negative effect on calculation time, especially when using MPC on-line calculation with long time horizons.
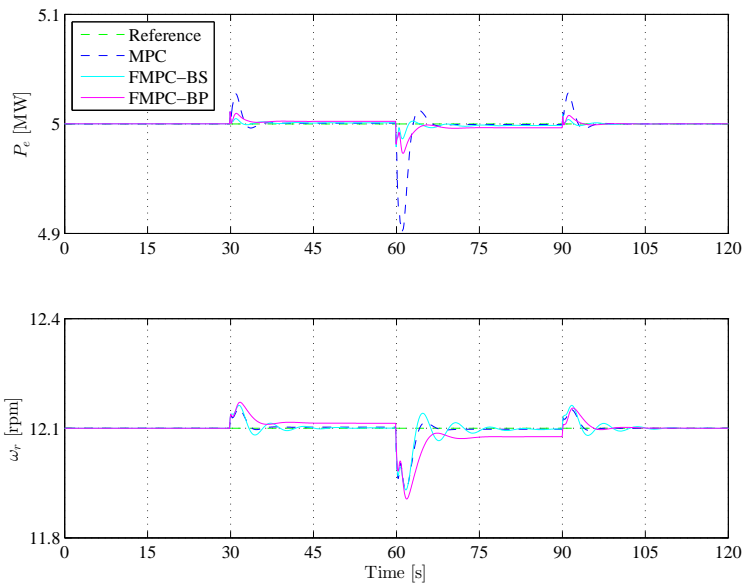
Figure 6.22: Measurements - P_e and ω_r (band-stop and band-pass filter on tower states)
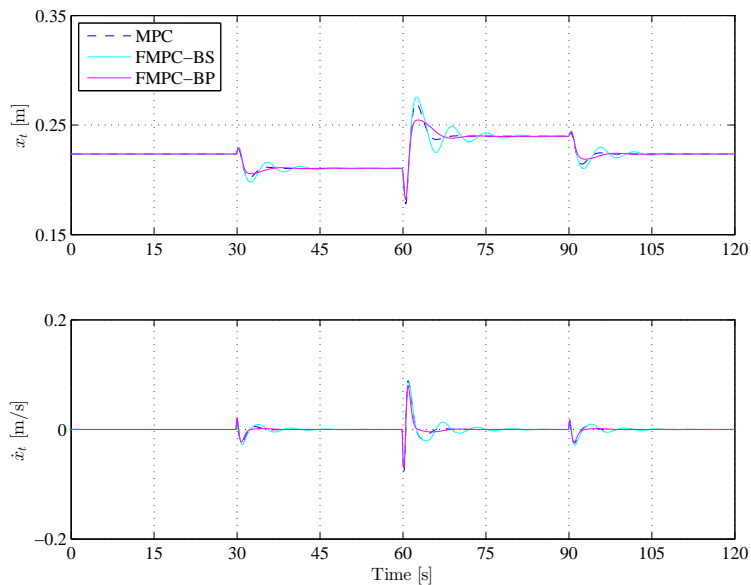
Figure 6.23: Tower for-aft movement (band-stop and band-pass filter on tower states)
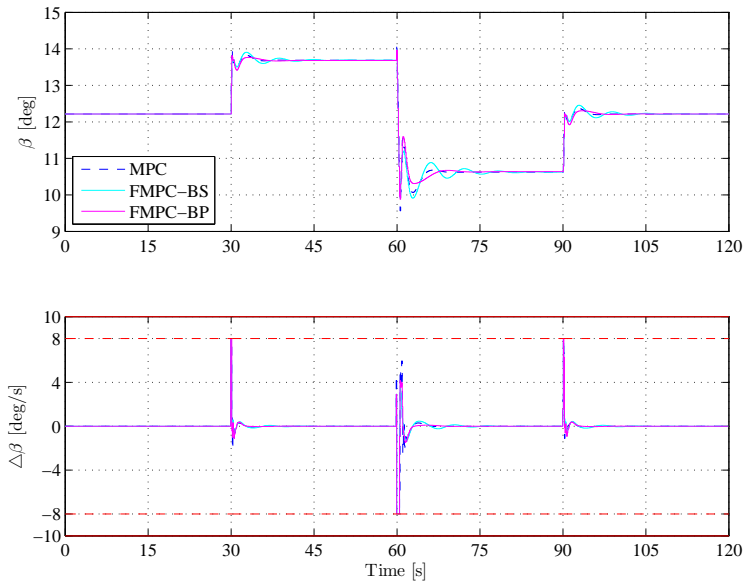
Figure 6.24: Pitch control inputs (band-stop and band-pass filter on tower states)
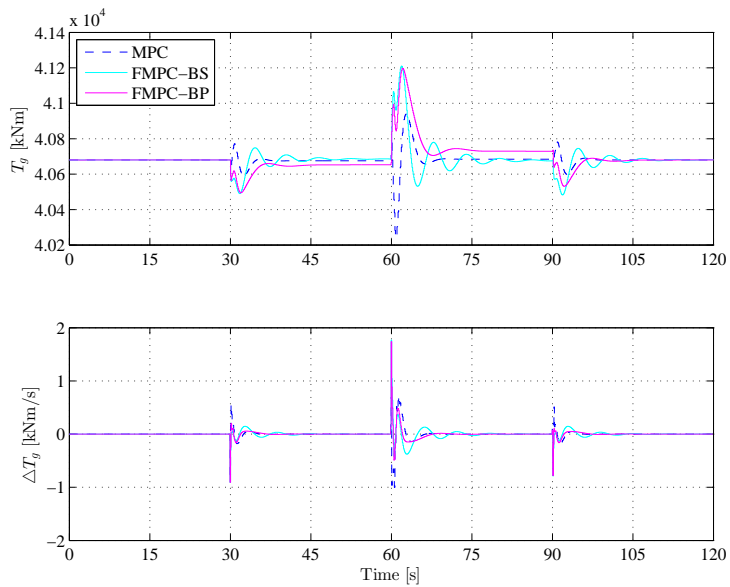
Figure 6.25: Generator torque control input (band-stop and band-pass filter on tower states)

6.2.4   Final tuning

Stochastic simulation has been performed with final tuning presented in chapter 5. As it was mentioned, low-pass filters are used on power output and measurement of the rotational speed, band-pass filters are considered on tower for-aft movement and high-pass filters are applied on control inputs. Wind speed profile applied to the system was shown in previous section (fig. 6.6).

Results are shown on following sets of figures. Comparison with standard MPC is made as well. Figure 6.26 shows the measurement of the rotational speed together with power generation. Notice slight increase in the variance of the rotational speed against standard MPC controller. On figure 6.27 notice, that tower oscilations are much more damped using FMPC controller than using standard MPC. Pitch control activity of FMPC is very similar to standard MPC (fig. 6.28), but high frequency activity is removed from generator torque control input (fig. 6.29). Such tuning on the generator torque action has been chosen due to the fact, that gearbox and drive train (which are not considered in this project) are very sensitive to high frequency changes in generator torque control activity. Last figure shows cumulative sum of control rates, often named as pitch travel (fig. 6.30). Slopes of pitch travel are very similar using both MPC and FMPC, but there is huge difference in slopes of cumulative sum of generator torque rate.
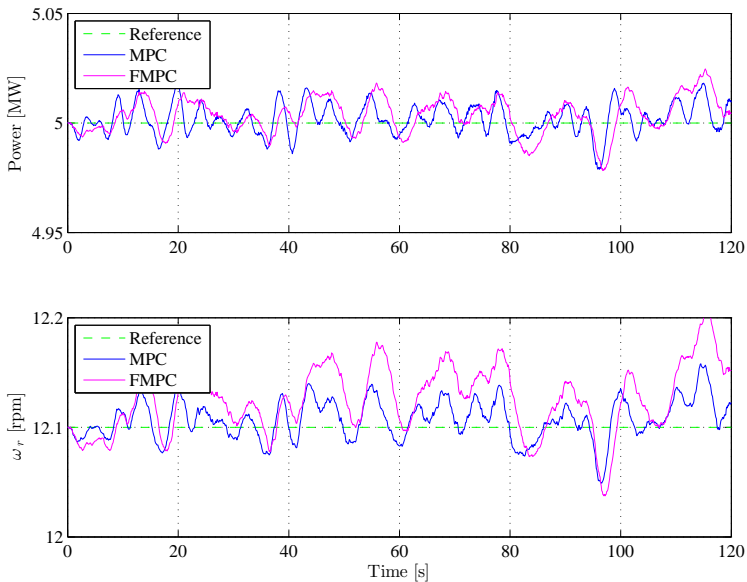
Figure 6.26: Measurements - P_e and ω_r (final tuning)
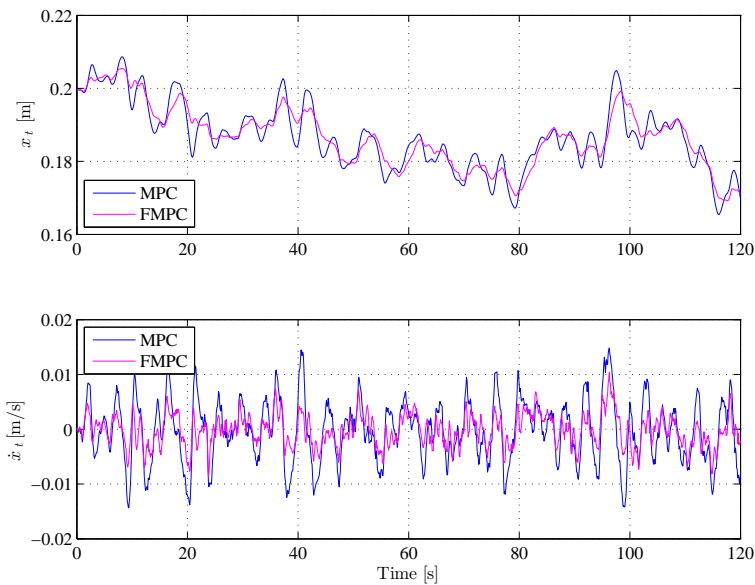
Figure 6.27: Tower for-aft movement (final tuning)
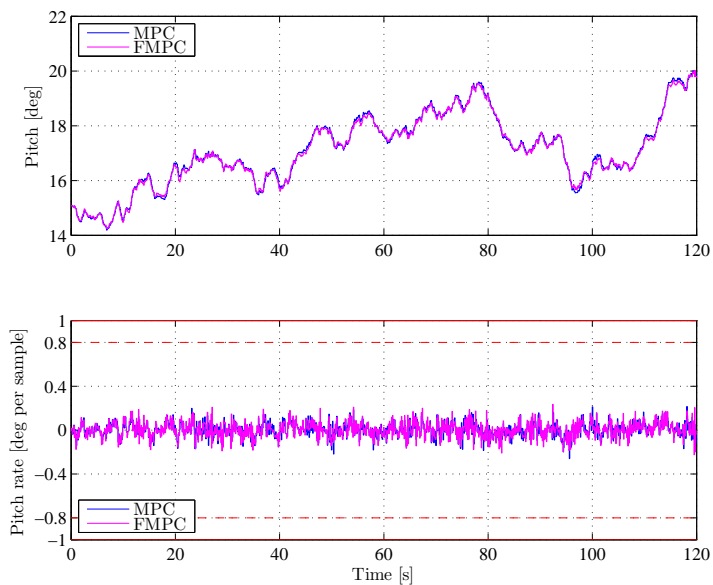
Figure 6.28: Pitch control inputs (final tuning)
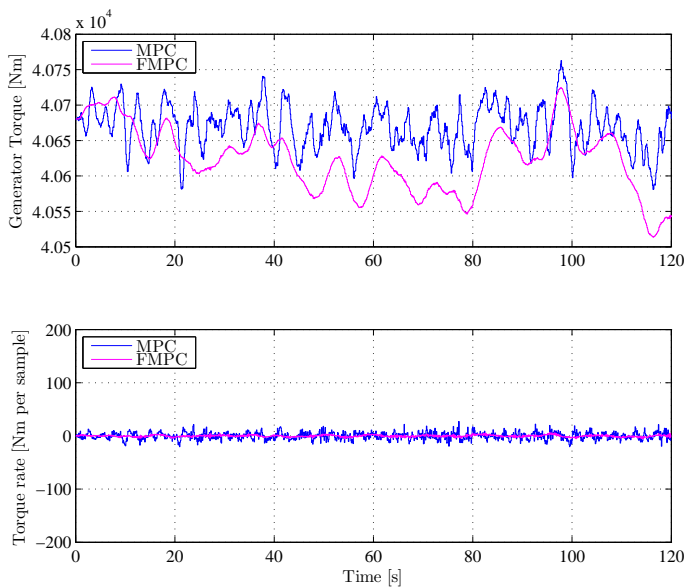
Figure 6.29: Generator torque control input (final tuning)
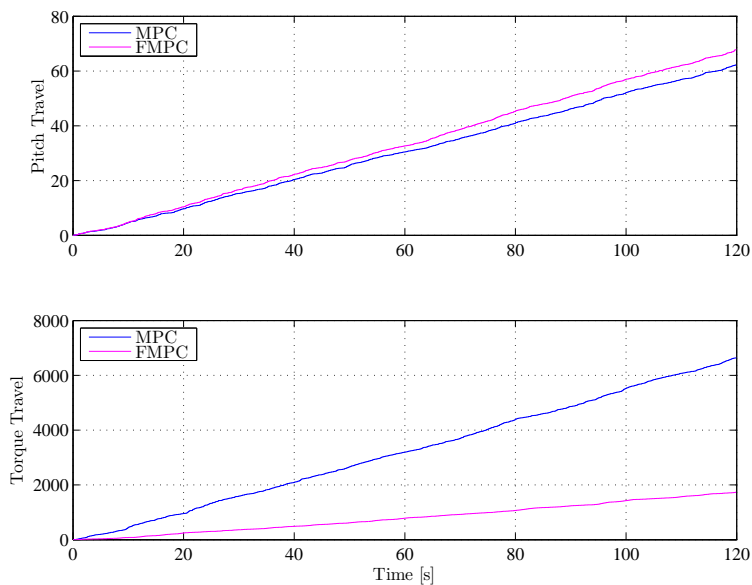
Figure 6.30: Cumulative sum of control moves (final tuning)

CHAPTER 7

Partial Load Simulations

In previous chapter attention was drawn to top region simulations. In this chapter the focus will be on partial load simulations (first three regions). Simulations are performed in each region separately. Stochastic simulations are performed between regions, so region switching is demonstrated. An overall simulations in all four regions is shown at the end of the chapter.

7.1 WT_0 model

Since controlling the wind turbine, is not a standard control problem, deterministic simulations with WT_0 model are made. Behaviour of the system will be demonstrated without any interference from tower for-aft movement or from stochastic influences in the wind speed.

7.1.1 Simulations in R-I

The objective of the controller in the region number 1, is to maintain the rotational speed at it's minimum speed, which is 6.9 rpm. Generated electrical power P_e is maximized. Wind speed profile applied to this system is shown on

figure 7.1, the estimation of the wind speed is shown as well. Measurements are shown on figure 7.2, in which we can see, that the rotational speed is maintained at its minimum speed, as well as the power is maximized. Green lines on these figures indicate the theoretical, or stationary values for actual wind speed. Figures 7.3 and 7.4 shows the calculated pitch action and generator torque. The pitch rate is well within limits, however constraints on generator torque rate are active.

Notice some oscilations in rotational speed and power output, when step in wind speed is made from 4.5 to 5.5 m/s. There is small overshoot in the estimation, and region 2 is reached. Once this happen, reference of the rotational speed is set to increase linearly with wind speed (region 2 control objective). However, when the wind speed estimation settles down to its value, tuning for region 1 takes place.
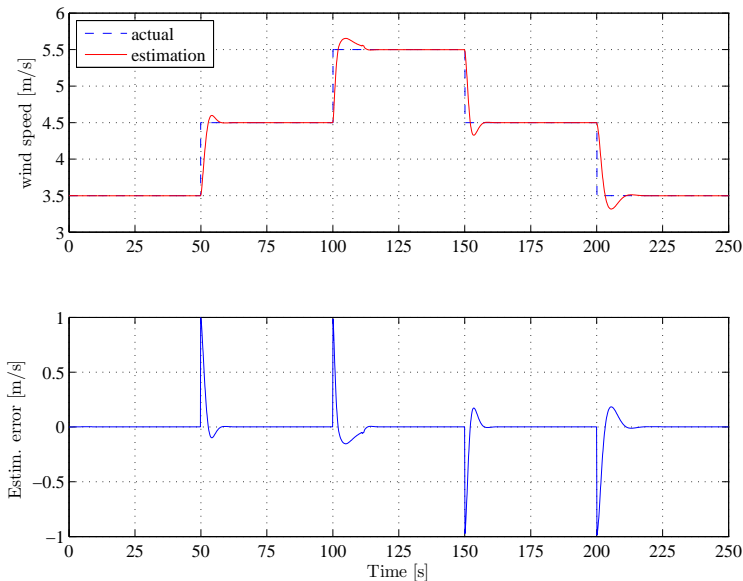
Figure 7.1: Deterministic wind speed profile - Region 1
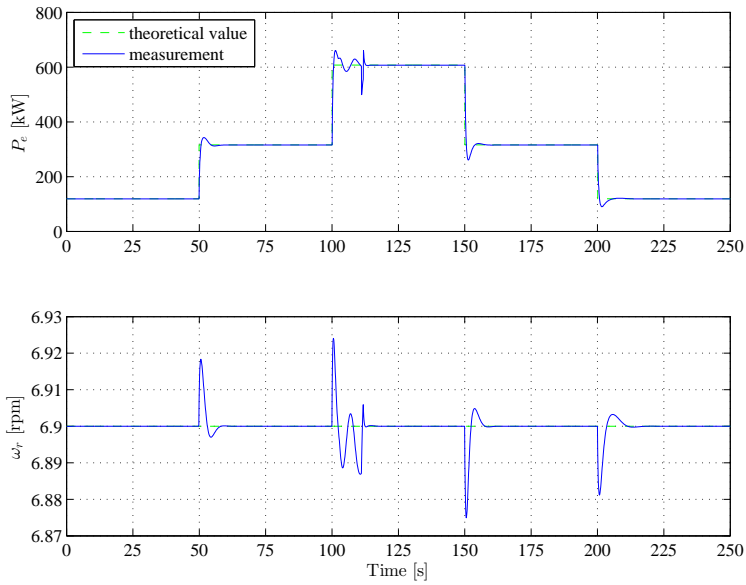
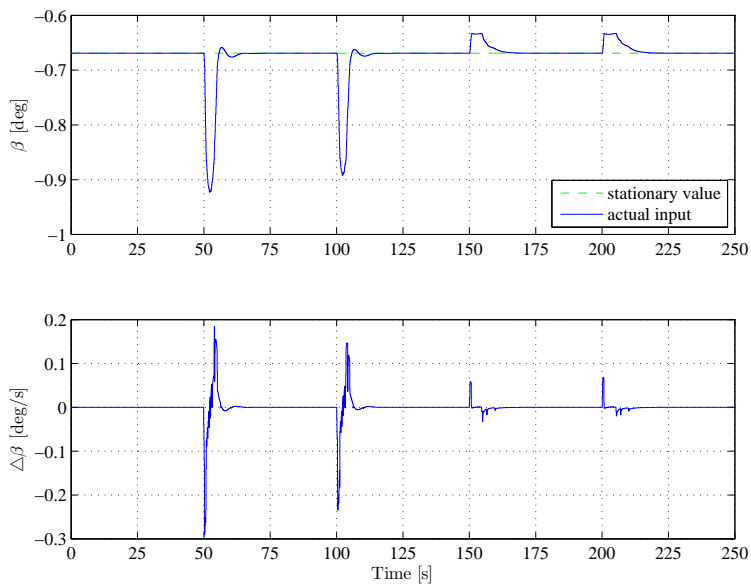**Figure 7.2:** Measurement of generated power and rotational speed of rotor
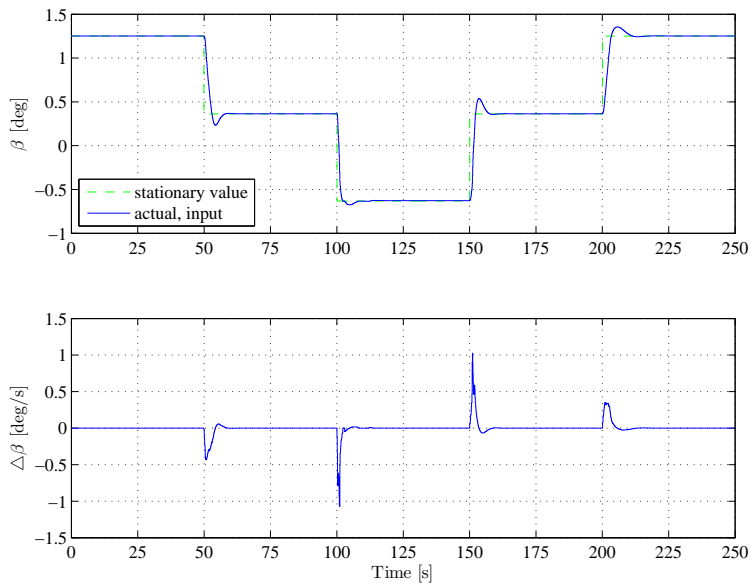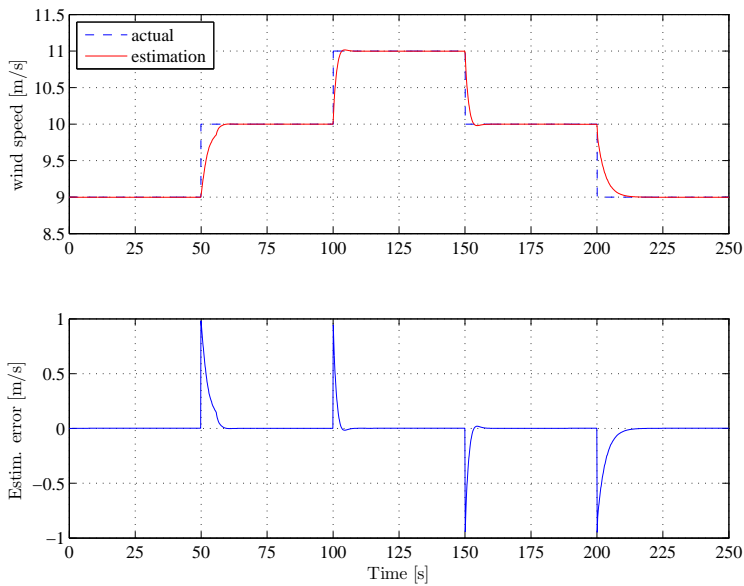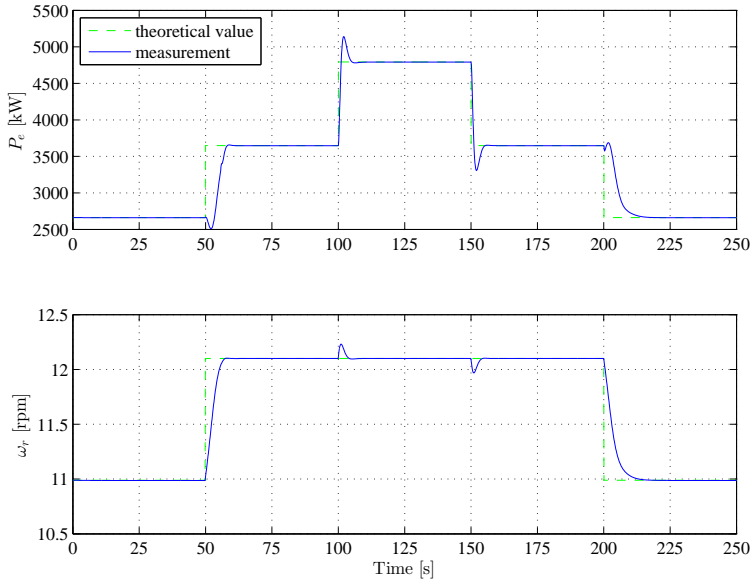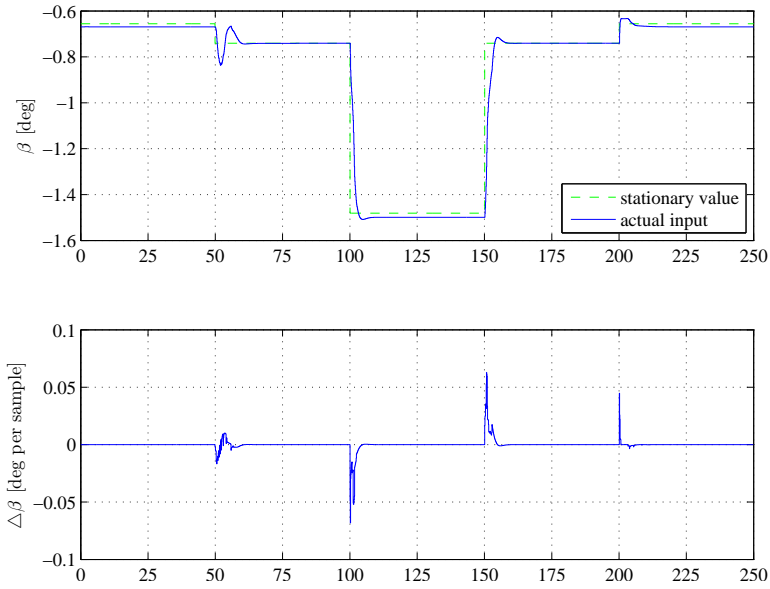


Figure 7.3: Pitch control input
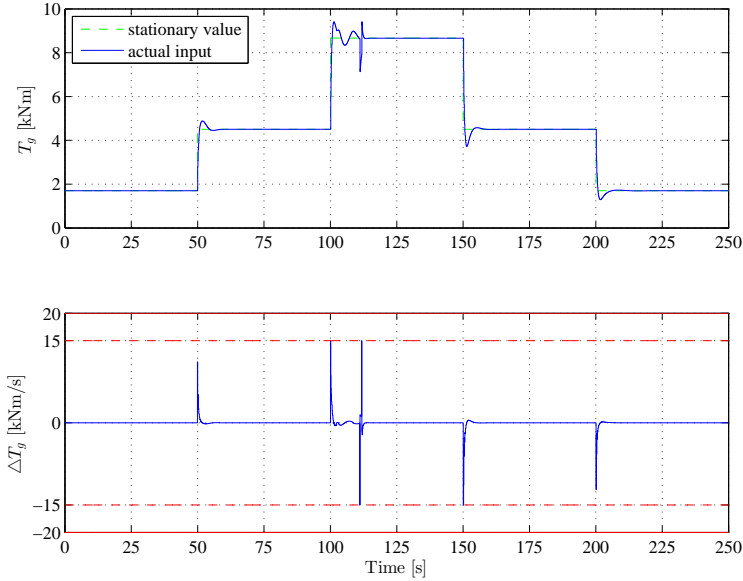
Figure 7.4: Generator torque control input

7.1.2 Simulations in R-II

In case of region number 2, main task is still to maximize power output, but the rotational speed isn't fixed like in region 1, but rise linearly with wind speed. This is achieved by setting the reference to the MPC based on wind speed estimation. Measurements are shown on figure 7.6. Notice power drops, when wind speed increases. Justification for this behaviour lies in formerly mentioned differential equation 7.1, which describes the changes in angular velocity of the rotor. From this we can understand, that if the wind speed increases, and the rotor speed must increase accordingly, generator action must be lowered 7.8. After such control action the kinetic energy of the wind will accelerate the rotor. Steady state value for the entire mid region for the pitch value is constant $\beta \approx -0.68 \ deg$, but in order to make the power extraction more efficient, calculations for the pitch angle are made as well (this was explained in refch:hawt). Pitch control action is shown in figure 7.7, followed by generator torque input 7.8.

$$J\dot{\omega}_r = \frac{P_r}{\omega_r} - NT_g \tag{7.1}$$
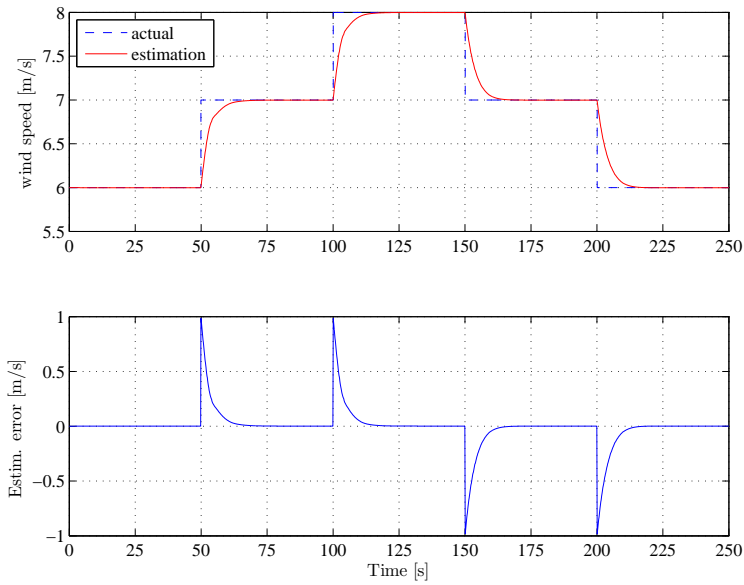
Figure 7.5: Deterministic wind speed profile - Region 2
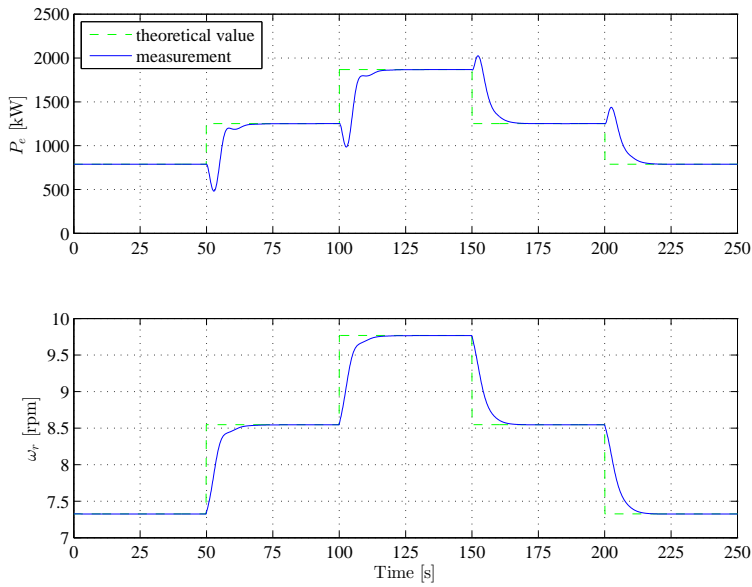
Figure 7.6: Measurement of generated power and rotational speed of rotor

Figure 7.7: Pitch control input
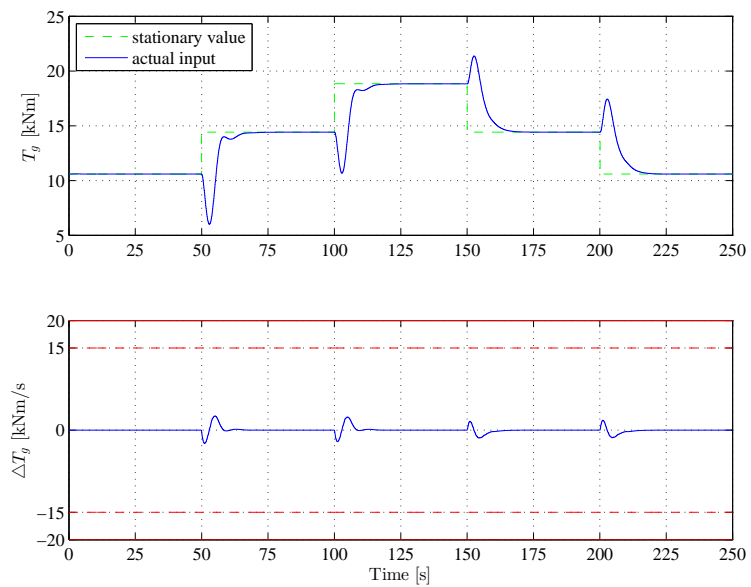
Figure 7.8: Generator torque control input

7.1.3 Simulations in R-III

Control performance in region number 3 is very similar to region number one. Nominal angular velocity of the rotor is reached (12.1 rpm), but the objective of maximizing the power still stands. Due to the fact, that this region is quite narrow compare to regions 1 and 2, simulation start at wind speed equal to 9 m/s, which is in the mid region (fig. 7.9). Measurements are shown in figure 7.10. In this simulation constraints are not active (fig. 7.12 and 7.11).

Figure 7.9: Deterministic wind speed profile - Region 3

Figure 7.10: Measurement of generated power and rotational speed of rotor

Figure 7.11: Pitch control input
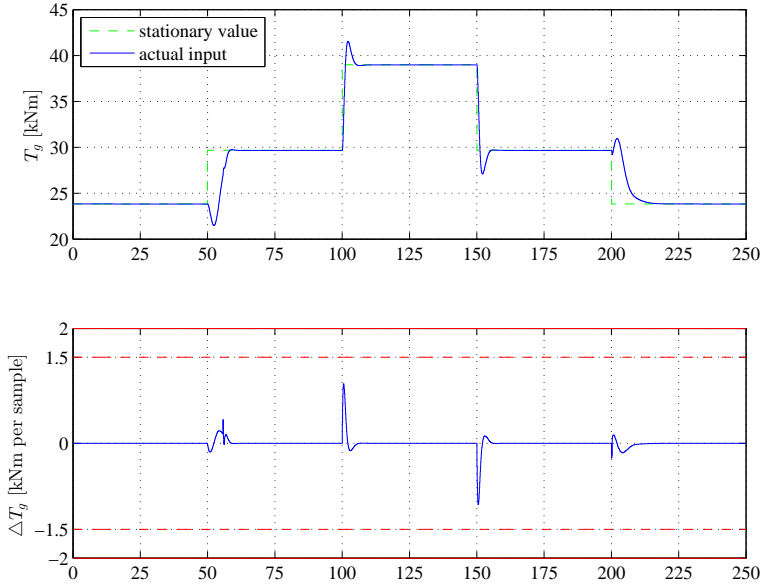
Figure 7.12: Generator torque control input

7.2 WT$_1$ model

Once the behaviour of the turbine in partial load is explained, attention can drawn to simulations with WT$_1$ model. Stochastic simulations are performed, in which mean wind speeds have been chosen precisely at wind speeds which defines particular regions. This servers as a demonstration of region switching controller.

7.2.1 Simulation between R-I and R-II

First simulation with wind speed profile with mean value is 5.6 m/s is performed (fig. 7.13). On figure 7.14 is shown when the region shift occurs. Since the regions switching is based on the estimation of the wind speed, there some minor delays occurs opposite to actual wind speed. This region switching is very easily observable on figure 7.15, which shown rotational speed besides power output.

Tower for-aft displacement along speed of the displacement is shown in figure 7.16. Control inputs are presented in figures 7.17 and 7.18. No constraints are active.
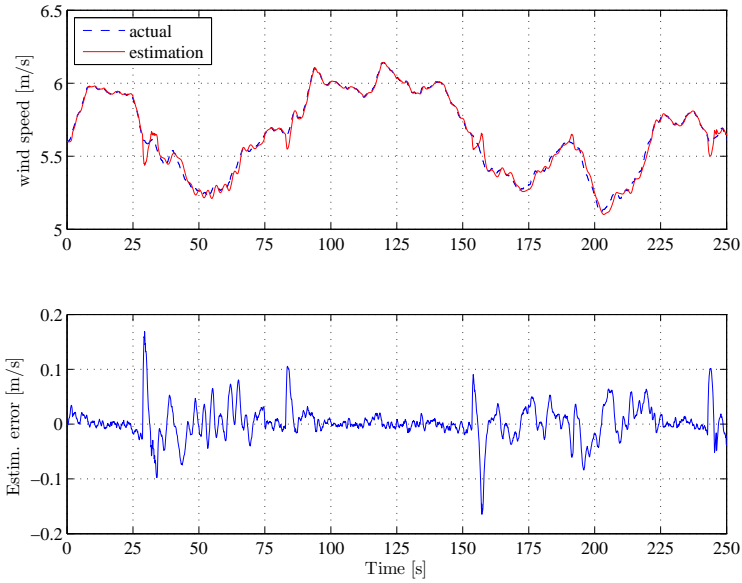
Figure 7.13: Stochastic wind profile R-I/II
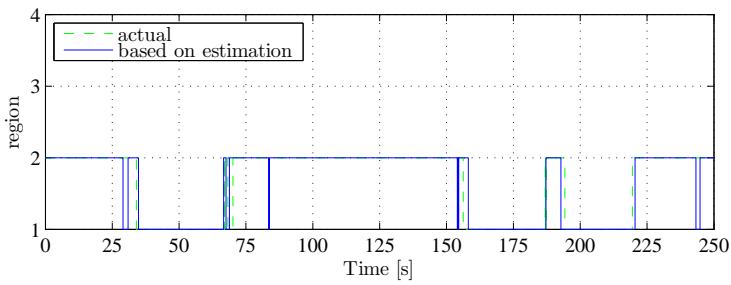
Figure 7.14: Region switching in partial load
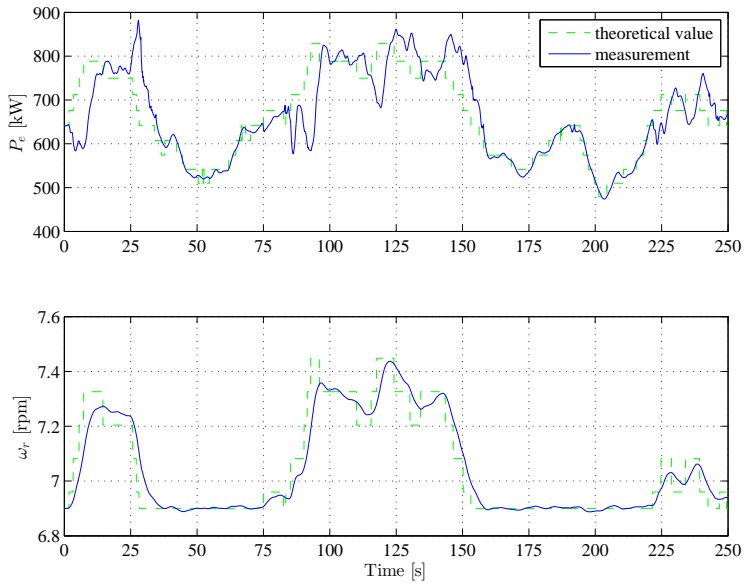
Figure 7.15: Measurement of generated power and rotational speed of rotor
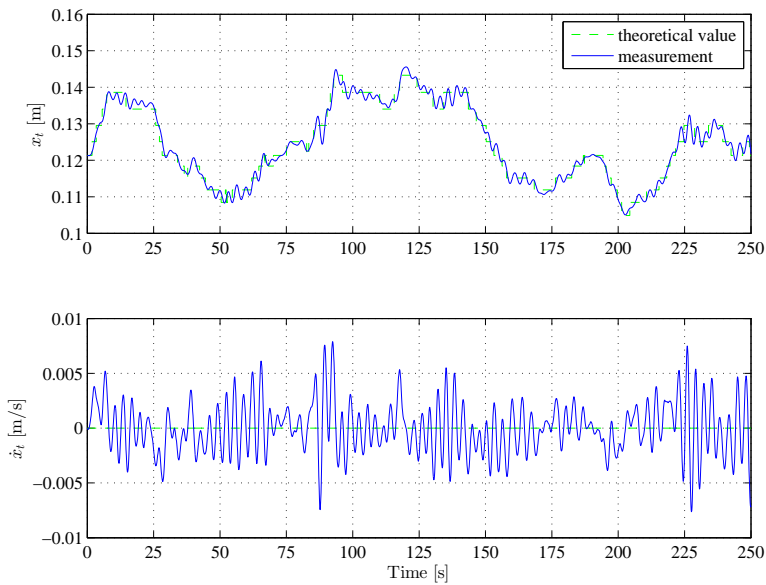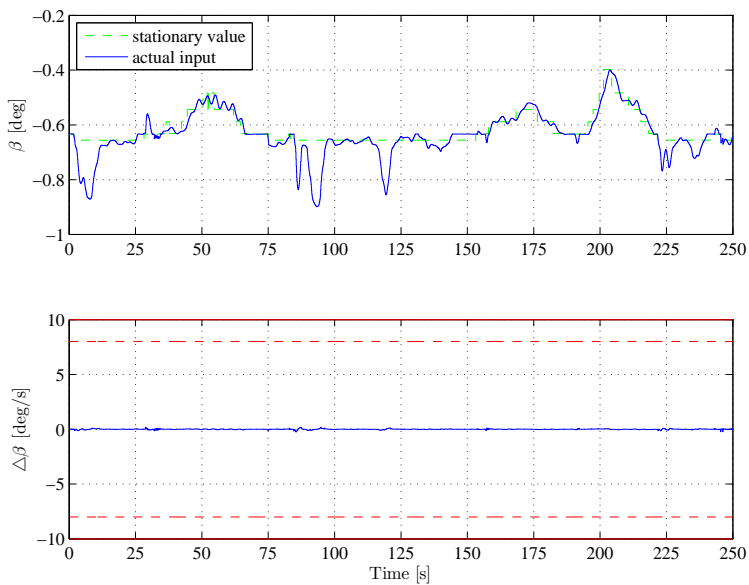

Figure 7.16: Tower displacement
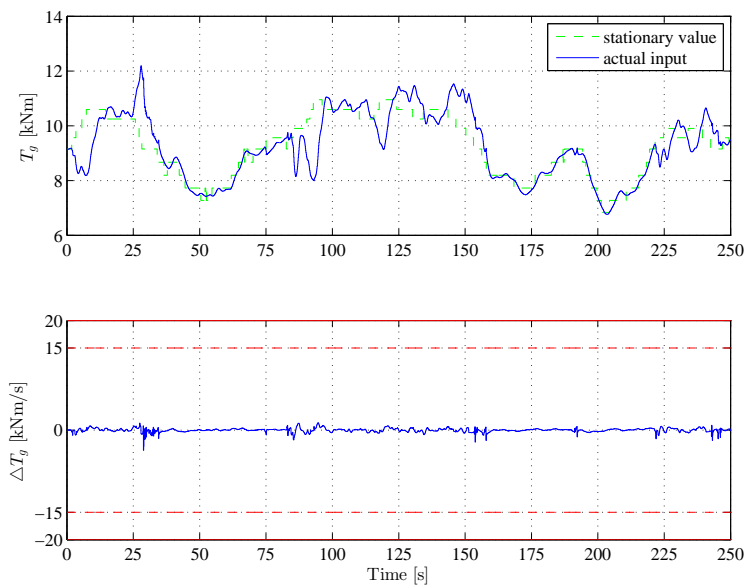
Figure 7.17: Pitch control input

Figure 7.18: Generator torque control input

7.2.2 Simulation between R-II and R-III

Stochastic wind speed profile with mean value of 10 m/s has been generated in order to perform simulation between region 2 and 3 (fig. 7.20). Notice, increased variance of the noise. Region switching is shown on figure 7.19. Since the region number 3 is narrow, and due to the increased variance of the noise, region 4 is reached for brief period of time.
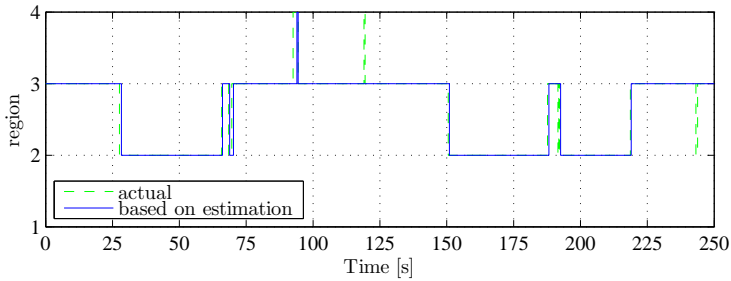
Figure 7.19: Region switching in partial load

Notice similar behaviour in the rotational speed, like in previous sets of simulations. In the R-III the rotational speed is kept at its nominal value, but when falling down to region 2, reference for the ω_r is set according to wind seed estimation (fig. 7.21). At time instances, when region is switched from R-II to R-III, power drops occurs. Reason for this is, that rather high weighting factor is placed on the ω_r control, and once the rotor is accelerated to nominal value, generator torque action (fig. 7.24) must be lowered for short time, so angular speed of 12.1 rpm can be maintained. Pitch values (fig. 7.23) are again calculated, so power output is maximized.
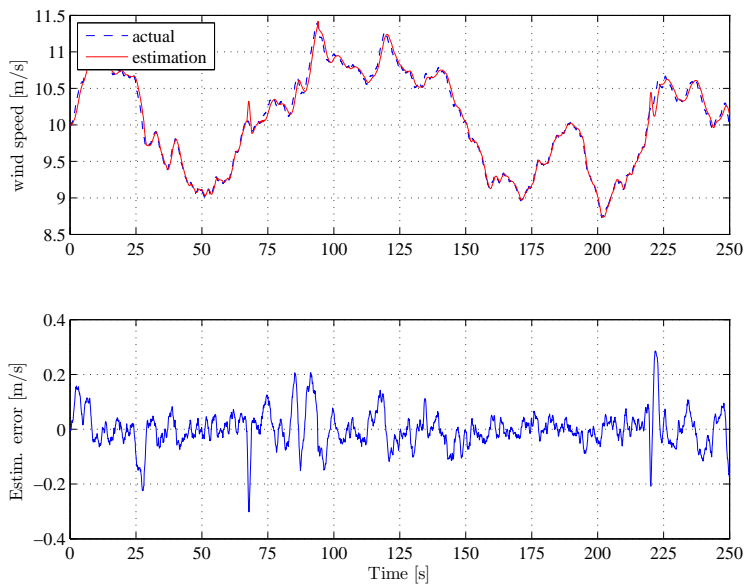
Tower for-aft movement is presented in figure 7.22.
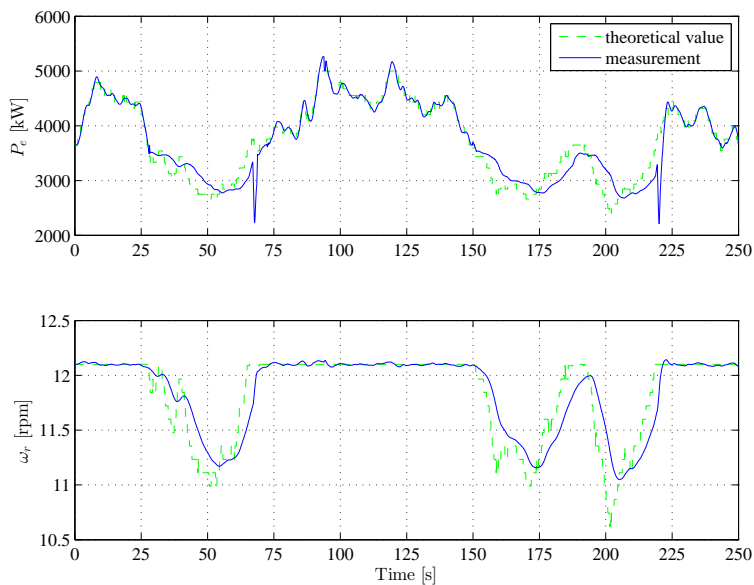
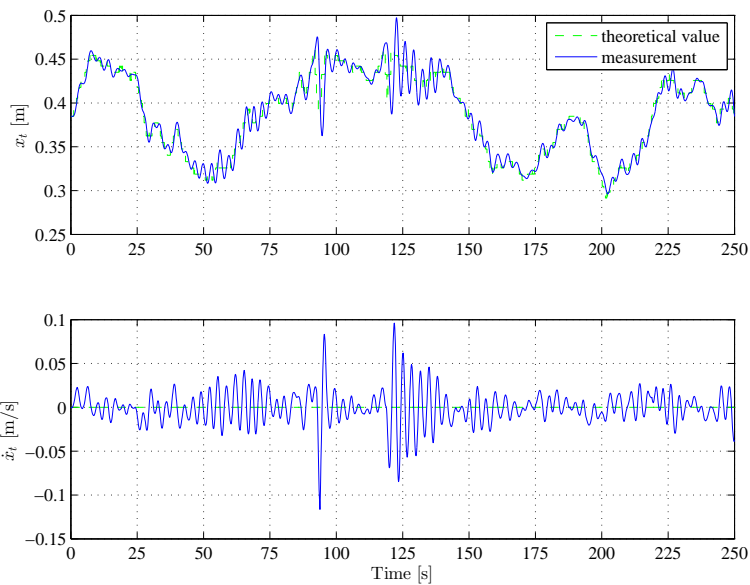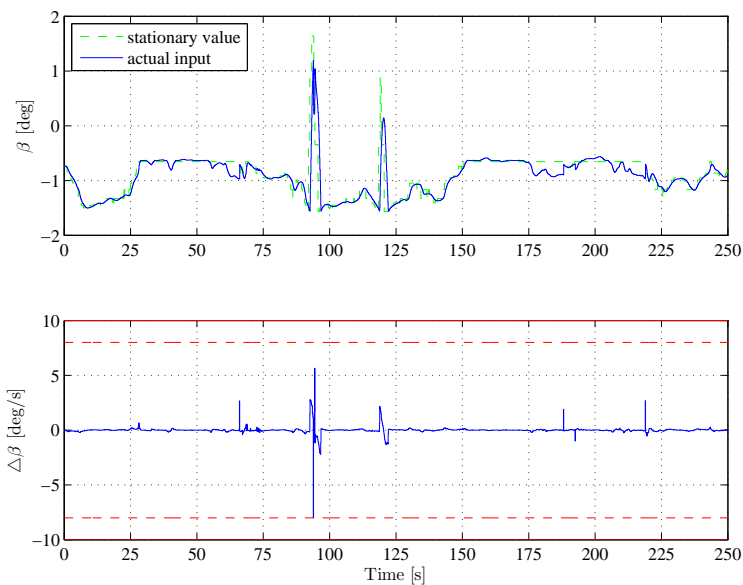**Figure 7.20:** Stochastic wind profile R-II/III

Figure 7.21: Measurement of generated power and rotational speed of rotor

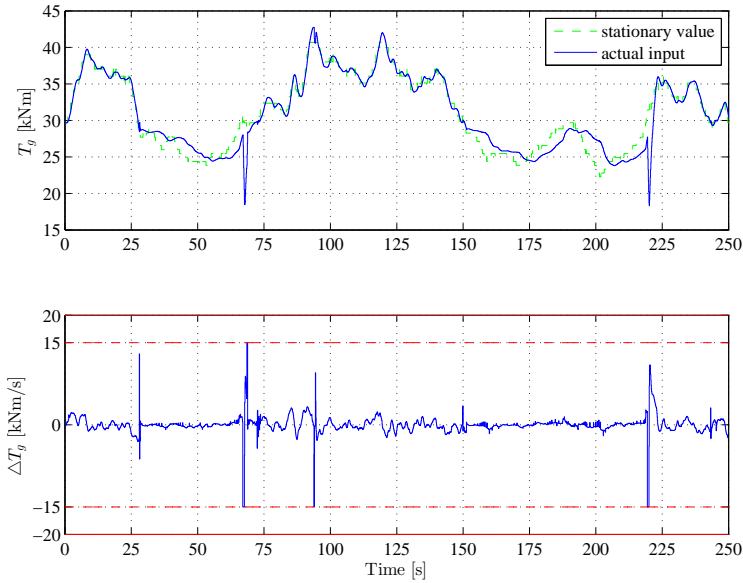**Figure 7.22:** Tower displacement

Figure 7.23: Pitch control input

Figure 7.24: Generator torque control input

7.2.3 Simulation between R-III and R-IV

Particular effort has been placed in tuning the controller at wind speed around critical wind speed 11.2 m/s. Reason for this is, that most of the wind speed conditions at nacelle hub height occurs precisely in the high region, and in the beginning of the top region. Such wind profile is shown in figure 7.25. How the regions change in this simulations is presented in 7.28.

Rotational speed is kept at its nominal value, even when short drop to R-II occurs (fig. 7.27). Region switching can been noticed on power output, which is dropping when, wind speed drops below 11.2 m/s. Rather rapid decrease of speed of the tower for-aft movement can be observed when top region is reached (fig. 7.28). In top region, controller has access to both inputs. Specially in this case, MPC controller with input constraints prove to be a good choice of a control strategy, because the constraints on both control signal are active, mainly when region switching occurs (figures 7.29 and 7.30). Also notice, that there is slight violation of the constraint on pitch rate at time $t \approx 220s$, where shift from R-III to R-IV occurs - this is a demonstration of the algorithm with different penalty on slack variable. High penalty was placed at generator torque rate slack, so this limit is not crossed.
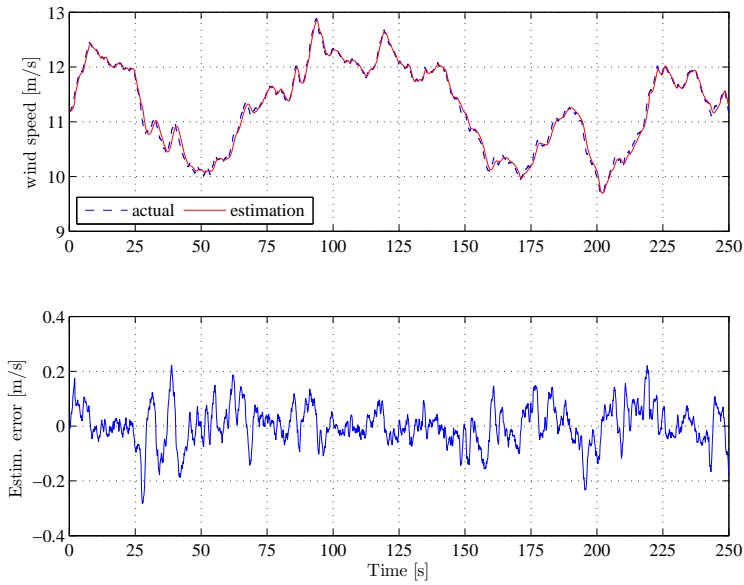
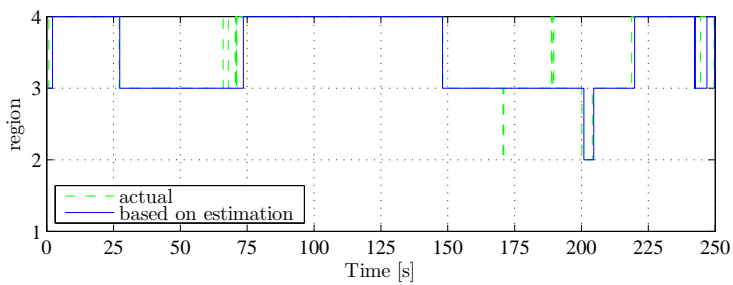**Figure 7.25:** Stochastic wind profile R-III/IV
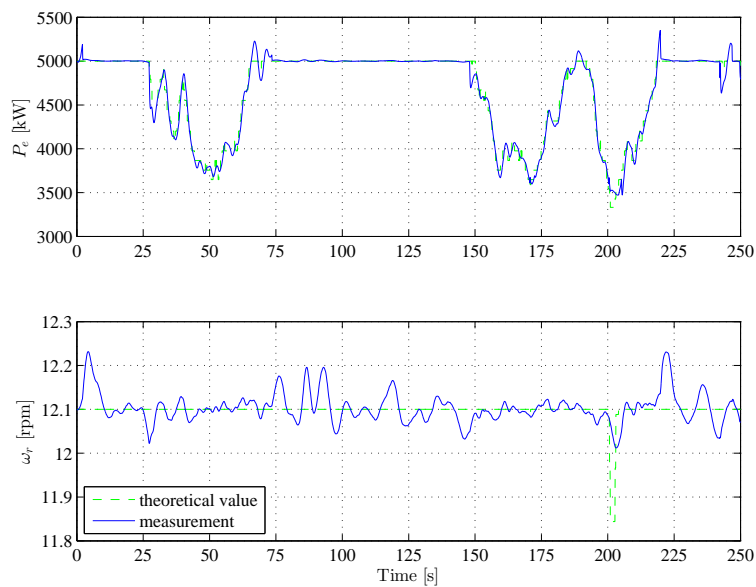

Figure 7.26: Region switching in partial load

Figure 7.27: Measurement of generated power and rotational speed of rotor
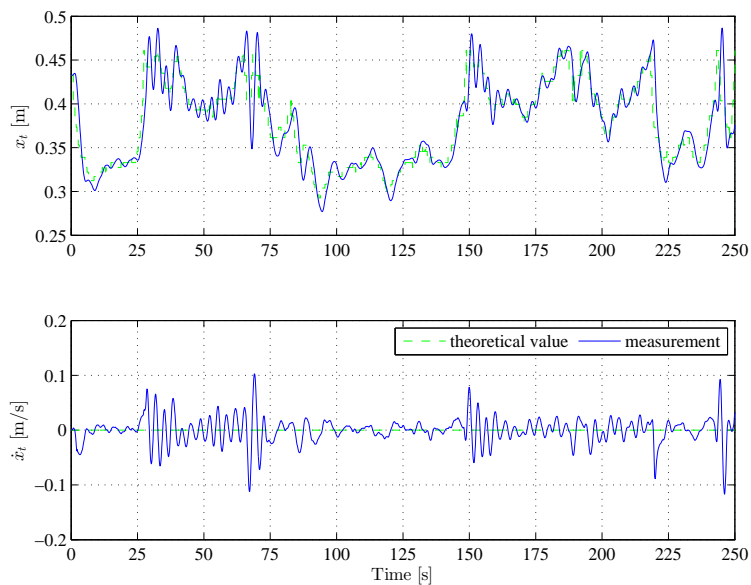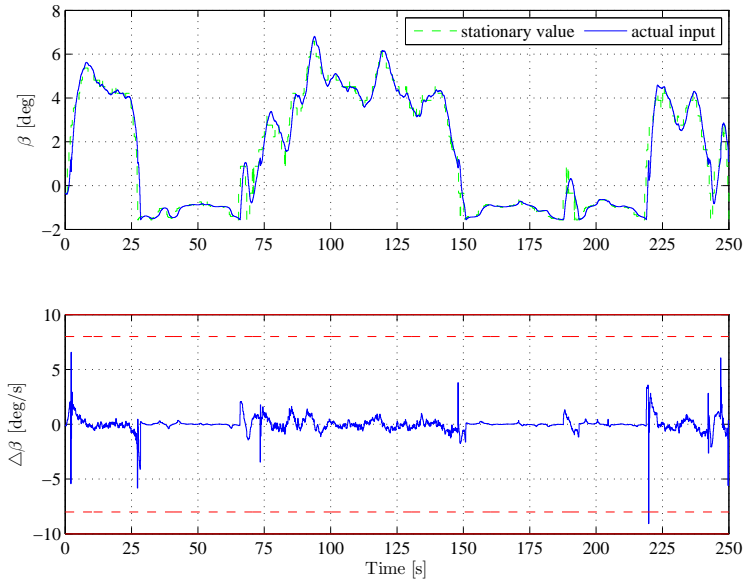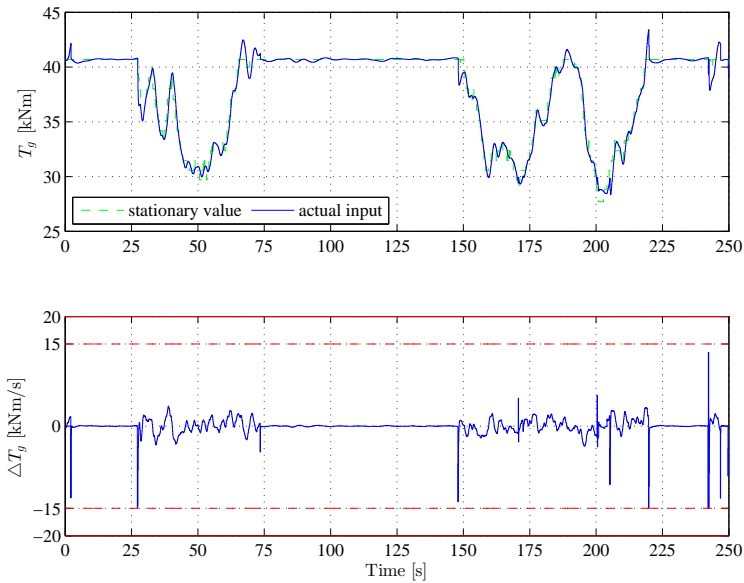

Figure 7.28: Tower displacement

Figure 7.29: Pitch control input

Figure 7.30: Generator torque control input

7.2.4   Overall Simulation

Last sets of figures shows an overall simulation, when the wind speed is varying from region 1 to region 4 (fig. 7.31). Which region is active at what time instance is shown on figure 7.32. Figures with measurement together with tower for-aft movement follows after that (fig. 7.33 and 7.34). Control signals are shown on figures 7.35 and 7.36. Notice that constraints are active when the regions are changes, specifically between R-III and R-IV.
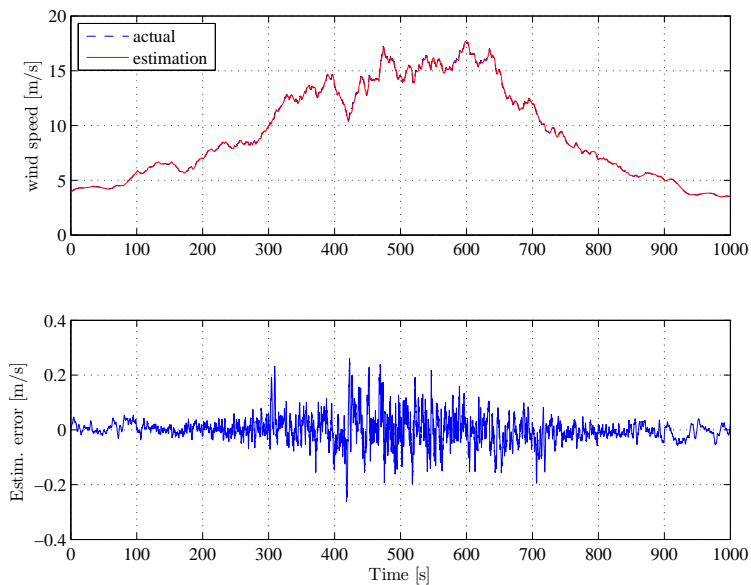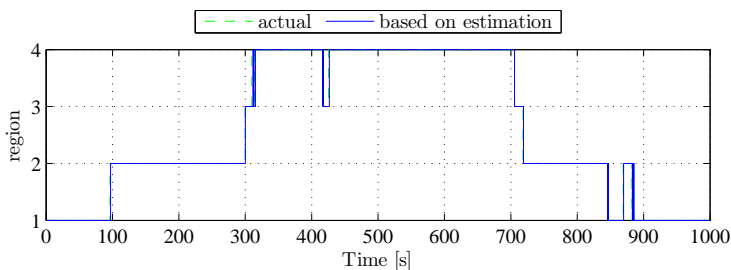

Figure 7.31: Stochastic wind profile

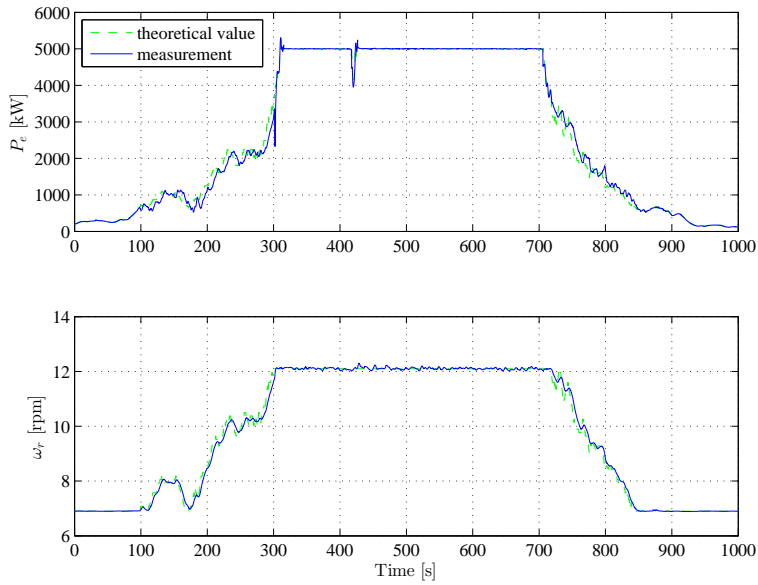**Figure 7.32:** Region switching in partial load

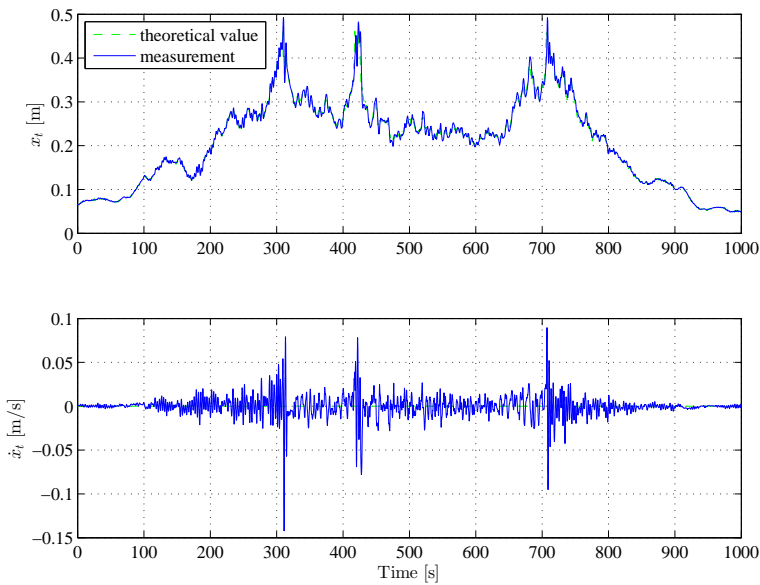**Figure 7.33:** Measurement of generated power and rotational speed of rotor
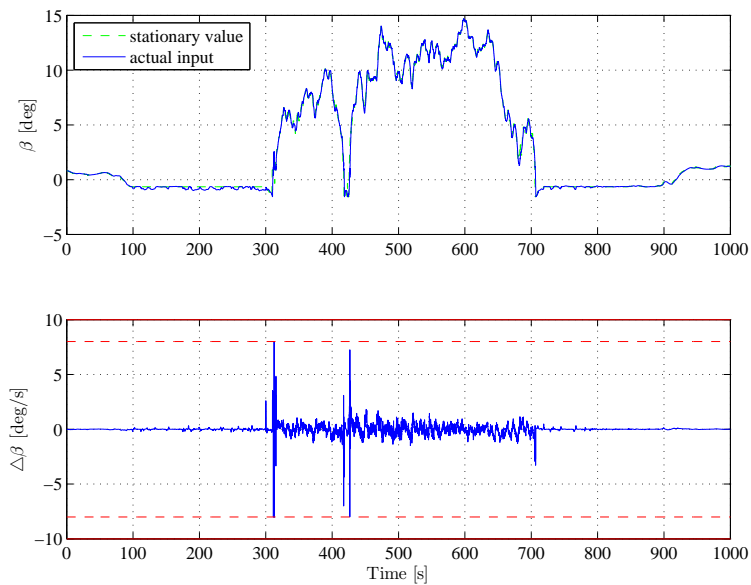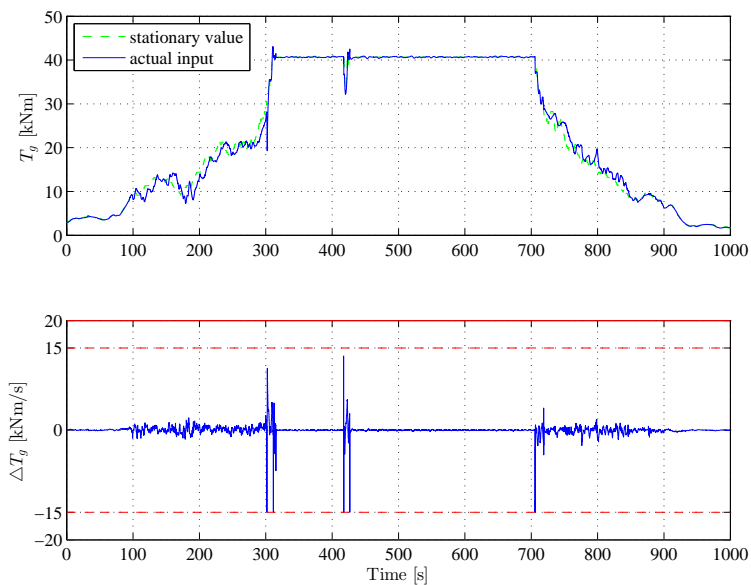

Figure 7.34: Tower displacement

Figure 7.35: Pitch control input

Figure 7.36: Generator torque control input

CHAPTER 8

Comparison of MPC Control with Baseline Controller

In this chapter we will compare the results from previous simulations, using MPC controllers, with currently implemented baseline PID controller. In the first section brief introduction to baseline controller will be given. The second section of this chapter is devoted into simulations and comparison of results.

8.1 Baseline Controller

This controller is implemented as a typical closed loop. The basic sketch of the system with the controller is shown on figure 8.1. The solely feedback input is the generator speed or rotor speed. Low-pass measurement filter is introduced on the measurement so high frequency excitation is avoided.

The baseline controller has two main parts; table look-up for generator torque, and PI controller for collective pitch rate. Simple gain scheduling for the proportional and integral gain is implemented. Both control signals are saturated if necessary, so the operational constraints are met. Contrary to the MPC design presented in (chapter 5), where the minimum blade pitch is set to $-5°$, in case of this PI controller, $0°$ is the minimum value. Further and more detailed

information can be found in (Jonkman et al., 2009).
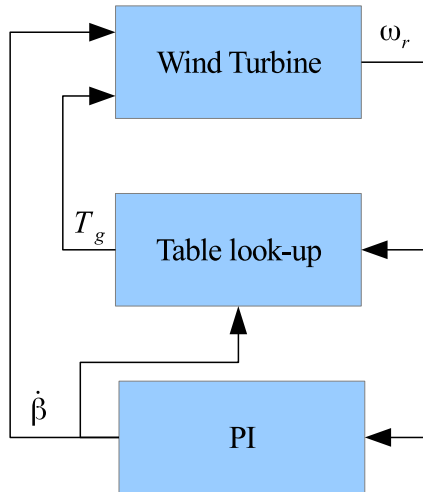
Figure 8.1: Sketch of baseline controller loop

8.2   Simulations with baseline controller

Baseline controller has been tested on same simulation model as MPC controllers. However, reader should keep in mind, that baseline controller presented by (Jonkman et al., 2009) has been tuned for FAST system, which represents the wind turbine much closely.

8.2.1   Full Load Simulations

Wind profile for the fourth region has been generated (fig. 8.2), and simulation with this profile has been performed, so MPC strategies can be compared with the baseline controller performance. Wind speed profile has been generated for mean values equal to 18 m/s.

Figure 8.3 shows generated power P_e and rotational speed ω_r. In both cases baseline controller performs worse than MPC strategies, but within acceptable
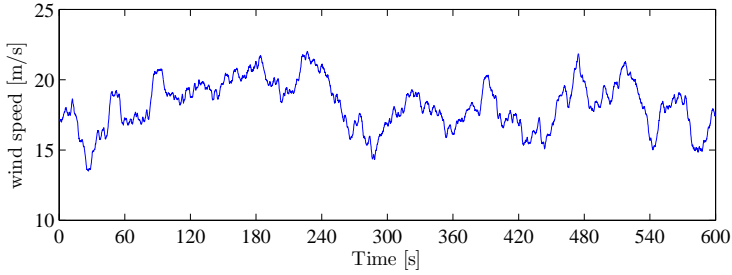
Figure 8.2: Wind speed profile

margins. Second set of figures shows time evolution of states related to tower for-aft movement (fig. 8.4). notice that tower oscillations are not damped using baseline controller. The speed of the tower displacement is gaining 10x higher values compared to model predictive controllers.
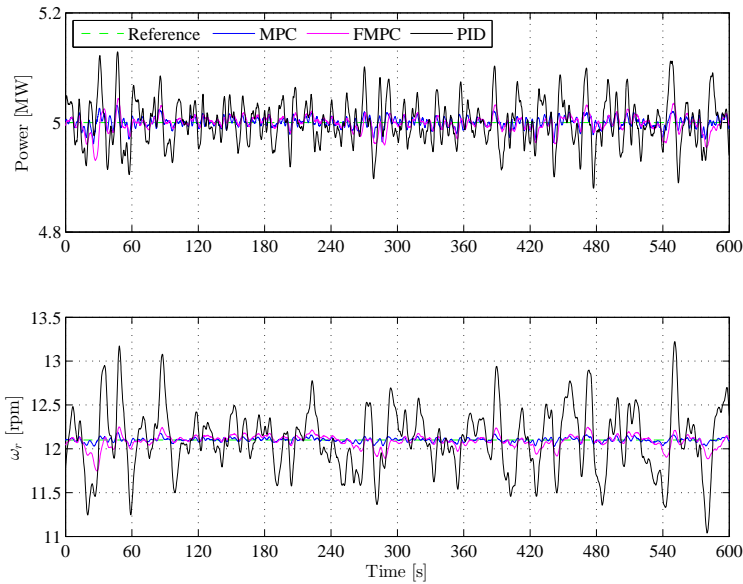
Figure 8.3: Measurements - P_e and ω_r

Figure 8.5 show the pitch activity. Slow dynamics of the rotational speed, which is the solely input to the baseline controller, results in slow variations in pitch regulation. Model predictive controllers on the other hand counteract the variations in wind speed much more aggressively. This behaviour of the pitch activity also results in higher tower oscillations, because tower for-aft movement

can be actively controlled only by pitch (see modelling section 2.1).

Variations of the generator torque activity using baseline controller are much larger than using MPC strategies (fig. 8.6). These variations naturally result in higher oscillations in rotational speed as well as in produced power.

Final comparison between baseline controller and MPC strategies is done by evaluating cumulative sum of control inputs rates. Figure 8.7 shows these results. Notice the difference in actual activity of the control signal and slope of e.g. pitch travel. In case of both MPC strategies, more work is done by the pitch input than but the generator torque input. Due to the fact, that MPC was designed to dampen the tower oscillations, higher pitch activity is necessary. Based on the fact, that the stationary value of the generator torque is throughput top region constant, slope of cumulative sum for T_g rate is small in case of MPC.

Resulting signals have been also statistically compared. Mean values (tab. 8.1) and standard deviation (tab. 8.2) has been computed. These tables also show comparison in such way, that resulting mean value (standard deviation value) of a signal from baseline controller is treated as 100%. We can notice that in all cases, except pitch, standard deviation is significantly decreased using one of the MPC strategies. In this comparison we can also notice that the standard deviation of tower speed of the displacement is decreased even more using FMPC.

Table 8.1: Mean values of signals

Signal	Original Values			Scaled Values		
	MPC	FMPC	PID	MPC	FMPC	PID
ω_r [rpm]	12.1008	12.0877	12.1017	0.9999	0.9988	1
x_t [m]	0.2005	0.2004	0.2015	0.9949	0.9943	1
$\dot{x}_t$ [10^{-3} m/s]	0.0169	0.0271	0.1162	0.1453	0.2336	1
P_e [MW]	5.0001	4.9985	5.0005	0.9999	0.9996	1

Table 8.2: Standard deviations of signals

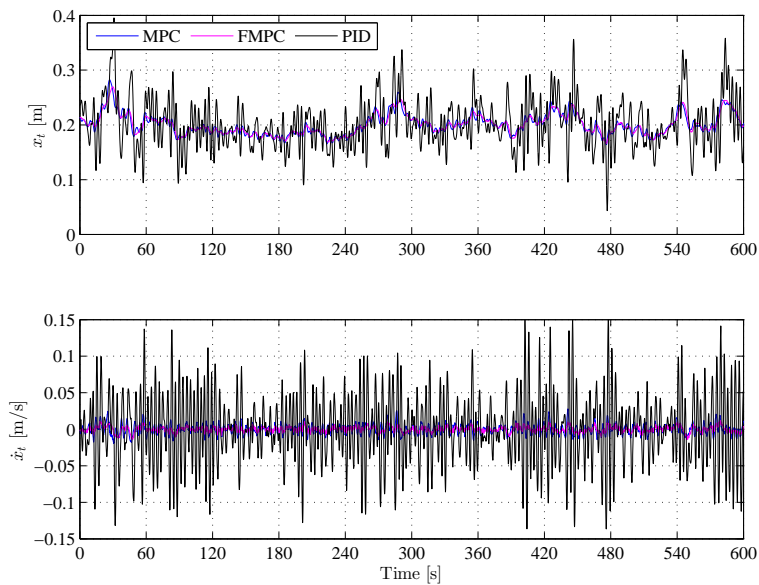| Signal	Original Values			Scaled Values		
	MPC	FMPC	PID	MPC	FMPC	PID
ω_r [rpm]	0.0026	0.0074	0.0384	0.0678	0.1933	1
x_t [m]	0.0192	0.0185	0.0446	0.4315	0.4146	1
$\dot{x}_t$ [m/s]	0.0068	0.0038	0.0477	0.1425	0.0805	1
P_e [MW]	0.0098	0.0142	0.0403	0.2436	0.3529	1
β [deg]	2.3618	2.3138	2.5014	0.9442	0.9250	1
T_g [kNm]	0.0391	0.1513	1.2056	0.0324	0.1255	1

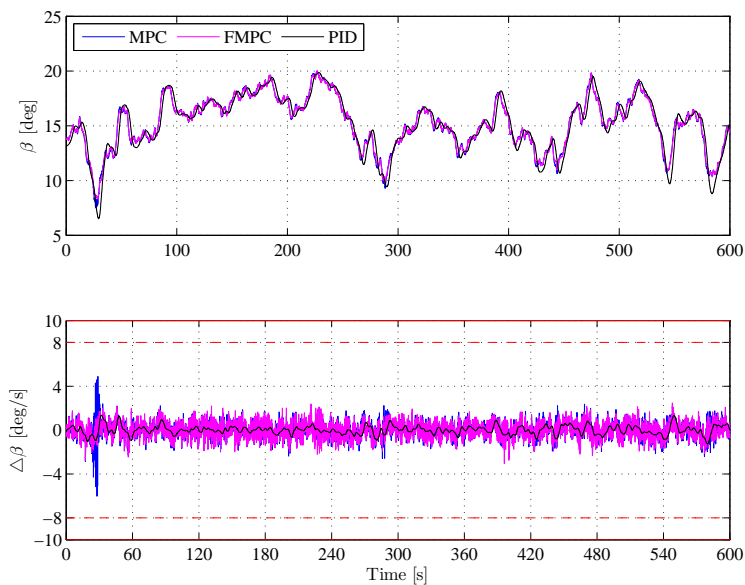**Figure 8.4:** Tower displacement x_t and speed of displacement $\dot{x}_t$

Figure 8.5: Pitch control action of baseline controller in full load
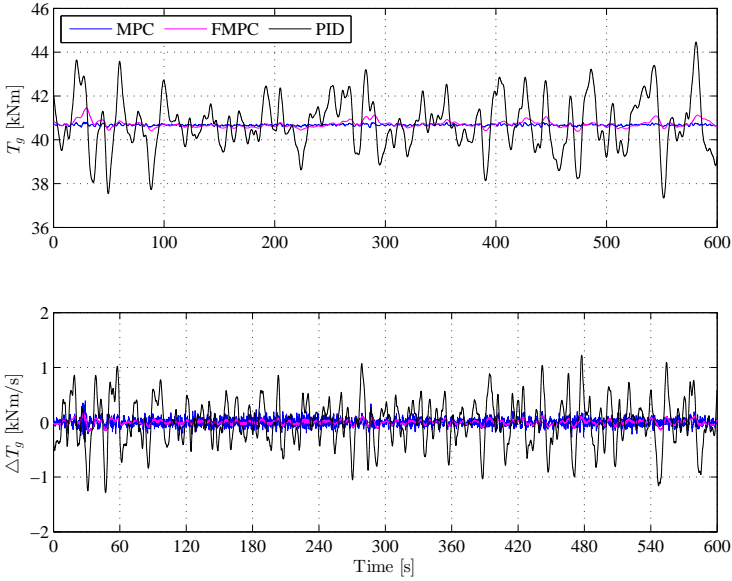
Figure 8.6: Generator torque control action of baseline controller in full load
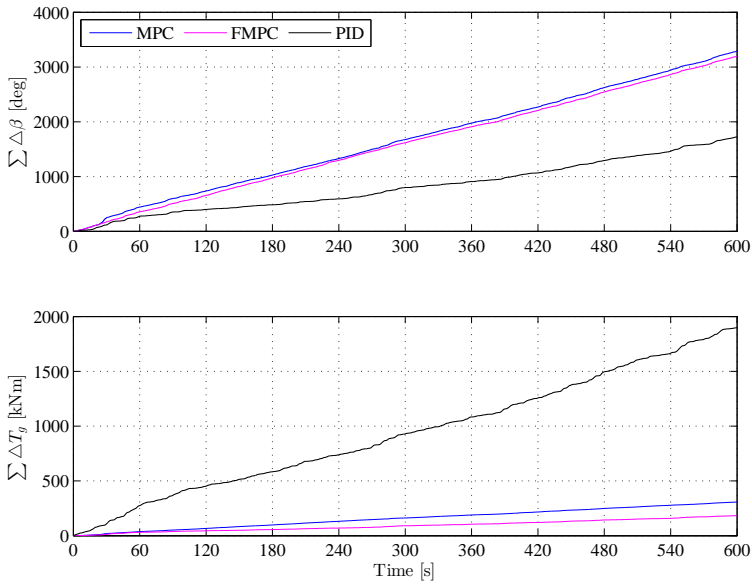
Figure 8.7: Cumulative sum of control inputs rates in full load

8.2.2 Partial Load Simulations

Comparison between MPC strategies and baseline controller is done as well. Wind speed profile applied to the system is shown 8.8. There is little difference in power generation (fig. 8.9), despite the fact, that the baseline controller is not pitching in the partial load (fig. 8.11). The trade of for this is, that the rotational speed is kept above the theoretical values in R-II and below in R-I. In case of generator torque control action MPC is more active than baseline controller (fig. 8.12). This is also demonstrated in cumulative sums of control rates (fig. 8.13).

Figure 8.8: Wind speed profile

Figure 8.9: Measurements - P_e and ω_r

Figure 8.10: Tower displacement x_t and speed of displacement $\dot{x}_t$

Figure 8.11: Pitch control action of baseline controller in partial load

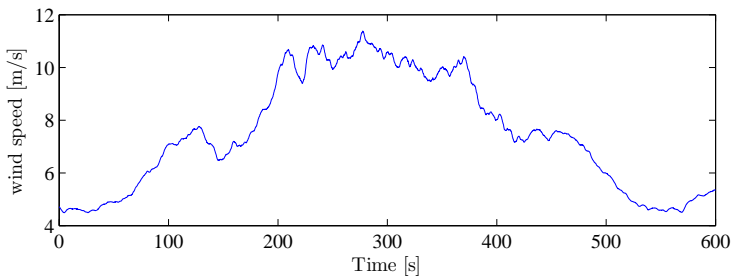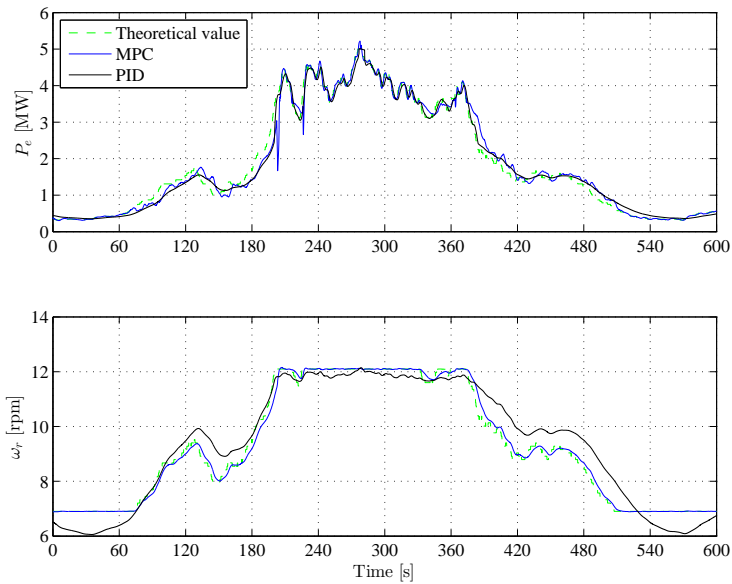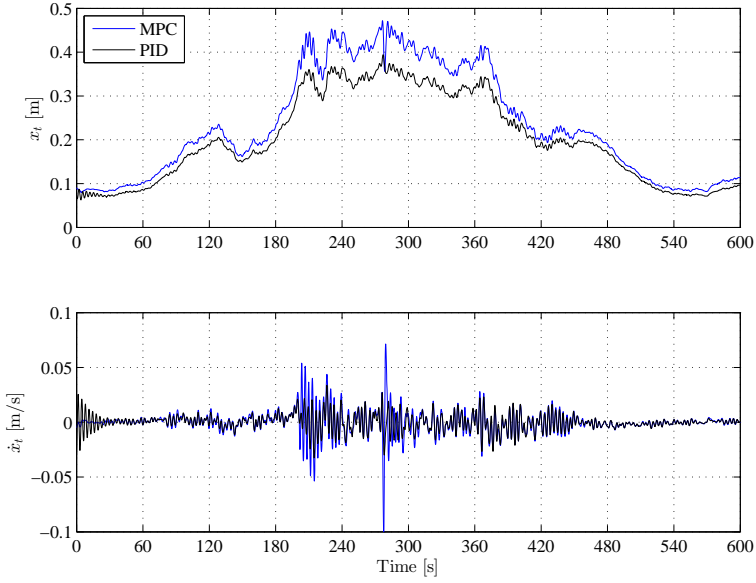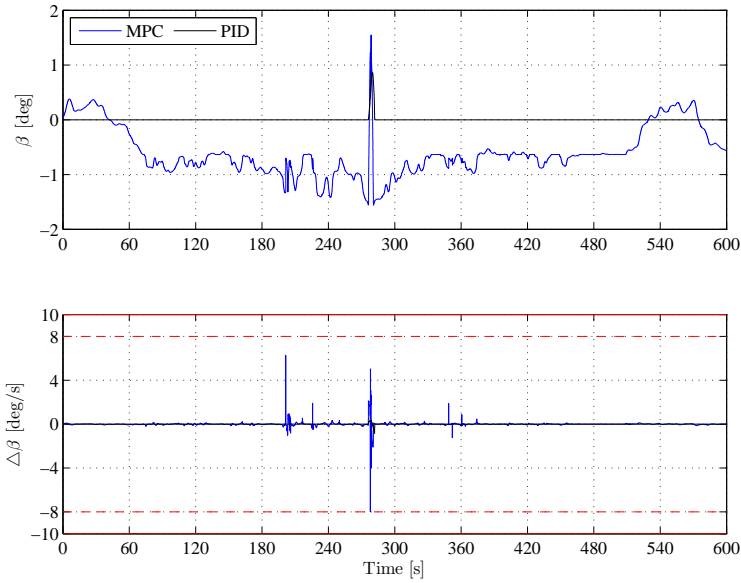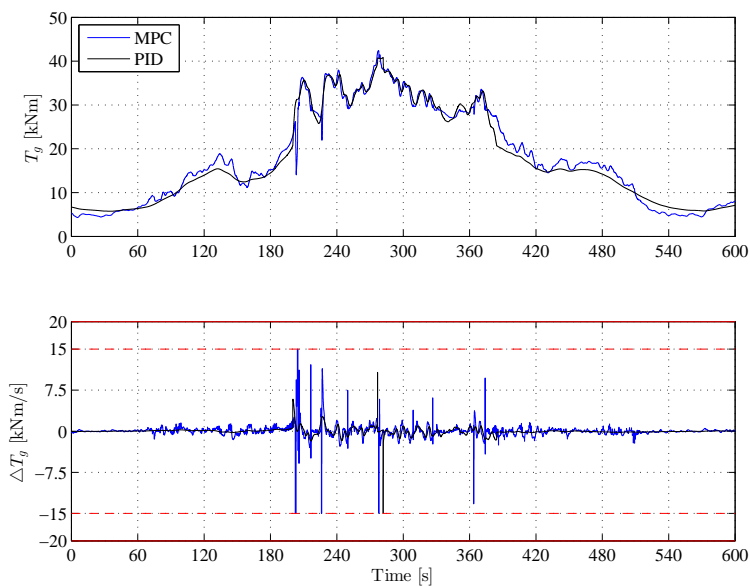**Figure 8.12:** Generator torque control action of baseline controller in partial
load
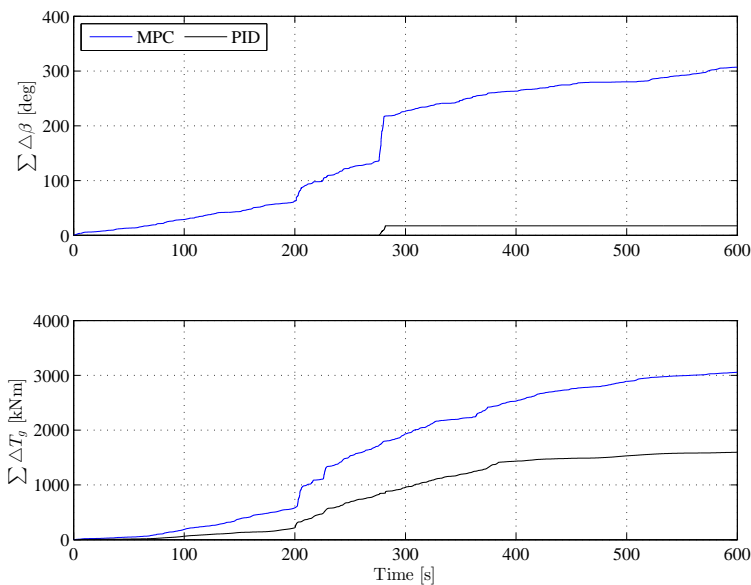
Figure 8.13: Cumulative sum of control inputs rates in partial load

CHAPTER 9

Conclusion & Perspectives

9.1 Conclusion

9.1.1 Theory and Methods

This project has been dealing with MPC control of the wind turbines. Before any controller can be designed, a mathematical model of the plant must be derived. In this project, third order system of the wind turbine has been considered. Since the controller proposed in this project is based on linear state space model, Taylor series expansion has been used to obtain LTI model.

Proposed MPC control with receding horizon policy is based on state feedback, thus state estimator must be used. Based on the facts, that wind speed measurement has not been considered, and that system dynamics change with increasing wind speed, wind speed must be estimated as well. Disturbance modelling has been used for this purpose. Estimator in the form of a stationary predictive Kalman filter was designed. This estimator is then used to estimate the states, the wind speed and unmeasured disturbances.

In this project two alternative MPC strategies has been investigated. Firstly standard MPC formulation, in which the tuning parameters are weighting matri-

ces. Secondly, frequency weighted MPC is considered, in which tuning is shifted from weighting matrices to designing filters in form of transfer functions.

9.1.2 Simulations and Results

Multiple simulations have been performed. In order to understand system behaviour at different wind speeds, deterministic wind profiles has been applied to the system. Simulations with stochastic wind speed profiles has been used to demonstrate how the system performs in "closer to reality" conditions.

Objective in the partial load case was to maximize power output. It has been demonstrated with satisfactory results, that MPC controller can fulfil this objective. Region switching algorithm has been used, in order to control the rotational speed, thus maximizing the power output. Several approaches of control has been investigated in this case. Since MPC controller can not control the turbine with pitch action, pitch must be calculated separately. Best power output has been gained by algorithm, that calculates the pitch action in such way, that maximum c_p value is found for given value of λ. Using this approach, rotational speed and power output has been kept closer to the stationary values.

In the full load case, where the objective is to control the power and rotational speed at its nominal values, two MPC controllers have been compared. Both MPC strategies yields satisfactory results. However, FMPC has proven to perform better in dampening tower oscillations, thus decreasing the physical strain of the tower.

Finally comparison between MPC strategies and baseline controller was done. Differences in energy production between MPC and baseline controller is extremely small. But if we take into consideration other objectives of the controller like damping tower oscilations, MPC strategies proven to do a better job.

9.2 Perspectives

In wind turbine control are many challenges, which were not addressed in the this project.

In general, taking into account more complex models, like flexible drive shaft, or blade momentum could improve the overall performance of the wind turbine power generation. Knowing the dynamics of the system also allows us to design

control strategies which address several issues i.e. decrease the structural fatigue, thus prolonging the lifetime of the entire wind turbine device. Proposed frequency weighted MPC prove to suitable to tool for fulfilling those control objectives. This combines together the advantages of model predictive control, such as constraints handling, together with frequency weighting, which is suitable for deceasing the physical stress on the tower. Since this approach has a form of gain scheduling, more precise estimation of the wind speed can prove to improve the overall performance. For this purpose we might use time varying Kalman filter or extended non-linear Kalman filter.

System Parameters

A.1 Physical Parameters of Wind Turbine

Table A.1: Physical Parameters

Quantity	Units	Value
R	m	63
H	m	90
J	$kg.m^2$	38768000
M_t	kg	422780
D_t	$N.m^{-1}.s^{-1}$	20213
K_t	$N.m^{-1}$	1654700

Constants M_t, D_t, K_t were taken from (Henriksen, 2007). Constants R, H, J from (Jonkman et al., 2009).

A.2 Calculated Matrices and Transfer Functions

In this section are presented state spaces models at 7 and 15 m/s. Also unscaled and scaled models are presented.

Continuous State-Space model linearised at 7 m/s unscaled

$$A = \begin{bmatrix} -0.0350 & 0 & -0.0149 \\ 0 & 0 & 1 \\ 0.5818 & -3.9139 & -0.1844 \end{bmatrix} \tag{A.1a}$$

$$B = \begin{bmatrix} 0 & -2.5 \cdot 10^{-6} \\ 0 & 0 \\ -0.0515 & 0 \end{bmatrix} \tag{A.1b}$$

$$B_v = \begin{bmatrix} 0.0149 \\ 0 \\ 0.1366 \end{bmatrix} \tag{A.1c}$$

$$C = \begin{bmatrix} 1398998 & 0 & 0 \\ 1 & 0 & 0 \\ 0 & 0 & 1 \end{bmatrix} \tag{A.1d}$$

$$D = \begin{bmatrix} 0 & 86.8210 \\ 0 & 0 \\ 0 & 0 \end{bmatrix} \tag{A.1e}$$

Continuous State-Space model linearised at 7 m/s scaled

$$\bar{A} = \begin{bmatrix} -0.0350 & 0 & -0.0149 \\ 0 & 0 & 1 \\ 0.5818 & -3.9139 & -0.1844 \end{bmatrix} \tag{A.2a}$$

$$\bar{B} = \begin{bmatrix} 0 & -0.1126 \\ 0 & 0 \\ -1.1331 & 0 \end{bmatrix} \tag{A.2b}$$

$$\bar{B}_v = \begin{bmatrix} 0.0149 \\ 0 \\ 0.1366 \end{bmatrix} \tag{A.2c}$$

$$\bar{C} = \begin{bmatrix} 0.3205 & 0 & 0 \\ 1 & 0 & 0 \\ 0 & 0 & 1 \end{bmatrix} \tag{A.2d}$$

$$\bar{D} = \begin{bmatrix} 0 & 0.8951 \\ 0 & 0 \\ 0 & 0 \end{bmatrix} \tag{A.2e}$$

Continuous State-Space model linearised at 15 m/s unscaled

$$A = \begin{bmatrix} -0.1362 & 0 & -0.0263 \\ 0 & 0 & 1 \\ -0.5836 & -3.9139 & -0.2223 \end{bmatrix} \tag{A.3a}$$

$$B = \begin{bmatrix} 0.0158 & -2.5 \cdot 10^{-6} \\ 0 & 0 \\ -0.1490 & 0 \end{bmatrix} \tag{A.3b}$$

$$B_v = \begin{bmatrix} 0.0263 \\ 0 \\ 0.1745 \end{bmatrix} \tag{A.3c}$$

$$C = \begin{bmatrix} 1398998 & 0 & 0 \\ 1 & 0 & 0 \\ 0 & 0 & 1 \end{bmatrix} \tag{A.3d}$$

$$D = \begin{bmatrix} 0 & 86.8210 \\ 0 & 0 \\ 0 & 0 \end{bmatrix} \tag{A.3e}$$

Continuous State-Space model linearised at 15 m/s scaled

$$\bar{A} = \begin{bmatrix} -0.1362 & 0 & -0.0263 \\ 0 & 0 & 1 \\ -0.5836 & -3.9139 & -0.2223 \end{bmatrix} \tag{A.4a}$$

$$\bar{B} = \begin{bmatrix} -0.3484 & -0.1126 \\ 0 & 0 \\ -3.2781 & 0 \end{bmatrix} \tag{A.4b}$$

$$\bar{B}_v = \begin{bmatrix} 0.0263 \\ 0 \\ 0.1745 \end{bmatrix} \tag{A.4c}$$

$$\bar{C} = \begin{bmatrix} 3945990 & 0 & 0 \\ 1 & 0 & 0 \\ 0 & 0 & 1 \end{bmatrix} \tag{A.4d}$$

$$\bar{D} = \begin{bmatrix} 0 & 122.9096 \\ 0 & 0 \\ 0 & 0 \end{bmatrix} \tag{A.4e}$$

Detailed Frequency Responses

More detailed frequency responses are shown in this appendix. 3D bode plots are made, so reader can see the evolution of magnitude and phase throughout operational wind speed interval. In all frequency responses we can see rapid change in responses starting at critical wind speed $11.2\ m/s$. This is caused by the fact, that we cannot control the linear model using pitch in the partial load, but only by generator torque.

(a) $G_{\beta,P_e}(j\omega)$

(b) $G_{\beta,\omega_r}(j\omega)$

(c) $G_{\beta,x_t}(j\omega)$

(d) $G_{\beta,\dot{x}_t}(j\omega)$
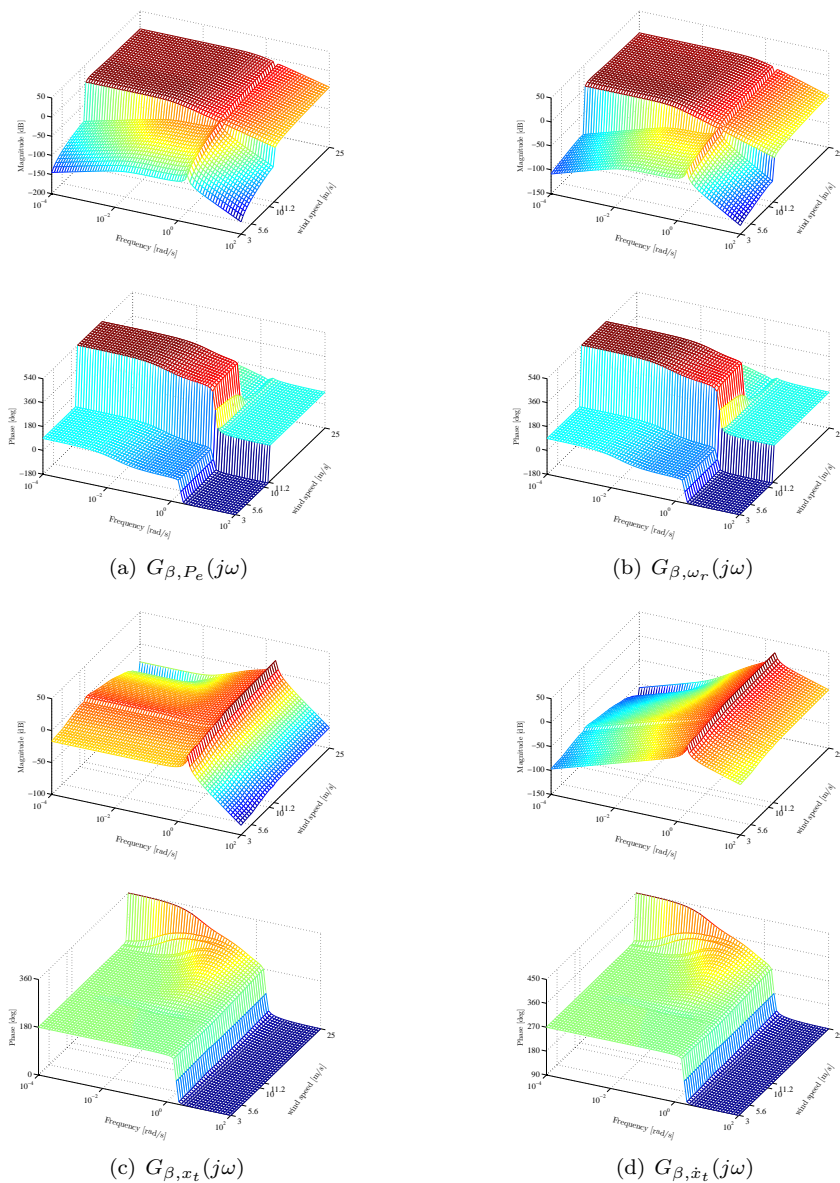
Figure B.1: Frequency response of transfer functions from pitch control input to outputs

(a) $G_{T_g,P_e}(j\omega)$

(b) $G_{T_g,\omega_r}(j\omega)$

(c) $G_{T_g,x_t}(j\omega)$

(d) $G_{T_g,\dot{x}_t}(j\omega)$
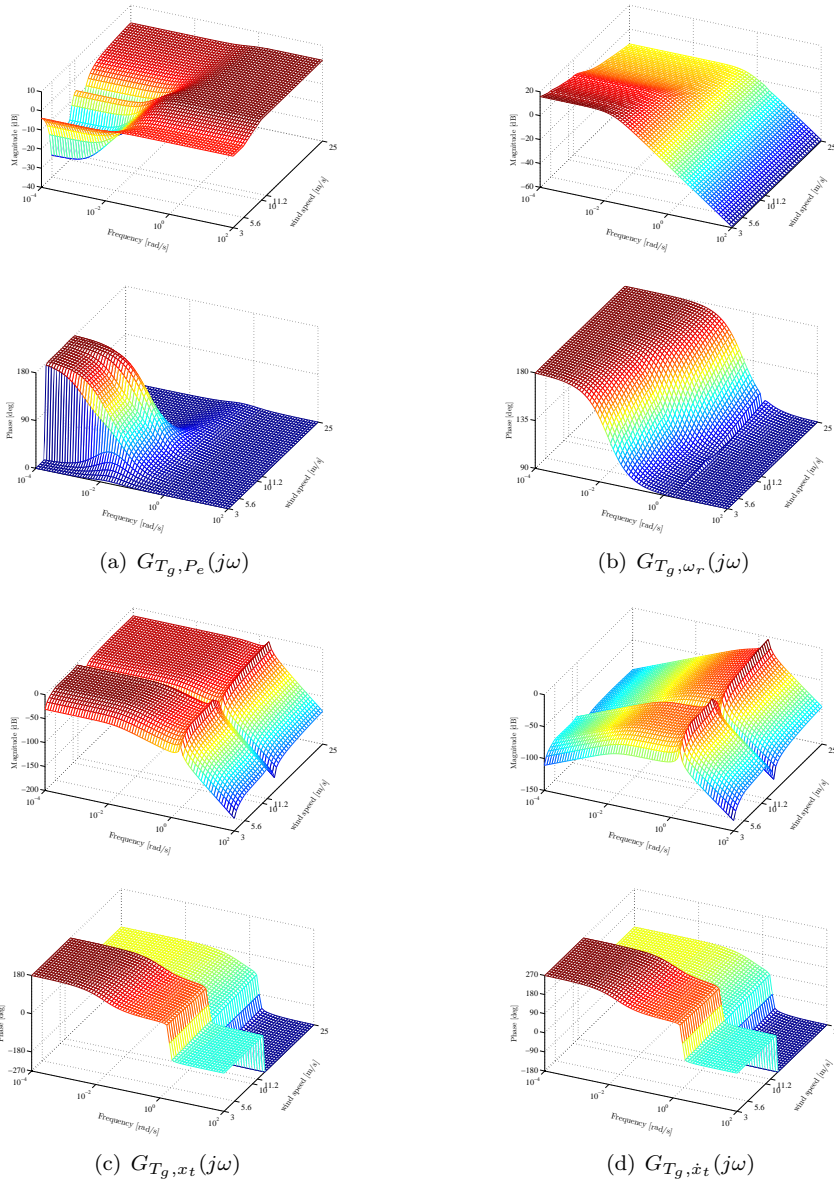
Figure B.2: Frequency response of transfer functions from generator torque control input to outputs

(a) $G_{v,P_e}(j\omega)$

(b) $G_{v,\omega_r}(j\omega)$

(c) $G_{v,x_t}(j\omega)$

(d) $G_{v,\dot{x}_t}(j\omega)$

Figure B.3: Frequency response of transfer functions from wind speed to outputs

Bibliography

Ahmad, A. and Wahib, A. (2007). Application of Model Predictive Control (MPC) Tuning Strategy in Multivariable Control of Distillation Column. *Reaktor*, Vol. 11:66–70.
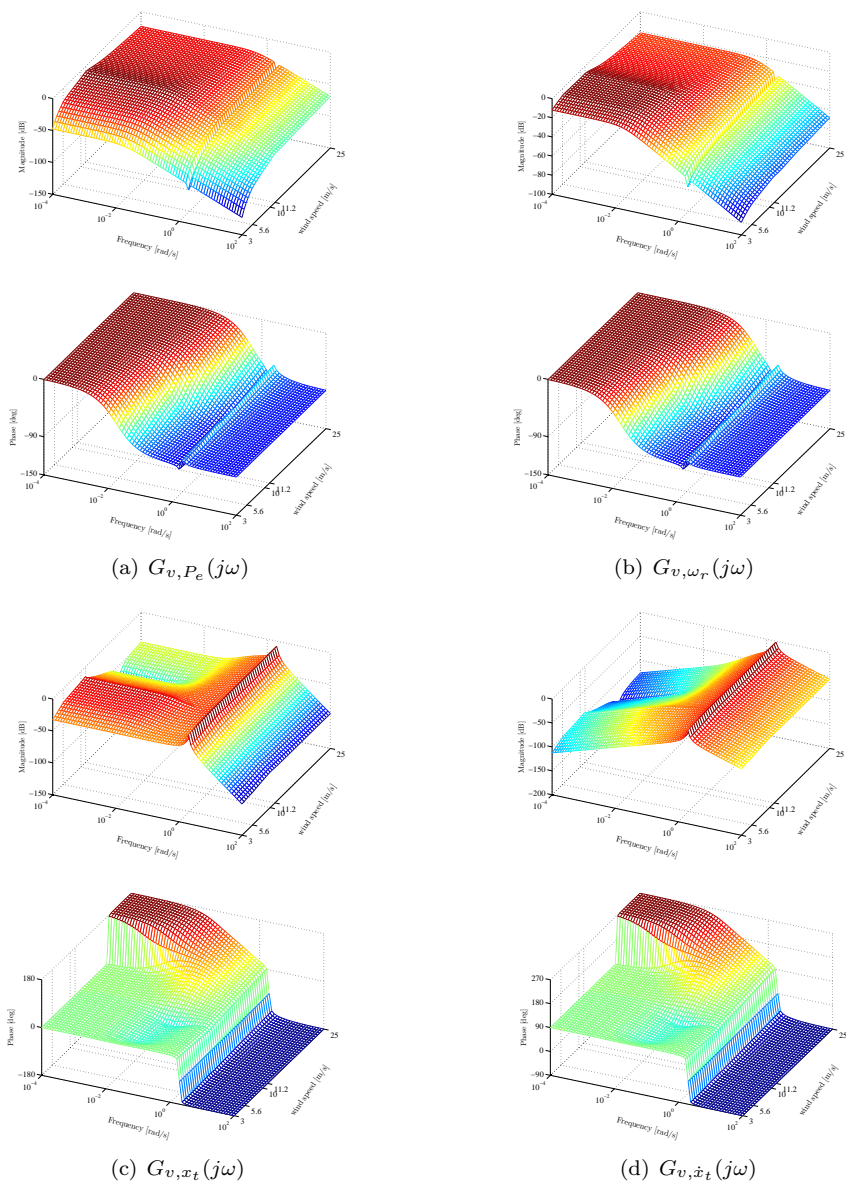
Åström, K. (1970). *Introduction to Stochastic Control Theory*. Dover Publications, Inc., Mineola, New York.

Bendtsen, J., Trangbaek, K., and Stoustrup, J. (2010). Hierarchical model predictive control for resource distribution. In *Decision and Control (CDC), 2010 49th IEEE Conference on*, pages 2468 –2473.

Bossanyi, E. A. (2003). Individual blade pitch control for load reduction. *Wind Energ*, 6:119–128.

Bourlis, D. and Bleijs, J. (2010). A wind speed estimation method using adaptive Kalman filtering for a variable speed stall regulated wind turbine. In *Probabilistic Methods Applied to Power Systems (PMAPS), 2010 IEEE 11th International Conference on*, pages 89 –94.

Boyd, S. and Vandenberghe, L. (2009). *Convex Optimization*. Cambridge University Press, New York, USA, 7th edition.

Brown, R. G. and Hwang, P. Y. C. (1997). *Introduction to Random Signals and Applied Kalman Filtering*, volume 2. John Wiley & Sons.

Burton, T., Shrape, D., Jenkins, N., and E., B. (2001). *Wind Energy Handbook*. J. Wiley.

Camacho, E. F. and Bordons, C. (2007). *Model Predictive Control*. Springer, 2nd edition.

Gosk, A. (2011). Model predictive control of a wind turbine. Master's thesis, Denmark University of Technology.

Hansen, M. (2008). *Aerodynamics of Wind Turbines*. Earthscan.

Henriksen, L. C. (2007). Model predictive control of a wind turbine. Master's thesis, Denmark University of Technology.

IEC-CDV (2004). *WIND TURBINES CDV STANDARD*. International Electrotechnical Commission, Geneva, Switzerland, 2nd revision edition.

J. Jonkman and Bir, G. (2007). Aeroelastic instabilities of large offshore and onshore wind turbines. Technical report, National Renewable Energy Laboratory, U.S.

Jonkman, J., Butterfield, S., Musial, W., and Scott, G. (2009). Definition of a 5MW reference wind turbine for offshore system development. Technical report, National Renewable Energy Laboratory, U.S.

Jonkman, J. M. and Buhl Jr., M. L. (2005). *FAST User's Guide*. National Renewable Energy Laboratory, USA.

Jørgensen, J. (2011). Model predictive control course. Lecture Notes.

Kalman, R. E. (1960). A new approach to linear filtering and prediction problems. *Transactions of the ASME–Journal of Basic Engineering*, 82(Series D):35–45.

Kvasnica, M. (2009). *Real-Time Model Predictive Control via Multi-Parametric Programming: Theory and Tools*. VDM Verlag, Saarbruecken.

Laks, J., Pao, L., and Wright, A. (2009). Control of wind turbines: Past, present, and future. In *American Control Conference, 2009. ACC '09.*, pages 2096 –2103.

Larsson, M. (2004). A model-predictive approach to emergency voltage control in electrical power systems. In *Decision and Control, 2004. CDC. 43rd IEEE Conference on*, volume 2, pages 2016 – 2022 Vol.2.

Maciejowski, J. (2002). *Predictive Control with Constraints*. PEARSON Prentice-Hall.

Mancuso, G. M. and Kerrigan, E. C. (2011). Solving constrained LQR problems by eliminating the inputs from the QP. In *IEEE Conference on Decision and Control*, Orlando, FL, USA.

Mirzaei, M., Henriksen, L. C., Poulsen, N. K., Niemann, H. H., and Hansen, M. H. (2012a). Individual pitch control using LIDAR measurements. In *IEEE Multi-Conference on Systems and Control*, Dubrovnik, Croatia.

Mirzaei, M., Poulsen, N. K., and Niemann, H. H. (2012b). Robust Model Predictive Control of a Wind Turbine. *American Control Conference.*

Muske, K. R. and Rawlings, J. (1993). Model predictive control with linear models. *AIChE Journal*, 39(2).

Nikolaou, M. (2001). Model Predictive Controllers: A Critical Synthesis of Theory and Industrial Needs. *Advances in Chemical Engineering, Academic Press*, Vol. 26:131–204.

Nocedal, J. and Wright, S. (1999). *Numerical Optimization.* Springer Series in Operations Research. Springer.

Østergaard, K. Z., Brath, P., and Stoustrup, J. (2007). Estimation of effective wind speed. *Journal of Physics: Conference Series 75.*

Østergaard, K. Z., Stoustrup, J., and Brath, P. (2008). Linear parameter varying control of wind turbines covering both partial and full load considitons. In *International Journal of Robust and Nonlinear Control*, volume 19.

Pannocchia, G. and Rawlings, J. (2003). Disturbance models for offset-free model-predictive control. *AIChE Journal*, 49(2).

Poulsen, N. K. (2007). *Stokastik Adaptiv Regulering.* Informatik og Matematisk Modellering, DTU.

Prasath, G. and Jørgensen, J. (2009). Soft constraints for robust MPC of Uncertain systems. In *International Symposium on Advanced Control of Chemical Processes.*

Prasath, G., Recke, B., Chidambaram, M., and Jørgensen, J. (2010). Application of Soft Constrained MPC to a Cement Mill Circuit. In *Proceedings of the 9th International Symposium on Dynamics and Control of Process Systems*, Belgium, Leuven.

Primbs, J. (2007). A soft constraint approach to Stochastic Receding Horizon Control. In *Decision and Control, 2007 46th IEEE Conference on*, pages 4797 –4802.

Skogestad, S. and Postlethwaite, I. (2005). *Multivariable Feedback Control: Analysis And Design.* John Wiley.

Wills, A. (2007). QPC - Quadratic Programming in C. http://sigpromu.org/quadprog/.

Xin, M. (1994). Modelling and control of a wind turbine. Master's thesis, Denmark Univeristy of Technology.

Xin, M., Poulsen, N., and Bindner, H. (1997). Estimation of the wind speed in connection to wind turbines. In *Proceedings of the IASTED Internation Conference CONTROL'97*, Mexico, Cancun.

Zeilinger, M., Jones, C., and Morari, M. (2010). Robust stability properties of soft constrained mpc. In *Decision and Control (CDC), 2010 49th IEEE Conference on*, pages 5276 –5282.